DISSERTATION

INTERFACIAL MODIFICATIONS IN FIBER REINFORCED GEOPOLYMER MATRIX COMPOSITES FOR IMPROVED TOUGHNESS

Submitted by

Patrick R. Jackson

Department of Mechanical Engineering

In partial fulfillment of the requirements

For the Degree of Doctor of Philosophy

Colorado State University

Fort Collins, Colorado

Fall 2017

Doctoral Committee:

Advisor: Donald Radford

Paul Heyliger
Arun Kota
Kaka Ma

ABSTRACT

INTERFACIAL MODIFICATIONS IN FIBER REINFORCED GEOPOLYMER MATRIX COMPOSITES FOR IMPROVED TOUGHNESS

Geopolymers have emerged in the recent decades as a potential matrix material for advanced composites. Geopolymers, or more generically inorganic polymers, extend the use temperature range over more common organic polymers, while retaining relatively low processing temperatures. In fact, some of the techniques used to process geopolymers are very similar to those developed for thermosetting polymers. This allows for processing of near net shape components without many of the complexities that would be associated with conventional ceramics or metals manufacturing technologies. To-date, fiber reinforced geopolymers have seen limited use, primarily in areas that emphasize high temperature resistance and good manufacturability over structural performance. The use of all-oxide geopolymer matrix composites (GMC) for high temperature structural applications remains uncertain due to limited toughness. Attempts to improve toughness in these materials through the use of an interphase material, such as those associated with ceramic matrix composites (CMC), have yielded mixed results. In some cases, an increase in toughness was observed, but at the expense of modulus and sometimes strength. The result was a composite that was less tough, or no tougher, than the composite with the untailored interface condition. Additionally, methods that would indicate differences between the tailored and untailored interface have not been employed leaving uncertainty as to what is providing improved toughness. This research examines the ability of weak

interface concepts, often employed in ceramic matrix composites and created using fiber coatings, as means of producing greater toughness in GMCs exposed to elevated temperatures. This was accomplished through examination of composite mechanical properties and interfacial conditions.

Geopolymer matrix composites reinforced with the 3M Nextel series of ceramic fibers were fabricated and exposed to elevated temperatures. From the fabricated composites, samples were prepared for testing in flexure, tension, short beam shear, and single fiber push-out. Microscopy techniques were employed to analyze fracture surfaces and results of push-out testing of composites. Both a model coating, carbon and thermally stable oxide coating known as monazite were applied to the surface of fibers and compared against a baseline condition to support the changes observed.

The results of the research indicate the importance of ensuring adequate cure time of the geopolymer matrix, which enhances it properties. In GMCs using carbon coated fibers to achieve a weak interfacial condition, low mechanical properties of inadequately cured matrix produced composites with limited shear resistance and limited ability to transfer stresses to fibers. A moderate increase in the mechanical properties of the matrix via extended cure time from 1 to 5 hours resulted in a roughly 50% increase in modulus and 150% increase in strength for GMCs containing the interphase material. In all cases the use of fiber coatings resulted in a reduction of interfacial strength. This was revealed by fiber push-out testing, which constitutes the first known use of this technique in GMCs to directly analyze the strength of the bond between the fiber and the matrix. Analysis of the

interfaces in specimens further revealed that simple reductions in bond strength are not sufficient for producing better toughness and mechanical properties in GMCs, but that there is a delicate interplay between the interface properties and improved mechanical behavior. Increased toughness was observed in the specimens containing the carbon coated and monazite coated fiber surfaces except in the instance where coating was degraded by the oxidizing environment. GMCs containing the monazite coated fiber demonstrated the greatest improvement in toughness. The improvement in toughness was the result of increased damage tolerance and also a roughly ~32 to 44% increase in strength as compared to GMCs without coated fiber surfaces. Both limited and elongated elevated temperature exposure did not limit greater toughness from being achieved in monazite coated fiber GMCs as compared to those composites without coatings. In general, the use of fiber coatings did improve the toughness of GMCs as result of weaker interfacial conditions and it was demonstrated that careful tailoring of the interfacial strength can result in retention of mechanical properties.

ACKNOWLEDGEMENTS

I was very fortunate during my four years of research to be surrounded by a great number of wonderful people. Some began and finished the journey with me and others flowed in and out over the time of my study, but they all played an important part in helping me to undertake and accomplish this amazing achievement. I am very humbled and grateful for any and all of the support everybody provided. As a small token of my gratitude I would like to acknowledge several individuals and groups that made a significant impact on my efforts

First, I would like to thank my advisor Dr. Don Radford for taking me on as advisee and sticking with me through the entire process. I am grateful for his guidance and mentorship in all things composites, which made this achievement possible. Also, a quick thank to all my committee members and for the support they provided in my effort to earn this degree.

I would like to thank my colleagues and lab mates. Specifically, I would like to thank Kent Warlick, Kevin Hedin, and Samsur Rahman for all of their help. Combined they did everything from helping me execute experiments to talking through my research and helping me overcome obstacles. I am very grateful for all of your help. I would also like to thank Trevor Aguirre for some of the same help. I wish all of you the best.

I am forever grateful to Air Force Research Labs RCXX research group at Wright Patterson Air Force Base for all of their support. The support they provided was very key to my

success. I would specifically like to Mike Cinibulk and Kristi Keller for providing access to and use of the lab. Additional, I would like to thank Kristi and Emmanuel Boakye for their help with coated fibers. I would also like to thank Triplicane Parthasarathy for his help in conducting the analysis of the push-out experiments. His expertise in this area was very helpful. Finally, I would like to thank Aric Ross for his help in preparing and testing samples and helping me with the use of the SEM. Aric went way above and beyond whatever was expected of him and was very instrumental in helping me finish my research. Aric, I couldn't have done this without your extraordinary effort. Thank you so much!

I would also like to thank all the individuals who helped with some of the "grunt work" of my research. There was lot of time and preparation that went in to the production of a single composite sample and I could not have done it without these individuals help. Ryan Aldrich, Tamara Haynes, and Jacob Dahlke thank you for all your help in preparing materials for the fabrication of composites. Ryan Dunn, thank you for helping me design and machine parts for the 4-point fixture. Kohl Jacobson, thanks for helping me conduct some of the flexural tests. Kate Radford, thanks for all of your help during the summer of 2016. There is no way I would have been able to get as much done that summer without your help. You were played a very essential role in helping me get all of lab work done prior to departing Fort Collins in January of 2017. I am very grateful of all of your hard work.

I would also like to thank Peter Nivala for his insight into working with the geopolymer material. You didn't have to help, but you did. I had some real breakthroughs in working

with the material after talking with you. This was very critical to the early stages of my research and set me on a path to completion. Furthermore, all the advice you offered was very encouraging and helped me through some tough times. Thank you.

In addition to those that helped me within the boundaries of CSU there were many that helped from a distance. I would like to thank LtCol Justin Rufa for guiding and mentoring me through this long process. It meant so much to me that you reached out (even while finishing up your PhD at Michigan) to help and encourage me in the early stages of my research and then all the way through to the end. I am glad that you got to share in the journey. I look forward to working with you again very soon.

I would also like to thank my church family at The Town Church, Fort Collins. This was one of the greatest local church experiences my family and I have ever been a part of. Many thanks to the elders of the church. Thank you for your leadership and for always pointing us back to our need for a Savior. My family and I are forever grateful. Thank you also to those friends and members of the church that prayed for us, encouraged us, and walked beside us during the ups and downs of this long season of life. Specifically, I would like to thank Sergei and Sarah and their family for all the support and fun memories. You are great friends. You made this season of life extra special.

Many thanks to my family. Thank you mom and dad for raising me up and for always being there for me. I am only barely learning the amount of care, concern, heartache, joy, hard-work, and self-sacrifice that you put in to raising me. You did it well. I am extremely

grateful that God gave me you as parents. Also, thank you mom and dad for taking the kiddos from time to time to let Corinne and I get some rest and relaxation. Thank you also to my father and mother-in-law for the same.

And of course, much thanks goes to my wife and kids. Thanks for enduring this long, arduous season of our lives. Thanks for sacrificing along with me. We had no idea what we signed up for when we started this, but it quickly became clear that it was going to be hard. Thanks Anastasia, Josiah, and Titus for all the giggles, the smiles, and the silly and sweet things you do. Thanks for giving up what you didn't even know you were giving up. I will do my best to make it up to you. Corinne thanks for caring so well for our kiddos. Thanks for doing it alone sometimes. Thanks for dealing well with all the missed dates, the lost family time, a stressed out husband, and the lack of help at times. Thanks for dealing with my slowness to get to all the "honey-dos." Thanks for sticking by my side when I was difficult to be around because the stress became so overwhelming. Thanks for encouraging me when I was so disheartened. Thanks for always calling me up. You make me a better man. You might think that you and the kids slowed me down and maybe that's true, but I wouldn't be half of who I was and what I have become through this experience without all of you by my side.

And to my Lord, who sovereignly orchestrated every minor and major event; who brought all these wonderful people into my life to challenge me, to encourage, and to delight in; who listened to all my complaining and frustrations; who carefully watched me dabble fruitlessly at times and then opened my mind to what was already there; who graciously

sustained me and my family in and out of every season of this 4 years; who brought glory and praise to himself and yet allowed it all for my good…all praise to Him! I am undeserving, but You are gracious and merciful. I am unfaithful, but you are ever present. You are my strength and my song!

And David said, "The Lord who delivered me from the paw of the lion and the paw of the bear will deliver me from the hand of this Philistine." (1 Sam 17:37)

TABLE OF CONTENTS

LIST OF TABLES

LIST OF FIGURES

Chapter 1 : Introduction

1.1 Objective

The main thrust of this research effort is to investigate the effectiveness of interfacial modifications for improving the toughness of geopolymer matrix composites (GMC). Toughness being defined as area under the stress-strain curve with increases characterized by improved damage tolerance through non-elastic deformation and non-catastrophic failure. The investigation explores weak interface concepts often used successfully to toughen ceramic matrix composites (CMC) to GMCs. While the technique varies little, the implementation and solution are unique for GMCs because of the large difference in mechanical properties between the geopolymer matrix and the fiber reinforcement.

The motivation for such a study is to explore the viability of using geopolymers, and more specifically GMCs, as a structural material for high temperature applications. Geopolymers offer higher temperature resistance beyond that of polymers, but can be processed using similar techniques and at low temperatures. They also have low density. This makes GMCs a very appealing material to replace the heavier metal components in auto, air, and space vehicles that are exposed to high temperatures during operation. The less complex and relatively low temperature processing associated with GMCs also makes them a more economical choice than conventional CMCs for use at temperatures between roughly 400 and 900 °C.

The aims of the study will be accomplished by examining the influence that interfacial modifications have on the mechanical behavior of these composites. The various characterization techniques used will aid in revealing and account for changes in the toughness of the material. The methods used will include both macro- (mechanical testing) and micro-scale (SEM and single-fiber tests) analysis in order to understand the influence of the interfacial region has on the toughness of GMCs.

1.2 Problem Background

Although many years in the making, the role polymer matrix composites (PMC) are playing as structural components in high performance automobiles, aircraft, and spacecraft are steadily increasing. The strength-to-weight ratio and tailor-ability offered by polymer matrix composites is hard to beat in comparison to sometimes heavier and bulkier metal components. That said, there are still areas within these technologies that are reserved for materials that can withstand thermal oxidative environments. The upper end use temperatures of some of the most thermally resistant polymeric materials is only near 400 °C [1]. Metals and their alloys can be considered for use in intermediate temperature range of 400 to 1100 °C. However, it is the mass of these components that often limits further gains in efficiency for systems trying to push the performance envelope. Advanced ceramic materials are lightweight and can easily operate at and above the upper end use temperatures of metals. Yet, despite advances in overcoming the very brittle nature of ceramics through various means, including fiber reinforcement, the complex and therefore ultimately costly processing procedures involved in their fabrication can limit production and implementation. Furthermore, the high temperature processing of ceramic matrix

composites (CMC) can often result in an unfavorable bonding condition because of the similar composition of the materials or residual stress state at the interface via a coefficient of thermal expansion (CTE) mismatch of the constituent materials [2], [3].

In recent decades, inorganic polymers, or more specifically geopolymers, have emerged among the "big three" as a potential matrix material alternative. As already mentioned, geopolymers offer temperature resistance beyond that of the best polymers, but do not require the complex processing procedures associated with conventional ceramics. In fact, the processing of geopolymers is very similar to that of thermosetting polymers and completed at temperatures ranging anywhere from room temperature to ~120 °C [4].

Geopolymer matrix composites (GMCs) show potential to be used as load bearing structures [5], [6]. Since the inception of GMCs [5], a great deal of research has been conducted on them with continuous fiber reinforcement [7]–[18]. The studies tend to focus on improving mechanical properties of the GMC through changes in processing conditions or evaluating the GMCs mechanical behavior after exposure to elevated temperatures. The use of carbon or silicon carbide (SiC) fibers is prevalent in studies involving GMCs. This is likely because both provide a great deal of reinforcing capability and some of the original experiments with GMCs used these fibers [5]. The incorporation of natural fibers in GMCs has also generated a bit of research because of the potential for a very economical composite with fire resistance. Very little attention in research has been given to the use of oxide fibers to reinforce geopolymers. In most all cases, fibers improve the mechanical properties of the geopolymer sometimes making them competitive with

some of the more common structural materials. From a specific property (value divided by density) standpoint, GMCs show good potential and even more so if one factors in their high temperature properties [19], [20]. Figure 1 shows one particular GMC compared to other common structural materials.

MATERIAL	Density kg/m^3	Tensile Modulus GPa	Specific Modulus MPa-m^3/kg	Flexural Strength MPa	Specific Flexural Strength MPa-m^3/kg	Maximum Temperature Capability °C
Fiber-Reinforced Concrete	2300	30	13.0	14	0.006	400
Structural Steel	7860	200	25.4	400	0.053	500
7000 Series Aluminum	2700	70	25.9	275	0.102	300
Phenolic-Carbon Fabric Laminate	1550	49	31.6	290	0.187	200
Phenolic-E Glass Fabric Laminate	1900	21	11.0	150	0.074	200
Geopolymer-Carbon Fabric Laminate	1850	76	41.0	245	0.132	> 800

Figure 1: GMC compared to properties of some structural materials[19]

Despite great improvement in strength and modulus of GMCs with the use of continuous fiber reinforcement, it has been found that GMCs, like ceramics, lack toughness when a strong interfacial bond forms with fibers [7], [21]. In constituents with similar chemical composition, this is exacerbated with elevated temperature exposure as diffusion of species can often result in an even stronger bond.

In advanced CMCs, reducing the interfacial bond strength between fiber and matrix has become a standard way of improving the toughness of the CMC. This often involves tailoring the bond utilizing a fiber coating. When properly applied, the fiber coating can

allow for the dissipation of crack energy. Direct analysis of interface in CMCs through mechanical testing or microscopy can generally reveal whether the tailoring will allow for greater composite toughness.

Tailored interfaces are one consideration for improving the toughness of GMCs. In previous work, GMCs utilizing a carbon coating on the fibers were exposed to various temperature regimes. The results indicated the potential to use CMC weak interface concepts on GMCs to improve toughness [21]–[23]. Despite potential for increased toughness, there were observed drawbacks for the use of this particular coating. After elevated temperature exposure, composite modulus increased and toughness decreased indicating that the coating potentially degraded under the oxidizing environment [21]–[23]. Degradation and loss of the carbon coatings is often expected after temperature exposure above 400 °C and in some cases the loss could theoretically be beneficial [24]–[27]. However, in this case it was not. The degradation of the coating and associated loss in toughness of the GMC points to a need to consider oxidation resistant fiber coatings. The carbon coating had one other not so obvious drawback. One study noted a significant drop in modulus of specimens utilizing the carbon coating as compared to uncoated fiber GMCs, which was attributed to reduced interfacial strength caused by the introduction of the interphase [23]. The drop was not completely unexpected. Geopolymers have a low modulus compared to the ceramics utilized in CMCs. Therefore, geopolymers rely on the properties of the fiber to enhance the modulus and strength of the composite, not unlike the effect of reinforcement of organic polymers. This occurs by means of shear transfer from the matrix to the fiber, which is influenced by the interfacial bond strength [2]. The

observed loss in modulus with incorporation of fiber coating intended to weaken the interface also appears to be the result of inadequate processing of the geopolymer matrix [28], [29].

Knowledge of interfacial tailoring in GMCs is scarce. Only a handful of studies have considered examinations of the interface for changes in composite mechanical behavior [10], [13], [30], [31]. Very little work on the use of interphase in geopolymers to improve toughness has been presented thus far [21]–[23], [32]. One publication [29] and one conference paper [33] generated from preliminary investigations of this dissertation (see Chapter 4) have added to the knowledge base and have begun to address concerns previously discussed: substantial loss in modulus of the composite and oxidation resistance of the fiber coating. Also, the previous studies have only suggested that improved toughness is a result of the interfacial modifications made at the interface. Yet, none of these studies have been able to provide a direct link to the interface.

The relationship between interface properties and composite toughness has been difficult to establish because of the composite configurations and the experimental program used in the earlier studies. In both cases, GMCs in these studies were exposed to increasing temperatures. However, it is recognized that after curing geopolymers can continue to undergo changes in their microstructure with additional thermal exposure [34]–[37]. For the particular geopolymer used in the studies using interfacial modifications [21]–[23], [32], the changes are now understood [28], [38]. Additionally, composite configurations (e.g. woven fiber architecture, multiple fiber types, and matrix fillers) added a greater

number of variables. This leaves some uncertainty in how changes at the interface have influenced the final toughness of the composites in these studies. To analyze the interface, the composite design should be such as to reduce the number variables that may influence composite mechanical behavior in the same way the interface might. Additionally, in order to demonstrate that these improvements in toughness are the result of the fiber coatings, techniques that directly assess the interface are necessary.

It is hypothesized that through the use of fiber coatings, continuous fiber reinforced geopolymer matrix composites can demonstrate improved toughness, while still retaining high degrees of strength and modulus even after exposure to elevated temperatures. The geopolymer characterization and interfacial studies have become the basis for this research. To address the hypothesis, the research will use an alumina-based oxidation resistant fiber with three different fiber surface conditions. Two of three conditions will be fiber coatings, one model non-oxide coating and the other an oxide coating, $LaPO_4$, known as monazite, which has been demonstrated to improve toughness in CMCs. The other fiber surface condition, a heat cleaned surface, will be the baseline, or worst case, condition to be used for comparison. Also, important to proving the hypothesis will be to leverage the accumulated knowledge on proper processing of geopolymers in order to ensure sufficient mechanical properties of the matrix. Mechanical characterization and microscopy techniques will be applied to directly assess the interface and analyze the effect of the interfacial conditions on mechanical properties of composites after heat treatment at elevated temperatures.

1.3 Thesis Structure

The thesis is divided into eight chapters. The topics of chapters include a literature review, background information, materials and processes used to fabricate composites, preliminary investigations, physical characterization of composites, investigation of toughness using fiber coatings, thermal aging of GMCs with fiber coatings, and a final summary.

Chapter 2 specifically covers the definition of toughness as it is used in this research and techniques that have been successful in promoting toughness in brittle matrix materials, especially CMCs. It also discusses the relevant research conducted on geopolymers and GMCs providing details on mechanical properties, thermal stability, and a more detailed look at efforts to toughen GMCs through the use of fiber coatings.

Chapter 3 examines the materials and processes used to fabricate the composites of this research. This includes all the constituent materials to include the fiber coatings.

Chapter 4 explains the two preliminary investigations that were conducted to support to the main efforts of this research. The results and analysis of these two studies are covered in this chapter.

Chapter 5 provides physical information about the composites of this research. The chapter contains measures of fiber volume fraction and porosity of composites used in the

primary investigations. Additionally, this chapter involves a brief discussion on the quality of manufactured composite specimens and the effect of thermal treatments on their physical appearance.

Chapter 6 investigates how the interfacial modifications made in GMCs through the use of fiber coatings are able to promote toughness. This was explored by series of mechanical tests that provided measures for modulus, strength, short beam strength, and toughness. A direct evaluation of the interface and fracture surfaces of the GMCs was also used to aid the investigation.

Chapter 7 investigates the effect thermal aging in an oxidizing environment has on the mechanical behavior of a GMC containing fibers with a coating. The discussion draws on results and data presented in previous chapters to aid the analysis.

Chapter 8 provides a summary of the research and addresses some of the key findings.

Chapter 2: Literature Review

2.1 Promoting Toughness in Brittle Materials

2.1.1 Terminology

The term toughness, as it will be used through the rest of this document, refers to a material's ability to absorb energy before fracture [39]. Toughness is somewhat of an abstract concept, but it can be quantitatively evaluated. Quantitatively, toughness can be calculated as the area under a material's stress-strain curve. A very closely related term to toughness is work of fracture (WOF). Also, an energy term, WOF is the area under the stress-displacement curve. The term toughness can also be used as shorthand for fracture toughness, but in the following discourse it will not be used as so. The terms toughness and fracture toughness have distinctly different meanings. That said, the mechanisms that might lead to greater toughness in a material might also improve that material's fracture toughness. In that regard, the two terms share a common link. However, a material that has a high value of fracture toughness may not necessarily be tough. This will be discussed in greater detail in the following sections.

There are two other terms associated with toughness, which may at times be used interchangeably throughout this document. The terms are graceful failure and damage tolerance. Like toughness, these terms are used in the evaluation of stress-strain, or in some cases, stress-displacement curves. These terms are commonly used in much of the

literature regarding efforts to improve toughness in ceramic matrix composites. Although both terms may be used in this document to suggest any increase in toughness, the term damage tolerance is generally applied to discuss the resistance to failure a material demonstrates that involves inelastic deformation. The term graceful failure is generally used to suggest non-catastrophic failure of the material.

2.1.2 Modifications to Improve Toughness

Brittle materials lack the inherent mechanisms needed to prevent cracks from initiating and then propagating. These mechanisms are referred to as intrinsic toughening mechanisms[39], [40] and are result of a materials make-up. For example, the particular structure of some metals such as aluminum and copper allow for prevention of cracks and dissipation of crack energy through dislocation and plastic flow. To promote toughness in brittle materials, such as ceramics, it is common to use a second phase or reinforcement. Nanoparticles, whiskers, short fibers, and continuous fiber are all types of reinforcements that can work to dissipate the energy of a crack and promote toughness. Increased toughness is achieved through the activation of mechanisms such as crack bridging, crack deflection, debonding, and/or fiber pullout [2], [39], [41]. Generally, the greater number of these mechanisms there are at work, the tougher the material.

2.1.3 Conditions for crack deflection

Crack deflection is an important factor in increasing toughness in composites. As such researchers have attempted to generate criteria for determining the appropriate conditions for crack deflection [41]–[43]. The model developed by He and Hutchinson is well cited and widely known. The model allows one to predict whether a crack propagating in one

material (e.g. the matrix) will deflect at the interface or penetrate into the second material (e.g. the fiber) based on three parameters: the fracture energy of the interface, the Mode I fracture energy of the second material, and a term developed from the elasticity of the two constituents. For elastically similar materials or where the matrix and fiber have similar moduli, their model predicts the ratio of interfacial toughness to fiber toughness need be less than 0.25 to allow for debonding [42]. This value is a good rule of thumb for CMCs designated for high temperature environments where the matrix and fiber are likely to be the same or very similar materials. In the case, where the modulus of the fiber is much greater than the matrix, the ratio predicted by the model is not as restrictive and deflection is more favorable. In other words, for the same fiber, the interfacial toughness can be much higher in a composite where the modulus of the matrix is significantly lower than the modulus of the fiber in order to allow for crack deflection.

The model provides a good starting point for determining what may happen at the interface between two materials or to conclude why a material may have exhibited a specific behavior. The long-standing acceptance of their model attests to its applicability in many cases [42]. However, it has been noted the criteria has difficulty predicting systems where debonding takes place ahead of the crack tip and also in coated fiber composites [3], [44], [45].

2.1.4 Achieving Toughness in Ceramic Matrix Composites

Ceramic materials make ideal candidates for structures exposed to high-temperature, oxidizing environments. Yet, ceramics, because of their lack of intrinsic toughening mechanisms, are very susceptible to failure in the presence of flaws i.e. cracks and voids. In

other words, they are brittle and their brittle nature often restricts their use in most relatively high load-bearing applications when the nature of the load is tensile. Their usage is especially questionable when a human element is involved as catastrophic failure could potentially result in injury or loss of life.

Continuous fiber reinforcement in ceramic matrices has proven to be one of the most effective ways to produce toughness in these materials [2], [39]–[41]. However, in the case of ceramic matrix composites (CMC), where the use of similar constituents (i.e. ceramic fiber and ceramic matrix) is common, understanding the interfacial bond created by fiber and matrix to becomes a critical area for promoting toughness. Often this requires very careful tailoring of the bond otherwise the fiber reinforcement may do little to enhance the toughness of the material. Further complicating this problem is this tailored interface can change due to reactions with the service environment.

There are three types of bonding that can occur at the fiber-matrix interface: chemical, mechanical, and physical [2]. Chemical bonding refers to primary atomic bonding and creates the strongest type of bonding at the interface. Mechanical bonds involve surface fiber roughness and expansions and contractions of the matrix and fiber, which create residual stresses at the interface. Finally, physical bonding refers to weaker secondary bonding.

Strong chemical bonds in conventional CMCs can be created as a result of the high processing temperatures. At these temperatures, diffusion can create a volume between

fiber and matrix with its own material characteristics. If this strong chemical bond is created at the interface in CMCs, the material behaves as a monolithic ceramic and is really no tougher than without reinforcement. On the other extreme, a condition where no chemical bonding takes place, the composite is really no better as matrix is a block of a material with a bunch of holes in it. This of course assumes other means of bonding are also virtually absent. This results in the same brittle behavior. Therefore, adequate care must be taken in tailoring the interfacial strength in order promote toughness in these materials.

Mechanical bonding in CMCs is also an important consideration for achieving toughness. Mechanical bonding is a combination of interface roughness and radially induced stresses. Radially induced stresses are the result of thermal expansions/contractions and interface roughness. Both interface roughness and radially induced stresses can greatly affect the mechanical behavior of the composite. Radial induced stresses can prevent debonding, increase friction, and limit fiber pullout [2]. Interfacial roughness can play a significant role on fracture and fiber sliding at the interface [46]–[48].

At present, there are two prevailing methods for the incorporation of fiber in ceramic matrices. In one method, a stronger bonding condition can exist at the interface and higher level of porosity in the matrix, or weak matrix, promotes toughness [49], [50]. The porosity in the matrix serves as a means to effectively stop crack propagation by relieving the stresses at the crack tip as it encounters these voids in the matrix. The other method involves the use of fiber coating, or interphase, to create a weak interfacial condition

between fiber and matrix [3], [51]–[53]. Unlike, the chemical bond discussed above, the interphase is intentionally placed becoming a discrete volume separating fiber from matrix. The weaker interfacial condition in these composite systems serves to absorb crack energy via crack bridging, crack deflection or meandering, debonding at the interface, and ultimately fiber pullout (see Figure 2). The presence of fiber pullout is often consistent with a weak interfacial bond and is an important fracture energy absorbing mechanism in composite materials [2], [39], [41]. Fiber pullout is generally dictated by the magnitude of the frictional sliding stresses. The lower the friction the longer the crack extends away from the original crack plane before stresses are transferred back from the matrix to the fiber [3].

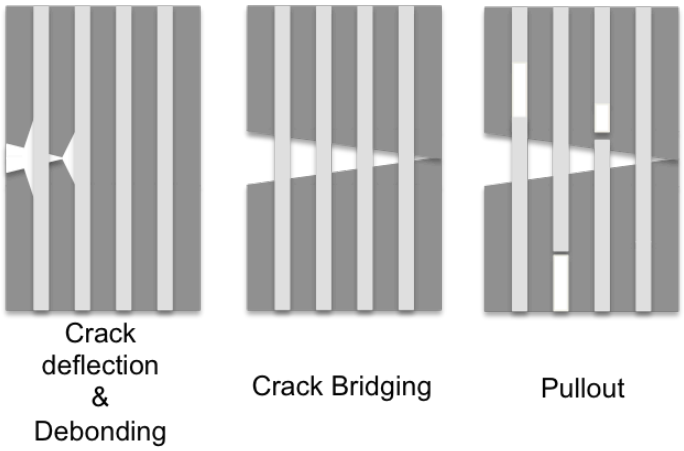

Figure 2: Graphical representation of the various mechanisms that promote toughness in fiber reinforced composites.

There are concerns to creating a weaker interfacial condition with interphase. If the fiber coating creates a very weak bonding condition, stress transfer from the matrix to the fibers via shear is limited. In the case where the mechanical properties of the fiber are much greater than the matrix (i.e. the incorporation of the fiber into the matrix material was

intended to take advantage of the properties of the fiber), an extremely weak bond can severely limit the mechanical properties of the composite, as the magnitude of the shear transfer between the constituent is reduced and thus any gains in toughness may be irrelevant. Therefore, careful tailoring of the bond in these materials where fibers are necessary to provide a reinforcing effect is even more essential.

2.1.5 Interphase Materials

Choosing an appropriate interphase material comes with many considerations. The chemical compatibility with constituents and thermal stability are concerns especially when considering the necessary high temperature processing steps needed in the case of conventional CMCs and the final use temperature of the material. Additionally, the thermal coefficients of expansion (CTE) of all constituents, including the interphase, must be considered. As previously noted, differences in the CTE of each material can alter interfacial conditions through the development of residual stresses [3], [51]. Coating thickness is also important as it can also alleviate residual stresses and also be a route to lower frictional sliding stresses [3], [54]. However, there is a give and take. Thicker coatings can reduce compressive residual stresses and cause increase in surface roughness, while thin coatings can reduce surface roughness and may effect compressive residual stresses very little [3]. Determining which is more important to the toughness of the composite generally requires experimentation. Also previously discussed, the degree of fiber pullout, which is considered a measure of interfacial strength, is highly dependent on these factors at the interface.

Interphase materials are generally applied using gas or liquid-phase techniques. Chemical vapor deposition (CVD) is a common gas-phase technique. Gas phase techniques are best for preforms and helps to avoid problems with bridging of fibers, which is a common issue when using liquid-phase coating techniques. Liquid phase techniques include transporting filaments or tows through a liquid medium or dip-coating the fibers or preforms. These techniques tend to be more economical, but are susceptible to a couple issues. Unless, much care is taken, liquid phase techniques are less precise in achieving constant thickness and could result in bridging of fibers or uneven coverage (see Figure 3). The bridging of fibers can effect infiltration of the matrix, especially when using preforms. Bridging and its subsequent effect on infiltration can definitely negatively affect stress transfer between the fiber and matrix.

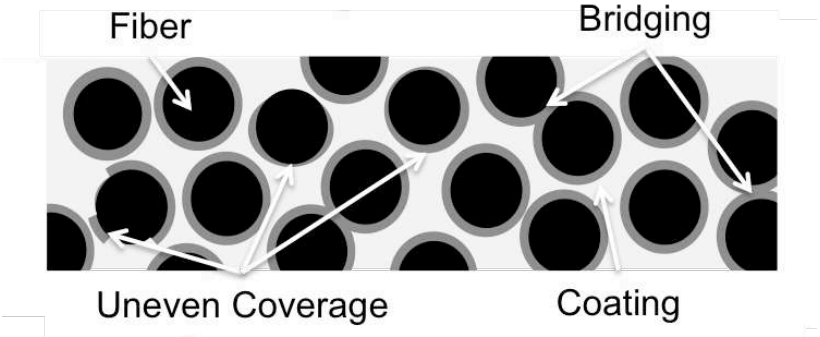

Figure 3: Graphical representation of bridging and uneven coverage of fiber coatings.

The use environment can dictate the type of interphase material one should use. Both carbon and boron nitride are very effective interphase materials for producing toughness in CMCs and have been extensively researched [3], [41], [55]–[62]. Unfortunately, these interphase materials, especially carbon, are not very resistant to oxidation. They are, however, relatively inexpensive and they can serve as model materials to initially test the

effectiveness of weak interface concepts in composite systems that will operate in oxidizing environments.

Creating all-oxide CMCs derived much attention during the last two decades. Many concepts and materials that have high-temperature stability in air have been considered as potential interphases that create a weak-interface condition. One method involves the removal of the coating after fabrication to produce the weak interface desired. This concept is known as a fugitive coating and has shown some promise at producing damage tolerant behavior [24]–[26], [63]–[65]. The most common of these methods utilizes an initial coating of carbon on the fiber although molybdenum has been tried as well [63]. Either through initial processing or additional heat treatment the coating is removed via oxidation creating a gap between fiber and matrix. The method relies on the roughness of the surfaces to provide a means of shear stress transfer between the fiber and matrix. Clearly, too large of a gap and shear stress transfer will be limited, negatively impacting the mechanical properties of the composite.

A very promising interphase material that has been used in CMCs is a rare-earth phosphate mineral, Lanthanum Phosphate ($LaPO_4$), referred to in the literature as monazite. Monazite bonds weakly to other oxides [52], [66], is not toxic, and does not dissolve in water, acids, or bases [67]. In addition, monazite exhibits excellent thermal stability. Its melting point is 2072 °C and it does not easily reduce below 1400 °C [67], [68]. The hardness of monazite is low (5.6 GPa) and the modulus of elasticity is 133 GPa as measured by ultrasonic resonance [66]. The thermochemical compatibility with oxide fibers and effectiveness of

monazite to produce mechanisms that promote toughness, such as crack deflection and fiber pullout, have been demonstrated (see Figure 4) [69]–[73].

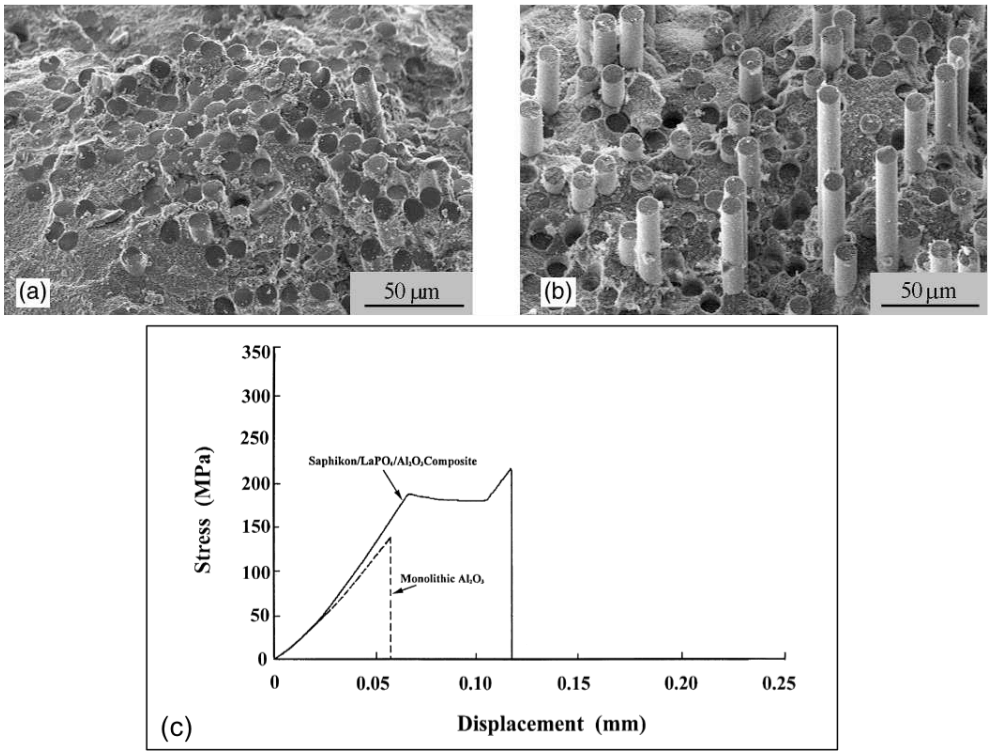

Figure 4: Fracture surface of Nextel 610/alumina matrix composite (a) without and (b) with monazite coated fibers [73]. Pullout in (b) indicates improved toughness. The curves in (c) show stress-strain of monolithic alumina versus saiphkon monazite coated fiber in alumina matrix with only ~1% fiber volume fraction [71].

A whole host of other concepts and materials for interphase have been tried and suggested in the attempt to produce tough, all-oxide CMCs. At what appeared to be the height of coating research in CMCs, these concepts included porous coatings, easy-cleave coatings, ductile coatings, reactive coatings, and interface weakening by segregation [3]. Reference [3] is a good resource for finding out more about the specific materials and their effectiveness in generating greater toughness in CMCs.

2.1.6 Characterization Techniques

Upon conducting a review of the literature on the use of interphase materials in CMCs one will find a small set of techniques commonly used to determine their effectiveness. In general, the techniques used for evaluation of fiber coatings include some type of mechanical testing to demonstrate improved toughness of the material. Often, to understand how the interphase coating is promoting toughness, single fiber tests and/or scanning electron microscopy (SEM) will be used in conjunction with the mechanical testing done on the whole composite.

Generally, whole composite mechanical testing will be done in the tensile configuration with or without a notch. 3-point flexural testing is also fairly common technique used. If such testing is conducted with a notched specimen, the specimens generally have reinforcement in at least two directions, which aids in guiding the propagation of the crack. From these tests authors report on stress-strain curves pointing to relative changes in toughness of samples with and without fiber coatings. As Figure 5 shows, in an ideal case, the introduction of interphase material would shift composite stress-strain behavior from graphic (b) to graphic (a). In the case of testing a notched sample, the sensitivity of the material to the presence of a notch is made by comparing strength and/or the WOF to the composite without a notch. Fracture toughness values of monolithic materials are commonly generated from notched samples, but based on this author's review of the topic the use of notched specimens is a somewhat rare occurrence in the literature involving CMCs with fiber coatings.

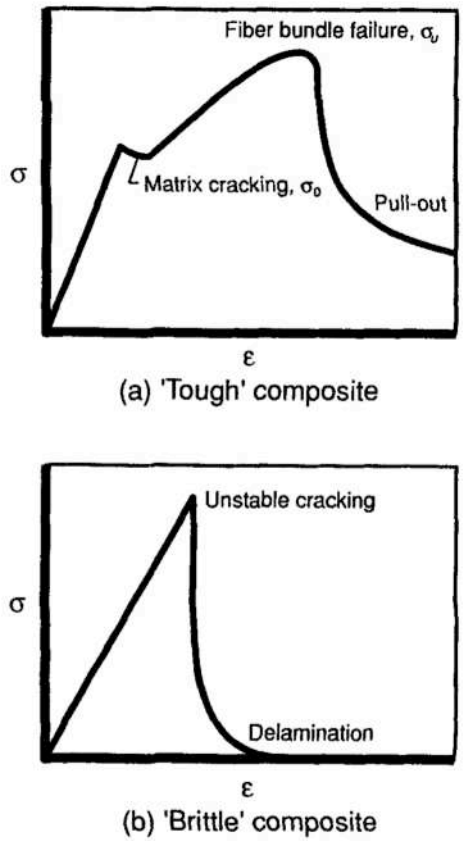

Figure 5: Model stress-strain curves for CMCs that exhibit (a) tough and (b) brittle behavior [74].

Referring back to Figure 5, the evaluation of toughness does not always include an objective value of toughness calculated as the area under the curve, but rather a subjective evaluation of the stress-strain curve for indications of improved toughness. Clearly, one can observe the two curves shown in Figure 5 (assuming the same scale) and qualitatively evaluate that the area under curve (a) is greater than the area under curve (b). However, one must be careful here. Greater area under the curve does not necessarily mean the material is tough because clearly, if curve (a) was simply curve (b) with higher ultimate strength, then it too would also have greater area under the curve. Yet, this does not constitute toughness in the sense being described here. Toughness implies resistance to

failure, or damage tolerance, which usually appears in the stress-strain curve as inelastic deformation, or at least the ability to support load after the initial failure. This is apparent in curve (a). Therefore, an assessment of toughness should include an evaluation of the stress-strain curve along with an evaluation, quantitatively or qualitatively, of the area under the curve. It should also be recognized here that materials like silly putty or bubble gum (extreme examples chosen to demonstrate a point), which would exhibit a lot of plastic strain, have low strength. This still results in a small amount of area under the curve. In other words, just because a material exhibits lots of inelastic deformation this does not mean that it is tough. Such a discussion also returns to the last part of Section 2.1.1 on terminology regarding differences between fracture toughness and toughness. These materials, silly putty and bubble gum would have high fracture toughness because of their ability to plastically blunt crack growth, but they are not considered tough materials because they don't absorb a great deal of energy.

Besides typical mechanical testing techniques, single fiber testing can be used to help evaluate the toughness of a material. The use of single-fiber tests serve to evaluate properties of the interface such as debond energy and friction stress both of which can be used to indicate the ability of the interface to absorb crack energy and promote toughness [44], [73], [75], [76]. The parameters also help infer the strength of the interface. Debond energy is an evaluation of the interfacial toughness, or the force needed to propagate a sharp Mode II crack at the interface [75]. As discussed previously, if the interfacial toughness is too high the fiber and matrix will not deflect at the interface and crack will instead penetrate the fiber. The measure of friction stress is the stress associated with the

sliding of the fiber, and can ultimately dictate the amount of fiber pullout observed[75]. If friction stress, or interfacial friction, is too high, fiber fracture will occur shortly after debonding. Push-in/push-out testing [44], [76]–[82] can be used to acquire one or both of these values and are relatively simple to execute. Fiber pull-out tests can be utilized as well [48], [75].

Often both types of mechanical testing are accompanied by supporting images produced using scanning electron microscopy (SEM), or in some cases, transmission electron spectroscopy (TEM). SEM can be used qualitatively to assess conditions at the interface. Figure 6 is a compilation of images demonstrating the various types of information that can be gathered from its use. The images of Figure 6a and Figure 6b when compared show the effectiveness of the coating to divert an incoming crack in the composite. The image in Figure 6c shows the smooth fibers and the identification of coating on fibers. Figure 6d shows the presence of fiber pullout, which was previously noted as an important measure of interfacial strength.

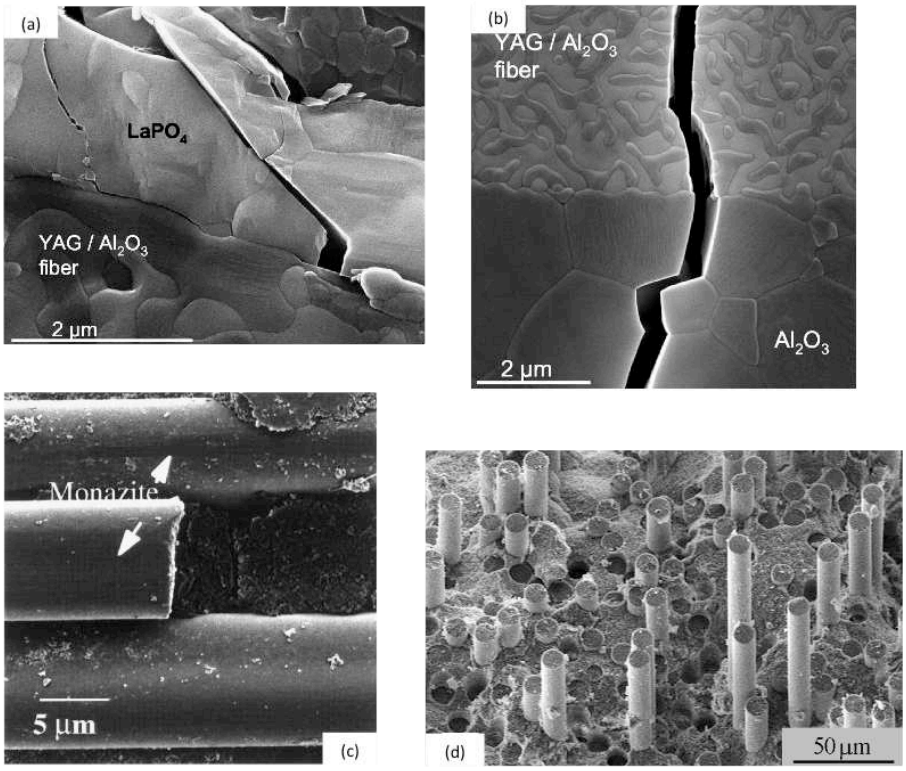

Figure 6: SEM images used to evaluate interfacial conditions and identify mechanisms that promote toughness. (a) Crack deflection at the interface of a sample with fiber coating and (b) lack of crack deflection at the interface in the same fiber-matrix system of an uncoated sample [3]. (c) Surface of fibers indicating the presence of interphase material on the fibers. Relative smoothness of fibers is generally a good indication of the strength of bond at the interface [72]. (d) Fracture surface showing fiber pullout and the presence of fiber sockets indicating fibers likely pulled out and existing on the other fracture surface [73].

2.2 Fiber Reinforced Geopolymers

Fiber-reinforced geoplymers are a relatively new composite material among the "big three:" polymer, metal and ceramic matrix composites. In addition to their attractive thermo-mechanical properties, geopolymer matrix composites (GMC) demonstrate excellent fire resistance [6], [8]. These combined attributes have led to their consideration for aircraft cabin materials, interiors of ships/submarines, and automotive components

[83], [84]. An initial use for GMCs was for high temperature composite tooling [4], [85]. Other important applications could include replacement of heavier metal components in aircraft engines and in other structures subject to temperatures that exclude the use of polymer matrix composites (PMC). The mechanical properties of GMCs even make them a consideration over CMCs for use in these environments because the means of fabrication is more economical [20]. These projected use environments of GMCs, much like CMCs, require the use of thermally stable constituent materials and a means to promote toughness in order to optimize the composite mechanical behavior.

2.2.1 What are geopolymers?

Inorganic polymers, or more specifically geopolymers, are derived from a chemical reaction of an aluminosilicate source with an aqueous alkali solution in highly alkaline conditions[85], [86]. The reaction ends in the formation of a 3-D network of SiO_4 and AlO_4^- tetrahedral linked units which form an amorphous to semi-crystalline structure [85]–[87]. Figure 7 shows the three fundamental oligomer units, all referred to as polysialate for short, that form the inorganic polymer based on Si/Al ratio [85], [87].

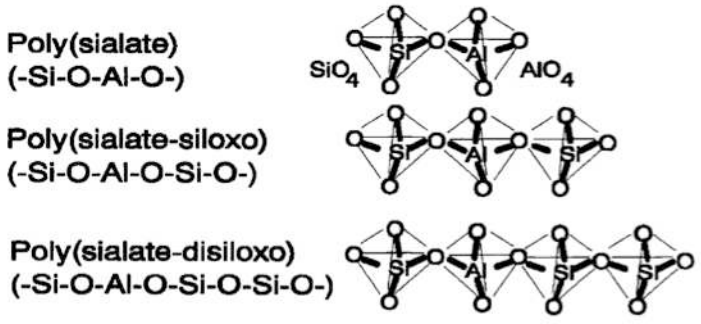

Figure 7: Diagram representing the various polysialate molecular groupings[88]

The formation of the geopolymer, or geopolymerization, is thought to consist of four steps [86], [89]–[91]. The first step, already mentioned above is the dissolution of aluminosilicate source and once this takes place curing of the geopolymer happens relatively quickly. The resulting material is ceramic-like in that it is brittle, hard, chemically resistant, and thermally stable at moderate-to-high temperatures [87], [92].

Unlike ceramics, geopolymers are generally processed at temperatures ranging from room temperature to 120 °C. However, cure time and temperature seem to have an important effect on the resulting mechanical properties of geopolymers. Two studies, one using unreinforced and the other reinforced geopolymers, reported an ideal cure temperature range for producing the best mechanical properties to be close to ~70-75 °C [12], [93]. Cure temperatures at or below these values are found in a majority of the literature. Also, the literature commonly agrees on the use of cure times of 24 hours or greater in a humid environment, which is thought to allow for full reaction of species [88], [94].

The reported mechanical properties of as-cured geopolymers can vary a great deal. In addition to processing parameters, the variation is caused by which source materials (in particular the charge balancing metal alkali, Na or K) are used and the ratio of those materials. The relatively low magnitudes of mechanical properties demonstrated by geopolymers differentiates them from advanced ceramic matrices. The metakaolin-based geopolymer used in this study, MEYEB, created by Pyromeral Systems is a potassium-based geopolymer. The mechanical properties of MEYEB after a 24 hour initial cure at 80 °C

followed by a 650 °C post cure can be found in Table 1 compared against other potassium polysialate geopolymers and also alongside more common matrix materials.

Table 1: Mechanical properties of some inorganic polysialate polymers versus other matrix materials

MECHANICAL PROPERTIES	Inorganic Polysialate Polymers	MEYEB*	LAS** Glass Ceramic	Mullite	Alumina	Epoxy
Tensile Strength (MPa)	3.7	--	100-150	83	250-300	7.6-96.5
Young's Modulus (GPa)	--	--	100.0	143	360-400	0.8-10.0
Compression Strength (MPa)	39-45	98	--	550	3000	13.8-279
Flexure Strength (MPa)	1.7-16.8	11-12	--	170	400	--
Flexural Modulus (GPa)	9.4-10.3	8	--	--	--	--
References	[8], [87], [88], [92], [95], [96]	[38]	[2]	[2], [97]	[2], [97]	[97]

* Values after a 650°C post cure; **Lithium Aluminosilicate

Table 1 highlights a few important facts about geopolymers. The first detail worth noting is the range of strengths displayed by geopolymers. The disparity is the result of different processing conditions and ratios of source materials used in each study. Secondly, the values of strength and modulus of geopolymers indicate a low strain-to-failure and therefore limited toughness much like ceramics. Finally, geopolymers display similar moduli to the best epoxies, which is relatively low compared to the ceramic materials. Geopolymers are truly a unique material, separate from ceramics, given their mechanical properties and structural make-up

2.2.2 Previous work

The first recorded use of the geopolymers as a matrix material occurred in the 1980s by the material's designer, Davidovits, who introduced GMCs as high temperature tooling for use in the plastic and foundry industries [85]. One silicon carbide (SiC) fiber reinforced geopolymer generated from this work demonstrated a formidable flexure strength of 380 MPa and retained strength after exposure to temperatures greater than 650 °C. This and other results spurred on the research generated by other researchers that occurred over the following decade [6], [8], [13], [98]. These pioneering studies generated a great amount of property data on GMCs reinforced with carbon and E-glass fibers.

A series of studies of most importance to the proposed research herein, occurring in the late 2000s, acknowledged the lack of toughness in GMCs with oxide constituents. The referenced works conceptualized and introduced the first studies on GMCs with tailored interfaces such as those widely studied in CMCs [21]–[23], [32], [84], [99]. In addition, these studies continued to focus on the projected use temperatures of GMCs by using oxide fiber and/or subjecting composites to elevated temperatures in excess of 650 °C.

Appearing in the mid-2000s to the present, a handful of studies using mostly carbon and ceramic fibers generated knowledge on the high-temperature stability of GMCs at temperatures from 650 °C to 1400 °C. The studies addressed important concerns related to the retention of mechanical properties, matrix thermal stability, and interactions at the fiber matrix interface at these temperatures [9], [10], [14], [17], [30], [31], [100], [101]. Welter and He et al. explored interactions at the interface with increasing temperature

exposure on basalt and carbon fibers respectively. After thermal exposure in air, Welter noted the creation of a single reaction zone after heating treating past 600 °C to 800 °C and two distinct zones after heating to 1000 °C. These were the result of chemical interaction between the fiber and matrix [30]. Investigating the geopolymer as a potential ceramic precursor, He et al. exposed carbon fiber/geopolymer composites to temperatures up to 1400 °C. Prior to 1100 °C composites demonstrated a drop in their mechanical performance, but then experienced gains after exposure to temperatures between 1100 and 1300 °C. The gains were attributed to completion of the crystallization of the matrix and appropriate interfacial strength between fiber and matrix [9].

Radford et al. and Mills-Brown generated underreported tensile property data on GMCs at room temperature, as well as, during high temperature exposure [14], [17]. To this author's knowledge, Radford et al. has been the only investigation conducted on the long-term exposure of geopolymers to elevated temperatures in order to simulate degradation under service conditions. For SiC_f/geopolymer composites, the authors' reported a substantial decrease in the mechanical strength after 500 hours at 650 °C [17]. The aged specimens, which were also tested at 650 °C, demonstrated a more brittle fracture, but it was uncertain whether this was due to changing properties of the matrix increasing the interlaminar strength or increased interfacial strength between fiber and matrix. Using the same GMC, Mills-Brown did note decreasing tensile strength for the composite when tested at temperatures from ambient up to 760 °C [14], [15].

2.2.3 Important considerations for evaluating GMCs toughness

2.2.3.1 Thermal stability

The survivability of geopolymers at operating temperatures above those of even the most thermally resistant polymers has brought this material significant attention. However, there is much to be understood about the changes that take place in the geopolymer at microstructural level from elevated temperature exposure. The changes clearly have implications for the mechanical behavior of geopolymers. The literature indicates that geopolymers can begin to form crystalline phases in the range of 650-1100°C [34]–[37], [102] and in some cases completely crystallize near the upper range of these temperatures [36], [103], [104]. Recall, prior to this shift the as-cured geopolymer is amorphous to semi-crystalline in structure. The onset of the phase change in geopolymers appears to be dependent on the initial source materials and processing conditions. Thermal stability up to 1400 °C has been noted for geopolymers that have the appropriate balance of starting source materials and are optimally cured [34], [36], [37]. Changes occurring in the geopolymer up until 800 °C are also generally related to dehydroxlyzation and sintering of the geopolymer accompanied by physical shrinkage and densification [34]. Figure 8 shows the changes in the microstructure of a particular potassium-based geopolymer after heat treatment at 300 and 600 °C. Figure 9 shows the evolution of the microstructure that occurs in MEYEB (the geopolymer used in this body of research) at different exposure temperatures. It is clear with increased temperature exposure the particles become more interconnected with total change in the structural appearance

occurring at 870 °C. Prior to this temperature, studies [38], [84] seem to suggest MEYEB to be thermally stable after 650 °C treatment (see Figure 10).

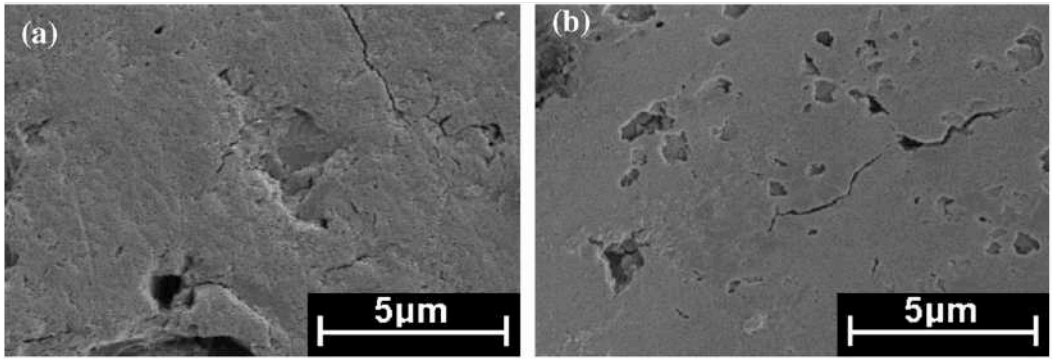

Figure 8: SEM micrographs of geopolymer after heating to (a) 300 °C and (b) 600 °C [34].

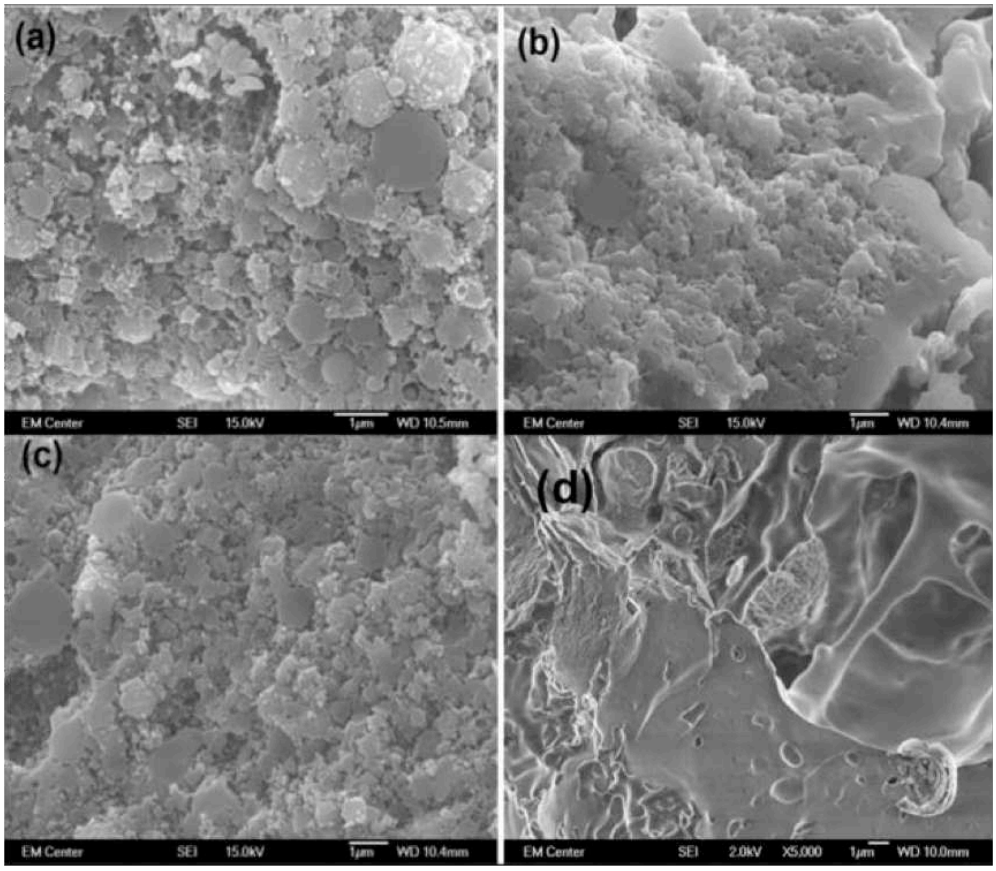

Figure 9. SEM images of MEYEB after (a) initial 24 hour cure at 80 °C then after heat treatment for 5 hours at (b) 250 °C, (c) 650 °C, and (d) 870 °C [38].

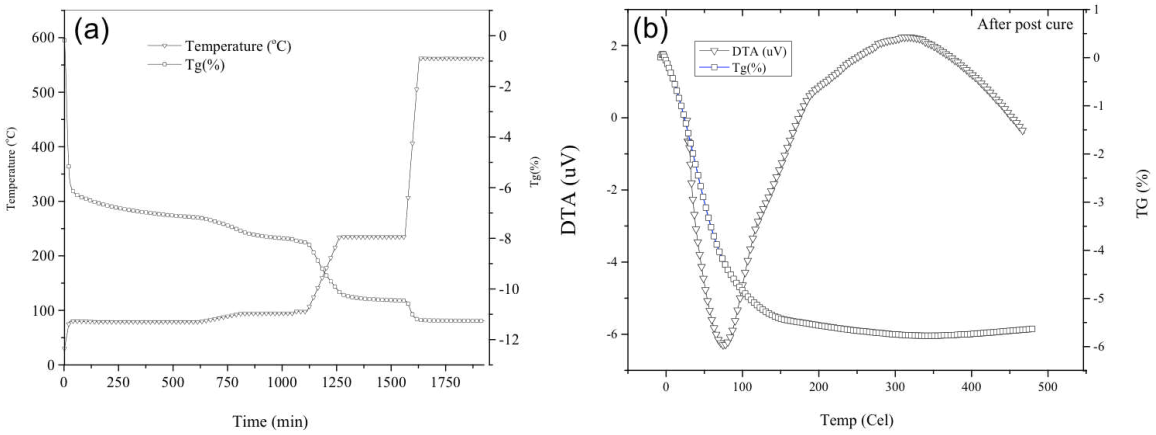

Figure 10: Thermal analysis of MEYEB (a) TGA of MEYEB after 24 hour, 80 °C initial cure (b) TGA and DTA of MEYEB after heat treatment at 650 °C for 5 hours [38]. Note: In (a) the rising curve is temperature.

Despite a good deal of information on changes to the physical nature of the geopolymer in these temperature regimes only a limited amount of information exists on how exposure temperature effects their mechanical properties. Only two known studies have provided a set of mechanical property data on unreinforced geopolymers after exposure to various temperatures [38], [103]. Figure 11 compares the flexural strength results of the two studies. Both show increasing flexural strength of a geopolymer with increased temperature exposure. Note the difference in strengths of the two geopolymers even at low heat treatment temperatures. Lin et al. attribute the significant increase that occurs after 600 °C to densification and crystallization of the geopolymer [103]. Rahman suggests densification for gains in flexural strength after 650 °C, but also reports a loss in the compression strength of the same geopolymer after exposure to 870 °C due to the complete loss of its particle nature (see Figure 8) [38]. These two studies exemplify the variability

between geopolymers, but also indicate that elevated heat treatment temperatures tend to improve their mechanical properties, at least up to a certain point.

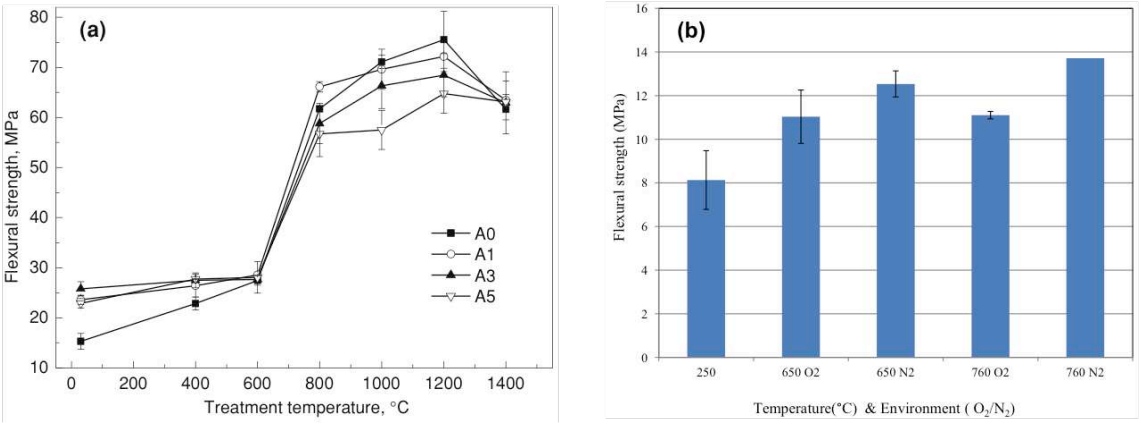

Figure 11: Flexural strengths of two different potassium-based geopolymers after various heat treatments compared. (a) as reported by Lin et al. [103]. (b) as reported by Rahman [38].

Studies characterizing the mechanical effects of elevated temperature exposure on GMCs with continuous reinforcement are also limited. In addition, to those already mentioned under Section 2.2.2, few other studies exist that explore the mechanical effects on GMCs containing oxidation resistant fiber [13], [21], [23], [85]. The work by Davidovits on GMCs revealed differing trends in changes to flexural strength with increasing temperature exposure. Reinforcing fibers, as well as, the type of geopolymer matrix likely played a role in the trends observed. With SiC fabric geopolymer composites, Hammel reports reduced strength and a slight reduction in damage tolerant behavior after exposure to 800 °C. Looking at the group of studies, a case could be made for decreasing flexural strength and toughness for heat treatment temperatures beyond 250 °C, but the results are not definitive. For the study examining interfacial modifications [23], the difficulty arises in separating interfacial effects from changing matrix properties.

2.2.3.2 Strength of the geopolymer

As previously noted in Table 1, the mechanical properties of geopolymers are relatively poor compared to more common ceramic matrices. The low tensile and compressive strengths for the unreinforced geoplymer indicate the matrix is also weak in shear. It's no surprise then that several authors predominately report failures in shear and compression (and/or fiber buckling) during flexural testing of geopolymers [8]–[10], [13], [105]. Even at span-to-depth ratios of 32:1, such as those reported by Welter, the tensile failure mode is usually absent in as-cured GMCs tested in flexure.

The weak nature of the geoplymer can make investigating the strength and toughness of the geoplymer difficult especially when involving interfacial modifications. Gains in strength obtained through careful development and processing of the geopolymer are possible [28], [94], [106] and may help prevent these types of failures in GMCs. A quick review of these sources and Table 1 reveals that further gains in strength are likely limited without an additional second phase to the geopolymer in the form of whiskers or nanoparticulates. As such, the use of different test configurations that reduce the effects of shear such as longer spans, tensile testing, or even four-point flexure should be used. It is also likely that the strength of the interfacial bond played a role in the failures observed for the studies reporting failures in shear and compression.

2.2.3.3 Promoting graceful failure

GMCs generally lack toughness except in systems where the interfacial bonding conditions are likely to be more ideal. These systems usually involve carbon or SiC fibers [8], [13], [16], [18]. However, carbon and even SiC are non-oxides and thus susceptible to oxidation. Given the amount of attention fiber reinforced geopolymers have received its interesting that very little attention has been given to interface evaluation in geopolymers. Most recently, Welter examined interfaces in a basalt fiber GMC indicating a transition of from physical to chemical bonding after exposure temperatures in air after 600 °C and He and Jia noted similar reaction in a carbon fiber GMC after exposure at 1400 °C in non-oxidizing environment [30], [31]. In both cases the composites became more brittle and decreased in strength.

As noted previously, two groups of researchers in the mid-late 2000s indicated that the use of more oxidation resistant fiber reinforcements in geopolymers resulted in reduced toughness [7], [21], [22], [99]. To promote toughness, both groups recognized that weak interface concepts employed through the use of an interphase, such as those studied extensively in CMCs, might be appropriate for GMCs.

In a series of experiments, originating in the Colorado State University Composite Materials, Manufacture, and Structures (CMMS) laboratory, MEYEB geopolymer composites were made with tailored interfaces. A model carbon coating was created on the surface of Nextel fibers, which was intended to create a weaker interfacial bond. The chemical similarity of the alumina-based Nextel fibers and the geopolymer was suspected to be a

worst-case scenario for the interfacial bond between fiber and matrix. Initial results were promising. Results indicated as much as a 50% increase in strength with samples containing the carbon interface, as well as, indications of fiber pullout [21]. Fiber pullout is generally consistent with a weak interface and as noted previously, an important fracture energy absorbing mechanism [2], [39], [41]. An attempt to characterize the interface using short beam shear was conducted, but the specimens did not fail in shear [22]. However, the investigators were unable to directly link improvements to composite strength via the use of interphase. Following these results, additional mechanical characterization was carried out on individual and combined effects of tailored interfaces with matrix fillers in unidirectional GMCs [23], [32]. While results indicated some potential gains in toughness of samples containing a weak interface (changes in interfacial strength evaluated by observing changes in modulus), the results did not clearly indicate the success of the interfacial modifications. At the time, the effect of the matrix fillers on composite strength and toughness was uncertain. It appears, based on a recent study, that some matrix fillers are beneficial to GMC mechanical properties [38]. As for the composites samples with only interfacial tailoring, the fibers with the carbon surface condition demonstrated an unacceptable drop in flexural modulus (as much as 40%) as compared to samples without and did not show any gain in strength [23] (see Figure 12). Another important aspect to note was that processing of the MEYEB matrix in these studies followed manufacturer recommendations and not the optimized cure cycle produced by Rahman and Radford [28] as it was not yet available to these investigators.

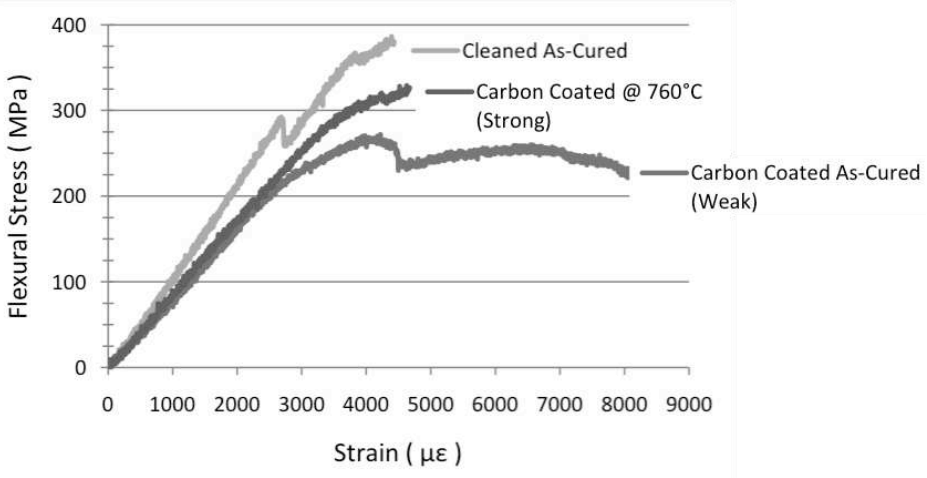

Figure 12: Stress-strain curves of Nextel 610/Geopolymer composites showing comparison between baseline specimen without coating and specimen with carbon interphase before and after heat treatment [23].

The drop in elastic modulus was consistent with a weaker bonding at the interface. In this case, the combination of weak interface and poor mechanical properties of the matrix were detrimental to composite modulus. Ideally, for the weak interface concept to be an appropriate means of toughening GMCs, gains in strength with minimal effects on composite modulus need to be observed.

2.3 Conclusions

The low toughness of the geopolymer without, and often with reinforcement has been established. Like ceramics, geopolymers lack the inherent intrinsic mechanisms to absorb crack energy. For consideration in load bearing applications these materials must display increased damage tolerance and non-catastrophic failure. A portion of the review of the literature summarized in this chapter has focused on applying the interface concepts established for promoting toughness in CMCs to GMCs. The incorporation of continuous fiber has produced the greatest gains in toughness in CMCs. However, careful tailoring of

the interface is often necessary. Without tailoring, the advantages of adding fiber can be lost and cracks still advance unimpeded. A great deal of theoretical models and experimentation has established that a low fracture energy and low friction interface creates the best means of absorbing crack energy. Crack energy is absorbed when mechanisms such as debonding, crack deflection, crack bridging, and fiber pullout are activated by this weak interface. Direct evaluation of the interface using methods like SEM and single fiber push-out are helpful in evaluating conditions at the interface.

The constituents in advanced CMCs generally have relatively high mechanical properties. Therefore, weakening of the interfacial bond does not generally cause significant changes in the mechanical properties of the whole composite. GMCs on the other hand rely greatly on the reinforcement to provide strength and stiffness to the relatively poor mechanical properties of the matrix much like thermoplastic and thermoset matrices do. Manipulating the interface in such systems becomes a unique problem. Attempts to alter the interfacial properties in GMCs have shown promise at improving toughness, but not without the potential for an unacceptable loss in composite modulus. Poor mechanical properties of the matrix were suspected to be one reason for the result. It is important to note that these attempts to improve toughness via the use of interphase did not have the advantage of a properly cured matrix. In these attempts, it was also uncertain how composite mechanical behavior was effected by the changing matrix properties due to elevated temperature exposure.

The temperature range and oxidative environment for GMCs makes their evaluation at relatively high temperatures necessary. As such, methods used to alter the interface to promote toughness must ultimately include the use of non-oxidizing materials. A variety of fiber coatings have proven to be successful in promoting relative degrees of toughness in CMCs. Researchers have reported success with an oxide coating known as monazite. That said, model-coating materials, such as carbon, have been helpful in demonstrating concept viability in both CMCs and GMCs.

Stress-strain curves generated from mechanical testing are often very helpful to determine the effectiveness of the coatings ability to improve toughness in the system. However, for geopolymers the weakness of the matrix can make shear failure a predominant failure mode thus potentially skewing interpretation of toughness gains. Attempts to reduce effects of shear using longer support spans in 3-point flexure or different test methods such as 4-point flexure or tensile testing would theoretically help.

Overall the review has the built the framework for the hypothesis of this research. As matter of convenience the hypothesis is restated following sentence in the same form as it was in Chapter 1. It is hypothesized that through the use of fiber coatings, continuous fiber reinforced geopolymer matrix composites can demonstrate improved toughness, while still retaining high degrees of strength and modulus even after exposure to elevated temperatures. The investigation of the hypothesis relies on linking the interfacial properties to improvements in toughness in GMCs as this has yet to be established in the research involving GMCs with fiber coatings. Furthermore, the experimental program of

these previous studies included a number of variables that made establishing this link difficult. Therefore, the GMCs of this research utilize a single fiber type and a state of the matrix for which properties are known. To observe for changes in toughness based on interfacial conditions GMCs are fabricated with different fiber surface conditions. A total of three fiber surface conditions are used: cleaned or uncoated, carbon coated, and monazite coated. Each GMC is subjected to elevated temperature exposure as this also important for the investigation of the hypothesis. 4-point flexural and tensile tests are conducted to establish measures for the mechanical behavior of each of the GMCs. Since it was established that the geopolymer is weak in shear and also that most flexural testing of geopolymers results in shear failure these particular test methods were chosen to limit the effects of shear on composite behavior. Short beam shear and single fiber push-out tests are conducted to establish interface properties, which will provide the linkage needed to address the hypothesis. Furthermore, microscopy methods are employed to examine fracture surfaces and push-out specimen surfaces to aid in drawing conclusions about the strength of interface and potential for the activation of crack energy absorbing mechanisms.

Chapter 3: Materials and Processing

All of the materials used in this investigation and the techniques used for processing geopolymer matrix composite (GMC) samples are addressed in the current chapter. The discussion will include details about the specific inorganic geopolymer used in this study. Properties and characteristics of the reinforcing fiber, as well as, the modifications to fiber surfaces will also be discussed in this chapter. Finally, the fabrication process will be discussed in full detail covering preparation of materials, details of processing, and final heat treatments. All additional or specific steps necessary for preparing specimens for testing will be covered in separate experimental sections in following chapters.

3.1 Matrix

The particular inorganic polymer used in this research goes by the trade name MEYEB. MEYEB was developed by Pyromeral Systems Inc. and is a research grade material not sold commercially. MEYEB is a potassium (K^+) charge balanced polysialate (PS) geopolymer derived from proprietary proportions of potassium silicate, aluminum oxide, silicon dioxide, aluminum phosphate, and water [19]. MEYEB shares many of the characteristics typical of geopolymers: non-ignitable, non-flammable, non-toxic, light weight, and fire resistant [19]. The starting materials and ratios used to create geopolymers dictate whether the structural make-up is more cementaceous or polymeric in nature [4]. MEYEB is polymeric. Only recently, properties of cured, unreinforced MEYEB were made available

as part of doctoral research. The mechanical and physical properties of MEYEB can be found in Table 2 and Table 3.

Table 2: Mechanical Properties of MEYEB* at various temperatures[28], [38]

Processing Temperature (°C)	Compressive Strength** (MPa)	Compressive Modulus (GPa)	Flexural Strength** (MPa)	Flexural Modulus** (GPa)	Fracture Toughness** (MPa√m)
80	52 - 61	12.43	--	--	--
250	70 - 88	---	6.9 - 9.5	4.1 - 5.6	0.23
650	92 - 105	20.63	9.8 - 13.0	7.4 - 8.7	0.42
760	102 - 132	--	11.0 - 13.5	9.5 - 11.6	0.53
870	67 - 77	--	--	--	--

*Properties are for MEYEB processed on optimum cure schedule as described in cited references
**Value or range of values is only an approximation of actual

Table 3: Physical Properties of MEYEB[19], [38]

	Density (g/cc)	CTE, linear (μm/m•°C) @ 100-600°C	Relative Density after 500°C
MEYEB	1.85	4.20	~96%

In addition to the tabulated data, thermal analysis of MEYEB revealed a majority of weight loss occurring prior to 300 °C and the after 650 °C [38]. The author reports on an increasing density past 300 °C indicating a temperature regime where the material undergoes increased densification [28], [38]. In additional to specific measurements this was validated via examination of microstructure. Microstructural examination of MEYEB at 250 °C and 650 °C revealed a slight reduction in the particulate nature of the microstructure and with heat treatments above 870 °C this particulate nature was completely eliminated (refer to Figure 9) [28], [38].

The MEYEB matrix is prepared by mixing proprietary liquid and powder components. The resin system consists of MEYEB resin and MEYEB hardener which, when mixed at a ratio of 5:1 and cured, produces a predominantly amorphous, potassium based polysialate [19]. After thoroughly mixing the components, it is stored at -25 °C to prevent polycondensation, which occurs relatively quickly at room temperature [19]. All samples used in the investigations described in subsequent chapters were fabricated within one day of the preparing the MEYEB resin. The only exception to this statement applies to composite samples prepared for the preliminary investigations (see Chapter 4).

3.2 Fiber and Fiber Surfaces

3.2.1 Unidirectional Nextel 610 fiber

The 3M™ Nextel™ 610 fiber roving is the reinforcing fiber for all composites in this study. Physical and mechanical properties of the Nextel 610 fiber can be found in Table 4.

Table 4: Properties of 3M Nextel 610 fibers[107]

	Tensile Strength (MPa)	Tensile Modulus (GPa)	Filament Diameter (μm)	Density (g/cc)	CTE (μm/m•°C) @ 100-1100°	Chemical Composition
Nextel 610 Filament	3100	380	10-12	3.9	8.0	>99% Al_2O_3

The metal oxide fiber, which is essentially pure alumina (Al_2O_3) can be used at temperatures up to 1200 °C with minimal strength degradation and is dimensionally stable [107]. In order to study the effect of interphase on the toughening of geopolymer matrix composites, the Nextel 610 (N610) fibers used are modified from their as-received condition prior to fabrication. All composites referenced throughout this document should

be assumed to contain the Nextel 610 fiber except when otherwise noted. Only one of the two preliminary studies used composites with a different reinforcing fiber. That fiber and its associated properties will be discussed in Chapter 4.

3.2.2 Fiber surfaces: Cleaned (CL)

The Nextel fiber is shipped with a sizing in order to protect it from damage during handling. The sizing on the fiber is 100% organic and mostly composed of poly-vinyl alcohol [107]. The as-received fibers are an off-white color and look very similar after the sizing has been removed. The cleaned (CL) fiber surface is the baseline condition of this study. It is so because the chemically similarity of the two constituents (fiber and geopolymer matrix) is expected to provide a worst-case scenario: strong bonding at the interface and a fairly brittle composite. Previous work and experimentation has suggested such conditions to exist [21]–[23]. To achieve the cleaned fiber surface small groups of fiber tows are placed in an oven, heated to 700 °C at 5 °C/min in air and held at temperature for 25 minutes prior to cooling to room temperature. The procedure closely follows the parameters set by the manufacture for removal of the sizing [107].

3.2.3 Fiber surfaces: carbon coated

Sizing on fibers is sometimes removed prior to composite fabrication; however, it has been found that the PVA sizing can be converted to a form of carbon through pyrolysis in inert environment [21], [22]. The new surface, which will be hereafter referred to as carbon coated (CC), is expected to create a weaker bond between fiber and matrix. It is one of two different fiber surfaces intended to demonstrate the effectiveness of interphase on toughening of geopolymer matrix composites. The CC fiber surface is achieved in a very

similar manner to that of the CL fiber surface, but fiber tows are heat treated in an inert environment. To create the inert environment, the oven chamber is evacuated and filled with nitrogen to roughly 85 Torr greater than atmospheric pressure. The chamber is evacuated and refilled two additional times. This is all done prior to 300 °C. For the remainder of the heating, hold, and cool down cycle the pressure is maintained between ~730 Torr and 780 Torr.

Like the removal of sizing on the fiber under oxidizing conditions, it is anticipated that the carbon coating will likely be removed or degraded in the GMC after heat treatment of composite samples in air above 400 °C. The loss of the carbon coating in the GMC creates two possibilities. First, this could result in a "gap" between fiber and matrix resulting in another weak interfacial condition. This is referred to as a fugitive coating and was discussed in Chapter 2. It should be understood that gap will likely be very small and no more than 100 nm in thickness. The specifications supplied by the manufacturer suggest this is the average thickness of the sizing when applied to the fibers. The other possibility is that the loss of the carbon coating will enhance the bond as diffusion occurs between the fiber and matrix. This condition is more likely. Evidence of such effects have already been reported in the previous studies involving very similar GMCs [21], [23].

3.2.4 Fiber surfaces: Monazite ($LaPO_4$) coating

Nextel 610 fibers coated with lanthanum phosphate ($LaPO_4$), or monazite (MZ) as it is referred to in most of the CMC literature, are expected to create a weak interfacial condition in the geopolymer matrix composites and therefore produce greater toughness in composite samples. Monazite coating is a part of a family of coatings known as weak oxide-

oxide [3]. Monazite is reported to be stable with alumina fibers up to 1550 °C and using proper processing techniques can be applied without causing strength degradation to the fiber [108], [109].

Monazite coated fiber was supplied by the Air Force Research Labs (AFRL) Structural Materials Division at Wright-Patterson Air Force Base (WPAFB). Figure 13 shows an SEM image of Nextel fibers coated with monazite. Note the porous structure of the coating.

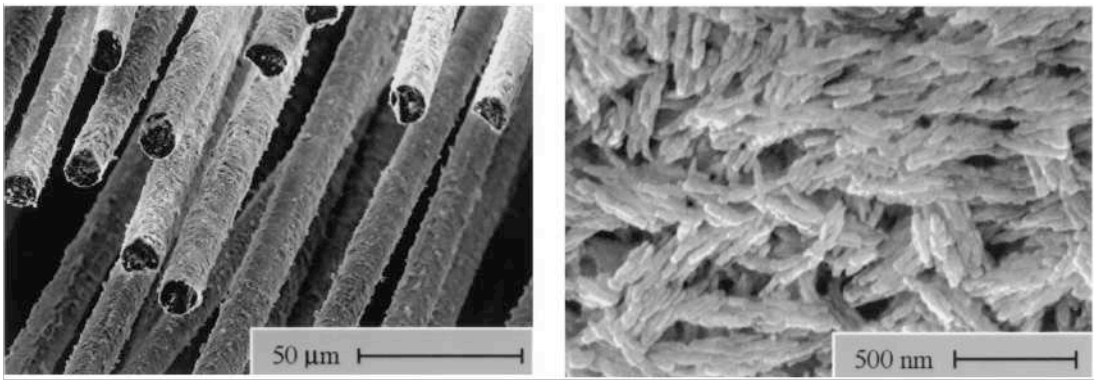

Figure 13: Monazite coated fibers[73].

The fiber was coated using a patented vertical coating system and method. The thickness of the coating was likely close to 500 nm based on the number of passes that yielded the best results for fiber strength [109]. This is approximately five times larger the carbon coated fibers. The precursor, collodial rhabdophane particles, were formed in water from lanthanum nitrate and phosphoric acid [109]. Prior to the fibers being coated the sizing was removed. Further details of the procedure for coating fiber tows can be found elsewhere [109]–[112]. Figure 14 shows the three different modified fiber surfaces.

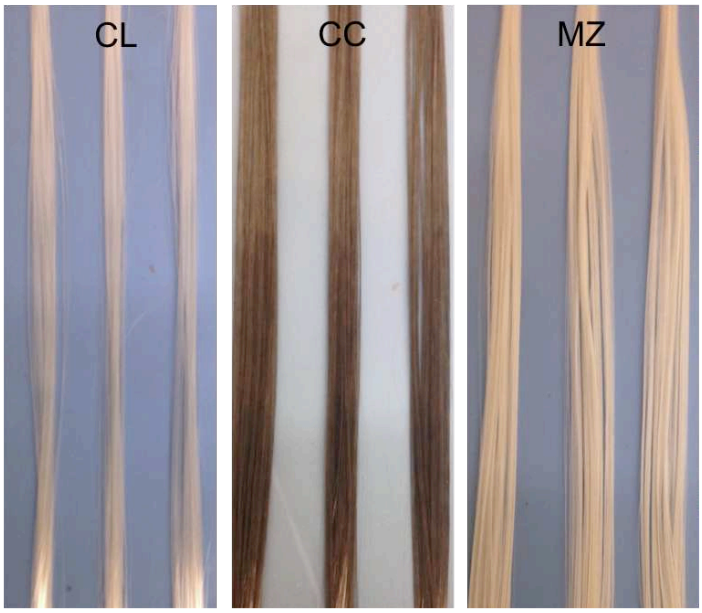

Figure 14: The effect of surface modification on Nextel 610 color: cleaned (CL), carbon coated (CC), and monazite coated (MZ).

3.3 Specimen Fabrication

3.3.1 Composite Fabrication

The MEYEB resin was removed from storage, stirred, and then poured onto a premeasured number of tows to achieve a 50% volume fraction. The fibers were wet out using hand lay-up techniques (Figure 15a & b). The wetted fiber tows were then placed in the cavities of an acetal mold designed to create samples with a rectangular cross-section (Figure 15c).

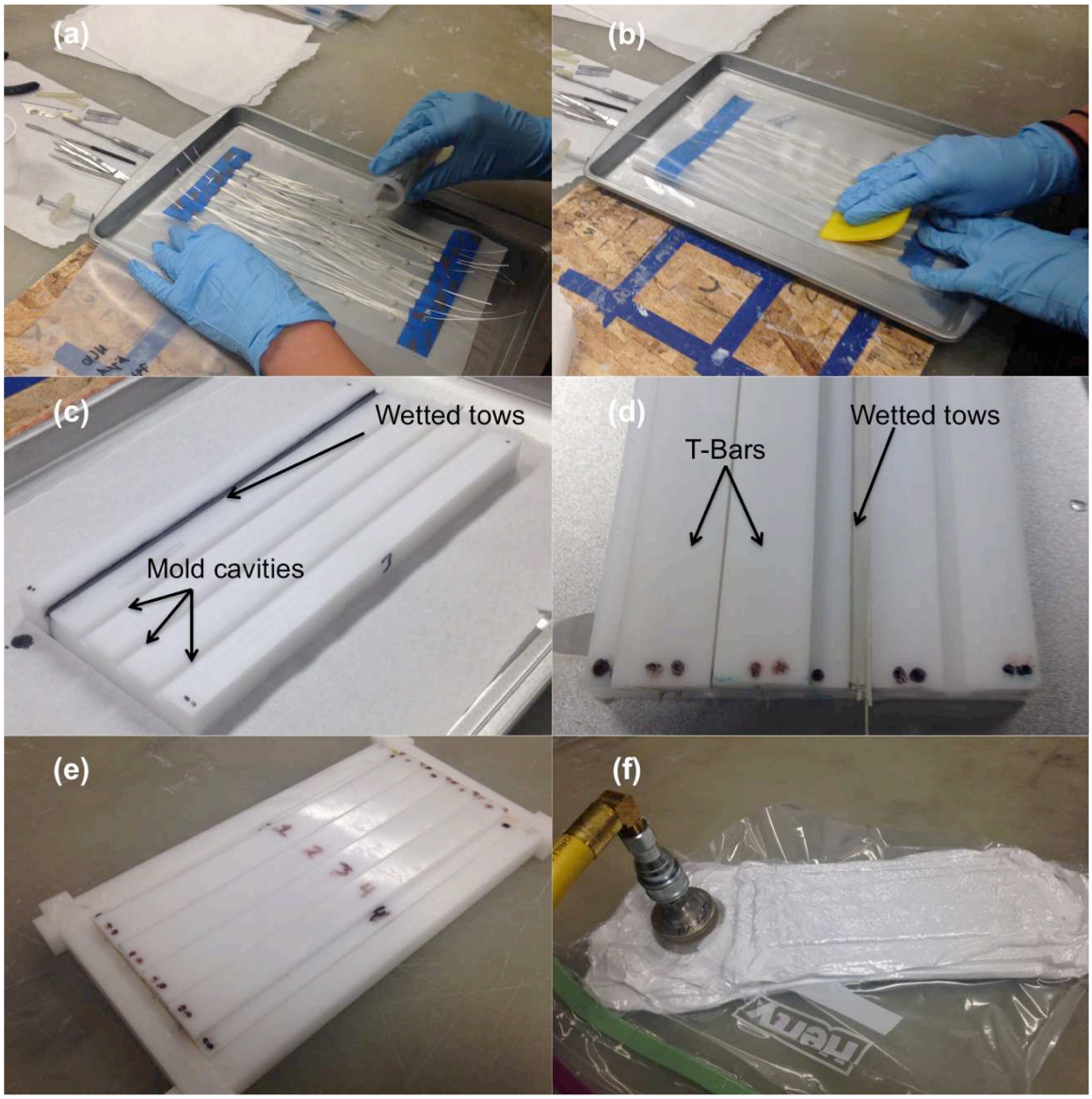

Figure 15: Processing steps using acetal multi-cavity mold

After placing the T-bars in the cavities (Figure 15d), the complete mold assembly (Figure 15e) was placed in an evacuated bag for four minutes to draw out excess resin and removed entrapped air (Figure 15f). The limited time under vacuum was to prevent moisture loss. Premature loss of humidity was previously shown to compromise the geopolymer structural properties [28], [38]. After the four minutes, the vacuum was

compromised and the mold assembly was transferred to a different bag. Before sealing the new bag, an ice cube was added to the bag to provide additional moisture content. The mold assembly was then moved to a hot press where heat and pressure were applied. The applied pressure was required to close the die to a fixed stop, generating constant cross-section dimensions. The temperature was programed to rise from room temperature at ~1 °C/min to 80 °C. After three hours at 80 °C in the hot press, the bagged, acetal mold was removed and placed an oven at 80 °C for 21 more hours to achieve a total initial cure time of 24 hours. Recall, this procedure was developed in a cure optimization study [28], [38] and results in a matrix with properties shown in Table 2. Using a 24-hour cure of the composite specimens in the primary investigation ensures the final cure state of the MEYEB matrix is in a form already documented in the aforementioned studies. After this initial 80 °C cure, the bag was vented to atmosphere, T-bars were removed, and the mold assembly remained at 80 °C for up to an additional 24 hour drying period before beginning the follow-on post cure. All composite samples of the primary investigation were produced in this manner.

Following the initial cure and drying period at 80°C, the mold was heated to 100 °C at 0.5 °C/min, held for 20 minutes and then ramped to 120 °C at 1 °C /min and held for 1 hour. The slow heating procedure was used to prevent rapid loss of remaining water to avoid internal damage to the composite. The samples were then removed from the mold while it was still hot. This more readily facilitated removal, given the differential CTE of the mold and the composite.

The resulting molded sample sticks created for flexure testing were nominally 203 mm (length) x 4.5 mm (width) x 1.5 mm (thickness). The sample sticks created to produce tensile test coupons were only 1.0 mm in thickness. All other dimensions were the same. Different thicknesses were achieved by using T-bars with different "T-leg" thicknesses. Upon removal, each sample was immediately placed back in the oven at 120 °C. Samples were then ramped at 5 °C/min up to 250 °C and subjected to a free-standing post cure for five hours at this temperature in air. After this step, samples were allowed to cool to room temperature and then heat treated for an additional five hours at 650 °C. The heating procedures closely follow the those optimized for MEYEB [28], [38]. Samples were either heat treated at 650 °C in air or at 650 °C in N_2.

The reason for the inert environment is to compare and contrast the effects of an oxidizing environment on each fiber coating type. Achieving the non-oxidizing environment for heat treating composite samples was accomplished in the same manner described for achieving the inert environment for converting sizing on fibers to carbon. For both air and inert environments, samples were ramped from room temperature to 650 °C at 5 °C/min.

After heat treatment, sample sticks were sanded to remove any flash produced during specimen processing. Generally, sample types will be referred to in shorthand notation throughout the remainder of this document. Table 5 gives the abbreviations of sample types, which indicates the fiber surface condition and final heat treatment environment.

Table 5: Shorthand notation for designating composite sample types

Shorthand Notation	Fiber Surface	Post Heat Treatment Environment
CL(A)	Cleaned	Air
CL(N)	Cleaned	Nitrogen
CC(A)	Carbon coated	Air
CC(N)	Carbon coated	Nitrogen
MZ(A)	Monazite	Air
MZ(N)	Monazite	Nitrogen

3.3.2 Unreinforced MEYEB

All unreinforced MEYEB specimens were fabricated in a manner similar to those produced in a prior study [28], [38] in order to provide for comparison. After preparation and removal from cold storage, the MEYEB resin was degassed to remove entrapped air that could create large voids in the cured material. To degass the resin was placed in a vacuum dessicator. To prevent premature polycondensation of the geopolymer, it was only placed in the dessicator for short periods of time, generally 3 to 5 minutes, and then returned to cold storage for about the same amount of time. Following degassing, the resin was poured into the designated mold. Once the mold cavities were filled with MEYEB, the resin was subjected to further degassing to remove the entrapped air that resulted from the transfer of the MEYEB resin into the molds. Once again, the MEYEB was moved back and forth between the dessicator and cold storage. Upon completion of degassing, the molds remained upright and were enclosed in an air-tight plastic bag and transferred to an oven. Additional moisture was added to each plastic bag in the form of an ice cube as was done for composite samples. The exact same cure cycle that was used on the composite

specimens was also used for the unreinforced specimens. It only varied from composite specimens in two ways. First, the cure for the unreinforced material did not involve putting the molds under additional pressure. Secondly, the unreinforced material was only heat treated in an air environment.

Two different mold types were used in processing the unreinforced material. This was done in order to produce cylindrical specimens and prismatic specimens for compression and flexural strength mechanical testing respectively. The molds used to create unreinforced specimens were also made of acetal. The mold used to produce cylindrical specimens were hollow acetal tubes that produced a final diameter of 6 mm (see the bottom right of Figure 16).

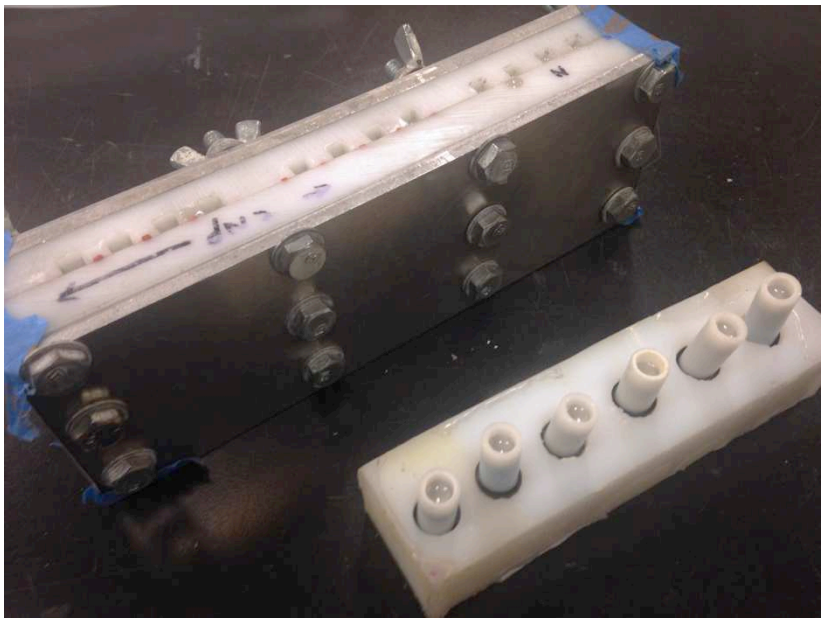

Figure 16: Molds used to produce unreinforced MEYEB samples. Picture shows molds filled with the uncured MEYEB resin.

Multiple cylindrical molds were used to produce individual specimens for compression testing. The molds were of slightly different lengths. Specimens were lightly sanded on both ends to produce two parallel, right angle surfaces. Specimens varied in length from ~15.5 mm to 19.5 mm. Cylindrical samples are shown next to the prismatic samples in Figure 17.

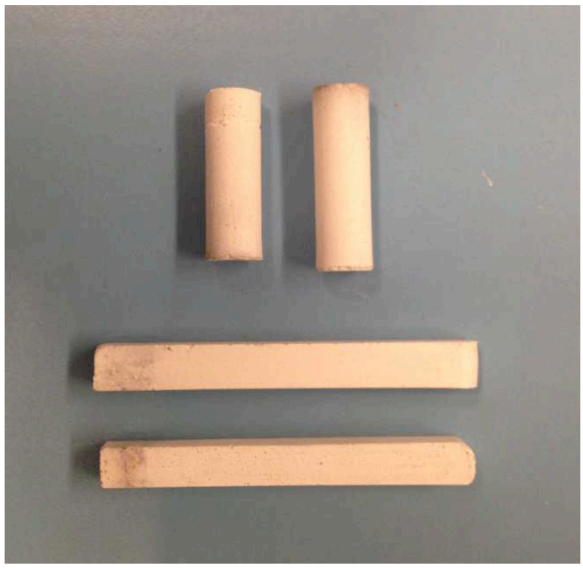

Figure 17: Unreinforced, cured MEYEB cylindrical and prismatic samples

The mold used to create unreinforced flexural samples is shown in the upper left corner of Figure 16. Samples were nominally 5 mm (depth) x 5.5 mm (width) x 45 mm (length) after removal from the mold. Samples were subjected to additional sanding to produce parallelism and remove any taper creating the final shape of specimens. Final dimensions of each specimen after sanding were nominally 4.25 mm (depth) x 4.25 mm (width) x 45 mm (length).

3.4 Thermal Aging

Some unreinforced and fiber reinforced MEYEB samples were designated for additional thermal aging beyond the baseline 5 hour heat treatment at 650 °C. Total exposure times of 50 hours and 500 hours at 650 °C were chosen to simulate general service conditions in order to evaluate the effects of long-term temperature exposure in an oxidizing environment. Unreinforced samples were not exposed to the intermediate aging duration of 50 hours.

To do this, samples were once again placed in a high temperature furnace at 650 °C. Samples were ramped from room temperature to 650 °C at 5 °C/min. The samples were then held at this temperature for an extended period of time to reach a total exposure time at 650 °C of 50 or 500 hours. Limitations of machine and personnel prevented achieving 500 hours without dropping back down to lower temperatures. To reach a total of 500 hours samples cooled until the machine dwell time could be reset. Upon resetting the program, the temperature was allowed to rise at 5 °C/min back up to 650 °C. The furnace had to be reset at least two times in order for samples to achieve a total exposure time of 500 hours.

Chapter 4: Preliminary Investigations

Two preliminary studies were conducted to investigate the influence of cure time on composite mechanical response and the initial use of 3M Nextel monazite coated fiber in a geopolymer matrix. The two studies will be referred to hereafter as "cure time study" and "monazite coated fiber study" for short. These studies sought to examine the influence of these factors on the mechanical response of composite specimens specifically evaluating changes in toughness. The cure time study originated as a result of the research already discussed in Chapter 2 and 3, which revealed changing mechanical properties of the geopolymer, MEYEB, when subjected to various initial cure times. Also recall, from Chapter 2 that studies revealed a detrimental effect on the modulus of geopolymer matrix composites that incorporated an interphase material. These preliminary investigations were conducted on the premise of demonstrating the appropriateness of weak interface concepts in geopolymer matrix composites (GMC) for improving toughness.

4.1 Materials and Processing

4.1.1 Matrix

The matrix material used in these studies was still the liquid inorganic polysialate polymer resin system, MEYEB, discussed in Chapter 3. However, the material used in these preliminary studies differs from the one used in the primary studies in a couple of ways. First, the resin system was not received in its different parts, but instead was mixed and

shipped in a cryogenic state from the manufacturer. The material remained in cold storage at -25 °C except when being used to process samples. Secondly, as a result of its premixed state, the material was used over an entire ten-week period from the time it was received. This differs from all other samples, which were processed using resin that was no more than a day old.

4.1.2 Fibers

Two fiber types were used in these preliminary investigations. The reinforcing fibers of the cure time study were Nextel 610 unidirectional fiber tows. In the same manner discussed in Chapter 3, the Nextel 610 (N610) fiber was modified from its as-received condition to create cleaned (CL) and carbon coated fiber surfaces (CC). For the monazite coated fiber study, Nextel 720 (N720) unidirectional fiber tow was used. At the time this study was conducted, only monazite coated N720 was available. Properties of the N720 fiber can be found in Table 6. Note the lower tensile strength and modulus as compared N610 fibers (see Table 4). Like the N610, the N720 fiber surface was modified to create CL and monazite (MZ) coated fiber surfaces. The Air Force Research Labs (AFRL) Structural Materials Division at Wright-Patterson Air Force Base (WPAFB) supplied the uncoated and monazite coated N720 fibers. As noted in Chapter 3, the procedures for producing MZ coated fibers can be found elsewhere [109]–[112].

Table 6: Properties of 3M Nextel 720 fibers[107]

	Tensile Strength (MPa)	Tensile Modulus (GPa)	Filament Diameter (μm)	Density (g/cc)	CTE (μm/m•°C) @ 100-1100°	Chemical Composition
Nextel 720 Filament	2100	260	10-12	3.4	6.0	85% Al_20_3 15% SiO_2

4.1.3 Fabrication

Fabrication of composite samples for these studies occurred in a very similar manner to those discussed in Chapter 3 with only a few minor differences. In these preliminary investigations, a steel mold was used for fabrication instead of one made of acetal (see Figure 18).

Figure 18: Steel Multi-Cavity Mold

To facilitate removal of specimens from the steel mold, the mold surfaces had to be pretreated with a release agent prior to placing the wetted fiber. The release agent used was Frekote NC-770. Additionally, time under vacuum in the mold was around three minutes rather than four. The resulting molded samples were nominally 203 mm (length) x 7.5 mm (width) x 2.5 mm (thickness). Recall samples produced from the acetal mold were 4.5 mm in width and 1.5 mm in thickness. The width and thickness dimensions of each mold type (acetal and steel) maintain the three-to-one ratio suggested by ASTM C1341 [113].

The cure times and final heat treatments for the specimens in these preliminary studies also differed slightly from the primary study. For the cure time study two different initial cure times were used. The N610 composite samples of this investigation were either cured at 80 °C for one or five hours. All N720 composite samples were cured for five hours at 80 °C. The N610 composites samples with CL fiber surfaces were heat treated in air at 650 °C, while composites containing CC fiber surfaces were heat treated in an inert environment at 650 °C for five hours. All N720 composite sample were heat treated in air at 650 °C for 5 hours. Procedures for creating the inert environment for N610 carbon coated samples are the same as those covered in Chapter 3.

4.2 Test Procedures and Calculations

All mechanical testing was conducted in 3-point flexure in accordance with ASTM C1341, except as noted. Specimens were tested at a displacement rate of 2.5 mm/min. The support span of the test fixture was 60 mm producing a roughly 24:1 span-to-depth ratio for samples. Loading was ceased when specimens experienced more than a 20% drop in load or demonstrated no change in load carrying capability upon further displacement. Load as a function of time was recorded for each test. Prior to the start of testing, a compliance calibration was conducted using a steel beam of similar dimensions to the composite specimens to enable compensation for the machine compliance and determine a corrected mid-span displacement from time and crosshead rate.

Flexural strength (S_u), flexural modulus (E), and toughness (U_T) of specimens were calculated using the following relationships from ASTM C1341 and ASTM C1275 [113], [114]:

$$S_u = \frac{3P_u L}{2bd^2} \tag{4.1}$$

$$E = \frac{L^3 m}{4bd^3} \tag{4.2}$$

$$U_T = \int_0^{\epsilon_f} \sigma \, d\epsilon \tag{4.3}$$

where P_u is maximum force recorded, L is the support span, b is the width of the specimen, d is the thickness of the specimen, m is the slope of the linear portion of the force-deflection curve, σ is the stress in the outer surface fibers, ϵ is the strain in the outer surface fibers, and ϵ_f is the strain at failure. Per ASTM C1341, failure was determined to be the force when test specimens split into two separate halves or when force dropped by 20% or more [113].

Measurements for strength and modulus were averaged within each set of specimens tested. The error bars on graphs indicate one standard deviation. The measured fiber volume fractions of N610 cleaned fiber and carbon coated fiber specimens ranged from ~48-52% and ~43-45%, respectively. The values of modulus for the study involving N610 composite specimens were normalized to a 45% fiber volume fraction (V_f) for purposes of

comparison. The measured fiber volume fractions of N720 specimens with the cleaned fiber surface ranged from ~42-46% and the N720 monazite fiber specimens from 39-41%. The moduli of N720 specimens were normalized to 40%. The strengths of the specimens were not normalized since a material's strength is very sensitive to the state of the microstructure.

4.3 Cure Time Study: Results and Discussion

4.3.1 Matrix cure state and composite mechanical properties

The flexural moduli of composite samples are compared in Figure 19. Using reported values for MEYEB and Nextel 610 fibers, a simple Rule of Mixtures (RoM) calculation yields a unidirectional composite modulus of ~171-175 GPa for a 45% fiber volume fraction [38], [107]. (The range of composite modulus values accounts for the range of possible matrix modulus values based on cure state as previously reported [28], [38].) The data contained in the study on MEYEB might even suggest it could be as high as 182 GPa using the value for compressive modulus [38]. However, for the purposes of this investigation, the smaller range will be used. To simplify reporting of percent variation from RoM, a mean value of RoM predicted modulus of 173 GPa is used. A RoM value is an estimate of the highest value of composite modulus that can be achieved assuming a perfect bond between the fiber and matrix. Thus, the variation from the RoM can give some information about the relative fiber-matrix bond strength for the experimental specimens. For the 1- and 5-hour cleaned specimens the resulting moduli are approximately 85% and 81% of the modulus predicted by RoM, respectively. The average modulus of the carbon coated specimens cured for 1

hour (CC_1hr) is 47% of that predicted by RoM and the average modulus for the carbon coated specimens cured for 5 hours (CC_5hr) is much higher, at 77% of the RoM generated value.

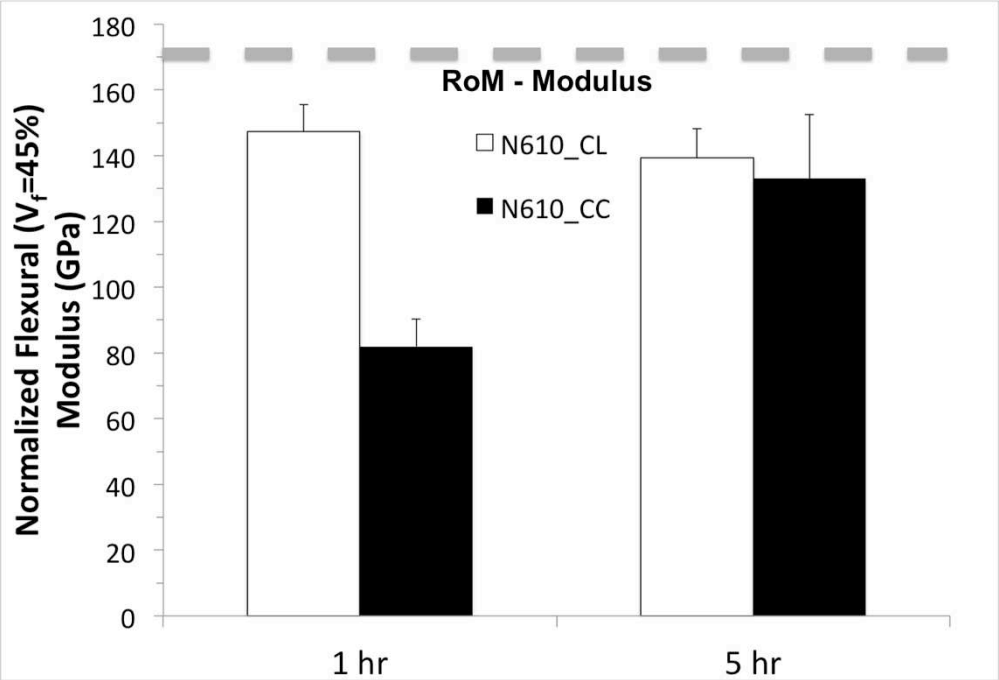

Figure 19: Flexural moduli (Normalized to V_f=45%) of CL and CC specimens compared based on initial cure time.

Based on the data presented in Figure 19, the effect of fiber surface condition on the measured geopolymer matrix composite flexural modulus is sensitive to the initial cure time. N610 cleaned specimens appear to be mostly unaffected by the longer duration cure. In stark contrast, the additional 4 hours of initial 80 °C hydrated cure time has a significant influence on the resulting flexural modulus of the carbon coated specimens. The increase for CC_5hr specimens is 60% over those specimens cured for just one hour. The extended cure brings the modulus of CC_5hr specimens very close to the values measured in specimens with the cleaned fiber surface condition. A two-tailed t-test indicates no

statistical significance in the modulus data between cleaned specimens cured for 1 hour (CL_1hr), cleaned specimens cured for 5 hours (CL_5hr), and CC_5hr specimens. This is important as it suggests that the decrease in modulus previously noted in the carbon interphase composites is more directly related to the geopolymer matrix state of cure and not to an inherent limitation of the stress transfer imposed by the carbon coating.

The average flexural strength of composite samples is shown in Figure 20. In the same manner as modulus, the strength of N610 cleaned specimens shows little sensitivity to changes in initial cure time, but once again, carbon coated specimens show a strong response to initial cure time. The average strength of CC_1hr specimens is relatively low compared to all other sample types, while the CC_5hr samples have strengths effectively equal to those of the cleaned fiber specimens. The strength of the carbon coated fiber specimens cured at 80 °C for 5-hours is over 150% greater than those cured for 1-hour.

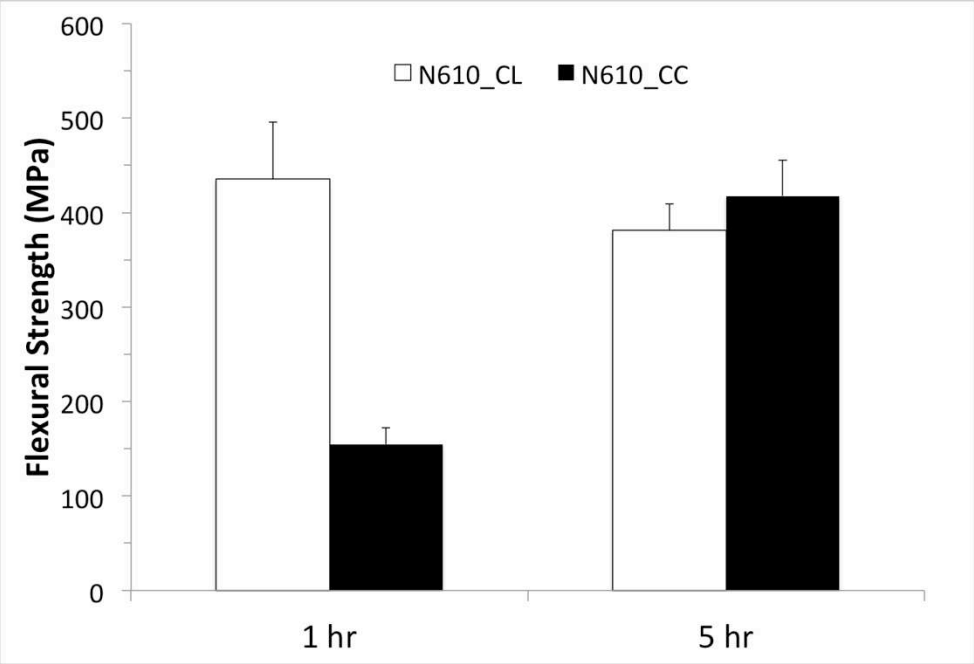

Figure 20: Flexural strengths of CL and CC specimens compared based on initial cure time.

The average modulus and strength of N610 cleaned samples is consistent with other reported values of unidirectional Nextel 610/geopolymer samples [10], [23]. As already noted, cleaned sample types also appear to show no sensitivity to initial cure time. The lack of discernible difference in the modulus of cleaned samples with different initial cure times makes sense in the case of a stronger interfacial bond. The increase in flexural modulus of the neat MEYEB matrix from a 1-hour to 5-hour cure is unknown; however, based on reported modulus data, measured in compression, it cannot be much more than 3 GPa [38]. Recall, the modulus of the Nextel 610 fiber is 380 GPa. A RoM calculation, which infers perfect load transfer between fiber and matrix, would not predict a significant change in the modulus of the overall composite even for the changes in modulus of the neat geopolymer related to cure time [19]. The measured moduli for CL_1hr and CL_5hr specimens in this study support this conclusion.

That said, there was a significant change in the measured modulus and strength of N610 carbon coated specimens exposed to the two different initial cure times. The lower modulus and strength of CC_1hr specimens was not unexpected as this was similar to values previously reported for Nextel 610/MEYEB composites [23]. As already noted, the drop in modulus was anticipated for the modified interfaces in Nextel 610/MEYEB composites, but the amount of decrease was unexpected and also undesirable. In carbon coated specimens, the extended initial cure time resulted in an increased composite modulus. An improved composite modulus in these specimens suggests that shear stress transfer from matrix to fiber was altered through the extended initial 80 °C cure. The changing moduli of carbon coated composite specimens in response to cure state of the

matrix, and the effect on the interface, confirms an important aspect of the use of interphases in GMCs. The large difference between the moduli of the constituents in GMCs, unlike those encountered in advanced CMCs, means that toughening GMCs through weakened interface concepts involves the added challenge of balancing shear stress transfer with the creation of energy dissipating mechanisms. This increase in shear stress transfer in CC_5hr specimens could be the result of an improved mechanical interaction at the interface, related to increased cure shrinkage and possibly to a larger coefficient of thermal expansion of the matrix. These changes in the matrix with extended cure time, which would contribute to larger radial compressive stresses at the interface, have been documented in recent studies involving the MEYEB matrix [28], [38].

The improvements measured in the strength of the carbon coated specimens are also most likely related to improved mechanical interaction, but the effect of cure time on the mechanical properties of the neat matrix seems to also be an important aspect. A study involving unidirectional Nextel 610/MEYEB composite specimens with carbon coating, reported little or no gain in strength and a large decrease in modulus for specimens with carbon coating [23]. This was surprising. Numerous studies indicated improvements to the strength of brittle matrix composites using weak interface concepts by preventing early failure of fiber bundles [3], [41], [115]. Additionally, other research reported, a 50% increase in flexural strength in MEYEB composite specimens cured for 1-hour made with carbon coated woven Nextel 440 fiber versus those made with cleaned fiber [21]. The authors attributed the increase in flexural strength to the ability of the modified interface to control crack propagation. This evidence along with the results of the current

investigation seem to reveal that the flexural strength exhibited by N610 CC_1hr specimens is the result of limited shear resistance of the matrix from insufficient cure. This is made clear by examining the load state the woven Nextel 440/MEYEB and unidirectional Nextel 610/MEYEB composites are exposed to in flexure. All other things being equal, in a woven configuration with Nextel 440 fiber, a composite would fail at a much lower force than a unidirectional Nextel 610 composite (compare Table 4 to Table 7). This also means that a woven Nextel 440 composite specimen experiences much lower shear stresses than a unidirectional Nextel 610 specimen.

Table 7: Properties of 3M Nextel 440 fibers[107]

	Tensile Strength (MPa)	Tensile Modulus (GPa)	Filament Diameter (μm)	Chemical Composition
Nextel 440 filament	2000	190	10-12	70% Al_2O_3 28% SiO_2 2% B_2O_3

Therefore, the loading condition that produced failure in these Nextel 440/MEYEB composites was not high enough to cause early shear failure of the fiber-matrix interface. Thus, the positive effects of the coated fiber on the mechanical behavior of composite specimens were observed, even though the MEYEB had only been cured for 1 hour.

The current results indicate cure state of the matrix and the interfacial conditions are key factors affecting the shear resistance of these composites. The N610 CC_1hr specimens show relatively poor flexural strength, but this is not the case for the N610 CL_1hr despite the same cure state of the matrix. Cleaned fiber specimens exhibited mixed-mode failures (see Figure 21a). Only shear failure was only observed in carbon coated sample types. In

CC_5hr specimens it is also possible the specimens failed in flexure, but the crack quickly diverted along planes parallel to the fiber making it difficult to observe (see Figure 21b). Furthermore, CC_1hr specimens were the only ones that showed a very small amount of deformation on the compression surface where specimens came into contact with the loading nose (see Figure 22).

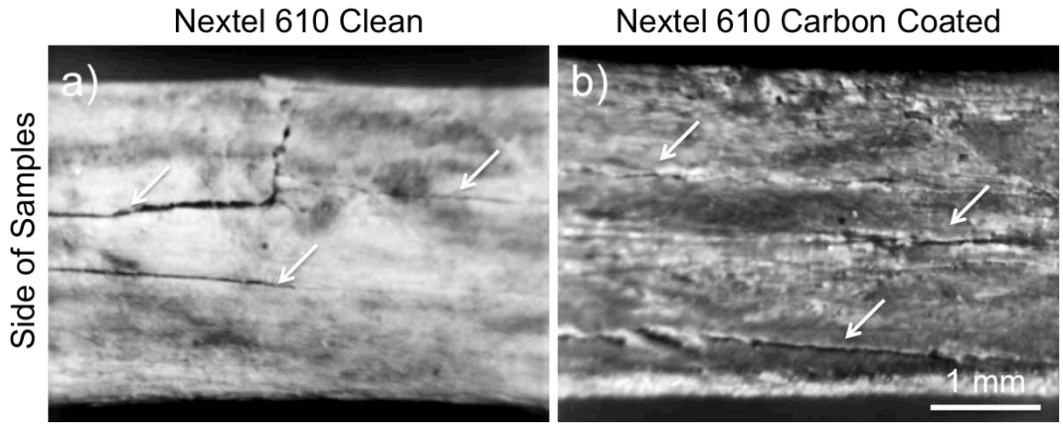

Figure 21: Representative images of damage observed in Nextel 610 clean and carbon coated composites. Images a) and b) are shown with the tensile surface at the top of the image. Fibers run left to right on the page. The white arrows indicate visible areas of shear damage.

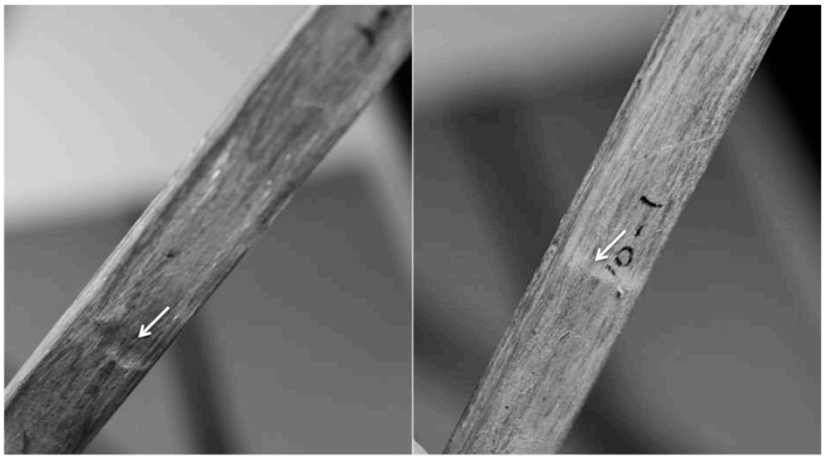

Figure 22: Damage incurred on compressive surface of CC_1hr specimens during 3-point flexural testing. Arrows indicate areas of deformation

This damage is believed to be directly related to lower matrix properties associated with the shorter 80 °C hydrated cure period. Recall, the MEYEB matrix is known to have increased compressive strength with extended hydrated cure. The reported data suggest a roughly 30 MPa increase in strength of the matrix from a 1- to 5-hour cure [28]. The increased matrix strength explains the lack of damage on CC_5hr specimens. However, the loading nose damage also has to be associated with interface conditions because CL_1hr specimens did not exhibit this damage. It appears that the low strength of the matrix and poor bonding conditions in CC_1hr specimens make it more likely for compression buckling of the fibers to occur. This explains not only the small amount of deformation on surfaces of these specimens, but also the relatively poor flexural strength exhibited by them. It is also possible that if damage did occur relatively early during the loading of the specimen, this may have affected the calculated modulus for CC_1hr specimens.

4.3.2 Improved Damage Tolerance with Modified Interface

While the previous sections have shown substantial changes in the modulus and strength of the Nextel 610 reinforced MEYEB with initial cure temperature, the principal goal of this study is to investigate the potential for improved toughness through the use of interphase. In fact, this is the first study to have done so using a more optimal initial cure. Figure 23 shows representative stress-strain curves of each specimen type. The stress-strain profiles from flexure testing reveal an immediate difference between those composites with the carbon interphase and those without. The 1hr results are consistent with the results of previous studies, showing substantially reduced modulus for the carbon coated fiber specimens. However, in combination with a more complete 5 hour cure, the carbon interphase shows much greater promise. The stress-strain curves of cleaned fiber

reinforced composite specimens are linear-elastic until failure, while the carbon coated Nextel 610 specimens have a non-linear region prior to peak stress.

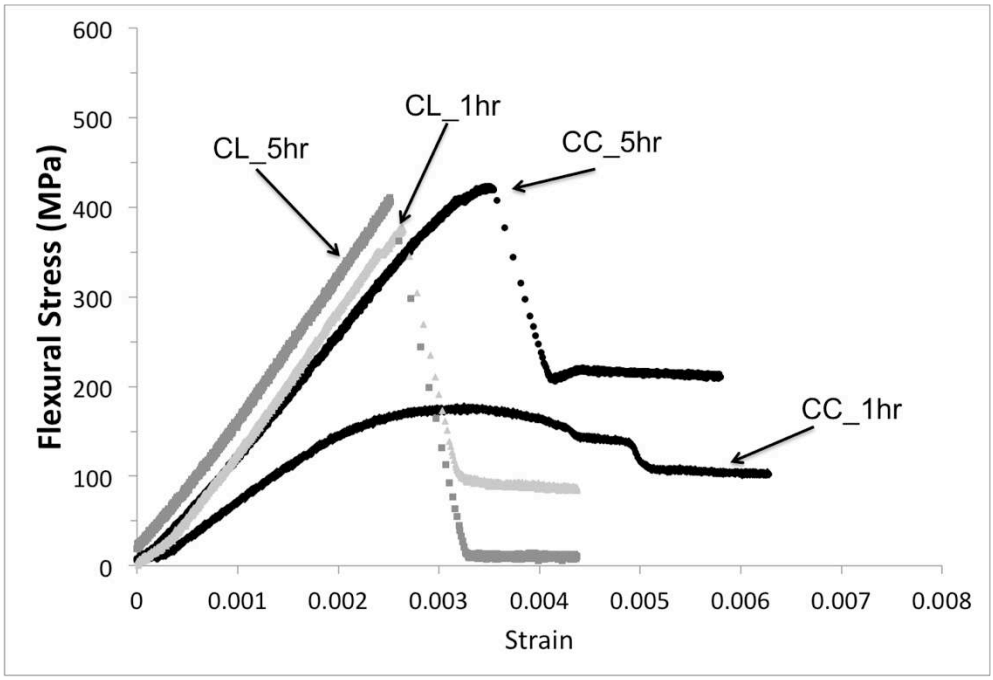

Figure 23: Representative stress-strain curves of Nextel 610 cleaned and carbon coated fiber composite specimens in flexure with differing initial cure times.

The non-elastic deformation observed in carbon coated Nextel 610 reinforced specimens is clearly a result of altered interfacial conditions, as it is not observed in cleaned specimens. The non-linear behavior prior to peak stress is consistent with the concept that the carbon coating is creating a weakened interfacial condition allowing for the deflection of cracks and the prevention of damage to the fiber [74], [116]. The more limited load drop after initial failure and the lack of catastrophic failure in the carbon coated samples also points to a weakened interface condition allowing a greater ability of these composites to dissipate fracture energy. Both this and the non-elastic deformation displayed by carbon coated samples leads to an increased area under the stress-strain curve, suggesting

improved toughness. Using Equation 4.3 to calculate this increased area, and thus an increased energy absorbed at fracture, confirms this conclusion (see Figure 24). The increase in toughness, as measured by area under the stress-strain curve, for the CC_5hr specimens over the CC_1hr specimens is ~76%. The toughness of the CC_5hr specimens over cleaned specimen types is ≥40%.

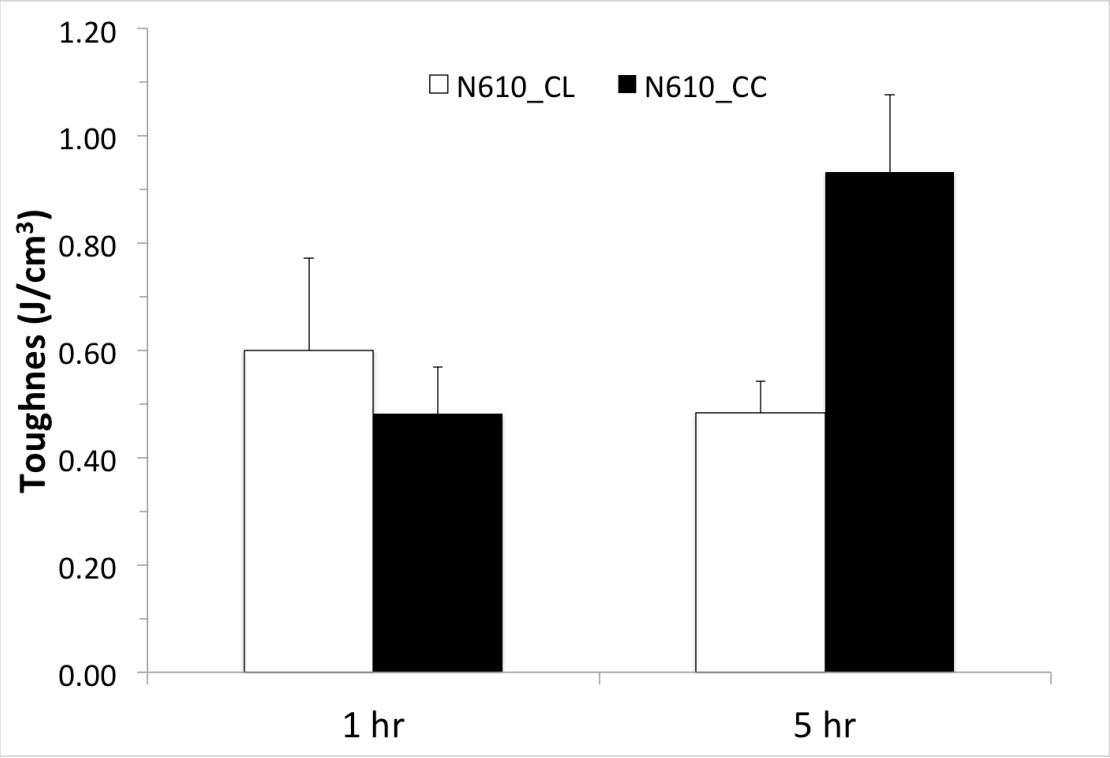

Figure 24: Toughness of composite samples with differing initial cure times as calculated from Equation 4.3

Recall these toughness values do not account for any area under the stress-strain curve beyond a 20% drop in max strength. This follows the stated method of defining failure in ASTM C1341. Especially in the case of CC_1hr specimens, it is uncertain whether the resulting shapes of the curves past peak stress were a result of the interfacial conditions activating the crack defeating mechanism or just inherent weakness of the matrix.

Regardless, the consistent ability of carbon coated specimens to fail non-catastrophically is a positive outcome in terms of damage tolerance (see Figure 25). In the same figure, it can be observed that some 1- and 5-hour cleaned specimens also demonstrate an ability to carry some reduced percentage of their max loading condition after initial failure. This seems to suggest low shear resistance of the matrix since in all other ways the profiles of these specimens were different than the specimens with carbon interphase. It is possible that it could be the result of debonding at the interface due to stress concentrations created at created at the tip of the Mode I crack in these specimens. The criteria of He and Hutchinson[42] might suggest this is the case (see also Chapter, Section 2.1.3) . However, if this is the case, clearly the interface in CL specimens is not as beneficial to composite toughness in the same way as the interface is in CC_5hr specimens.

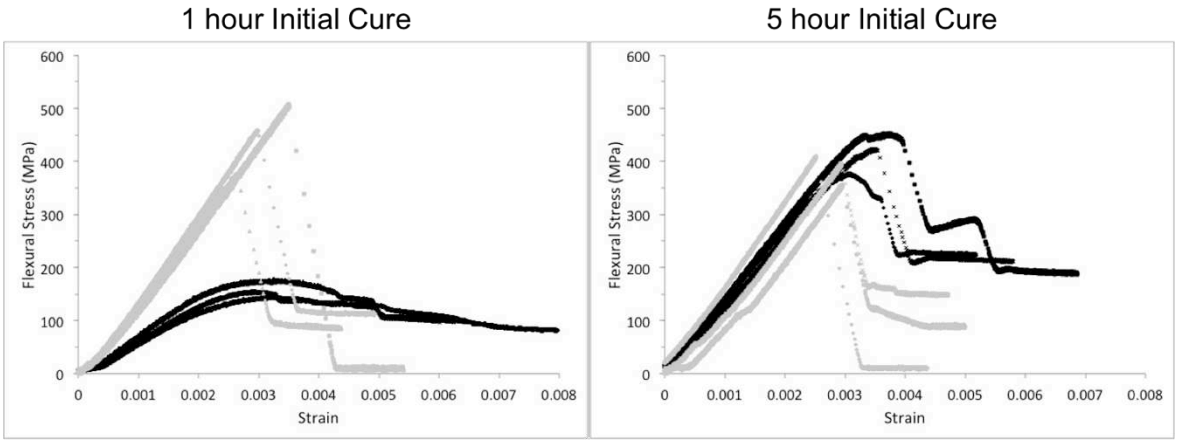

Figure 25: Stress-strain curves of Nextel 610 cleaned (gray) and carbon coated (black) specimens

Comparing the stress-strain profiles of the CC_1hr to the CC_5hr specimens, the damage tolerant behavior exhibited by each is fairly similar up to peak load. However, beyond the peak load, the two sample types differ considerably. The CC_1hr specimen curve shows a gradual decline from peak load rather than an abrupt load drop like the CC_5hr and even

the cleaned sample types. Clearly, such behavior is influenced by the cure state of the matrix and possibly even more directly related to its effect on interfacial conditions. The comparison of CC_1hr and CC_5hr curves also highlights the large difference in modulus and strength of these specimens. With these differences in mind it is important to recognize that combination of the increase in mechanical properties of CC_5hr specimens and region of non-elastic deformation results in large gains in area under the stress-strain curve which is commonly related directly to toughening.

The concept of weak interfacial conditions, attained through the incorporation of an interphase material, promoting toughness by the development of shear-dominated failures is observed in carbon coated specimens (Figure 21). As noted previously, it appears that both weakness in the matrix and interfacial strength limit the shear resistance of the CC_1hr specimens leading to unacceptable reductions in flexural modulus and strength. Thus, it now seems clear that the toughness benefits related to the modified interfacial condition is only realized when these Nextel 610 reinforced MEYEB matrix composites are subjected to a longer duration initial cure.

4.4 Monazite Coated Fiber Study: Results and Discussion

The following sections describe the results of the preliminary evaluation of a monazite interphase in a GMC as tested in 3-point flexure, which utilized Nextel 720 (N720) as the fiber reinforcement. Measures of strength and modulus are presented along with stress-strain profiles of samples tested in flexure. These are reviewed and discussed along with images that capture the damage produced in specimens from flexure testing.

4.4.1 Effect of MZ coating on mechanical properties

The average modulus of each composite is shown in Figure 26. The measured values are very close to the theoretical value of 104 GPa predicted from RoM approximation using the reported properties of both MEYEB and Nextel 720 fiber [38], [107]. The result is not completely unexpected in light of evidence provided by the cure time investigation. These composite samples were also cured for 5 hours. The coating type, MZ as opposed to CC, might also be a factor influencing this behavior. In fact, research with MZ in ceramic matrix composites seems to suggest the MZ does not create a weak interfacial bond between coating and matrix, but instead acts as a weak interface by failing within itself and/or failing at the fiber-coating interface [66], [73], [117]. Both mechanisms have been suggested. Regardless, the data indicates that in the current state of the matrix the use of the monazite fiber coating on Nextel 720 samples does not alter the shear transfer mechanism when compared to the CL samples. This is a positive outcome of this study, demonstrating once again that interphase can be used without a significant loss in composite modulus.

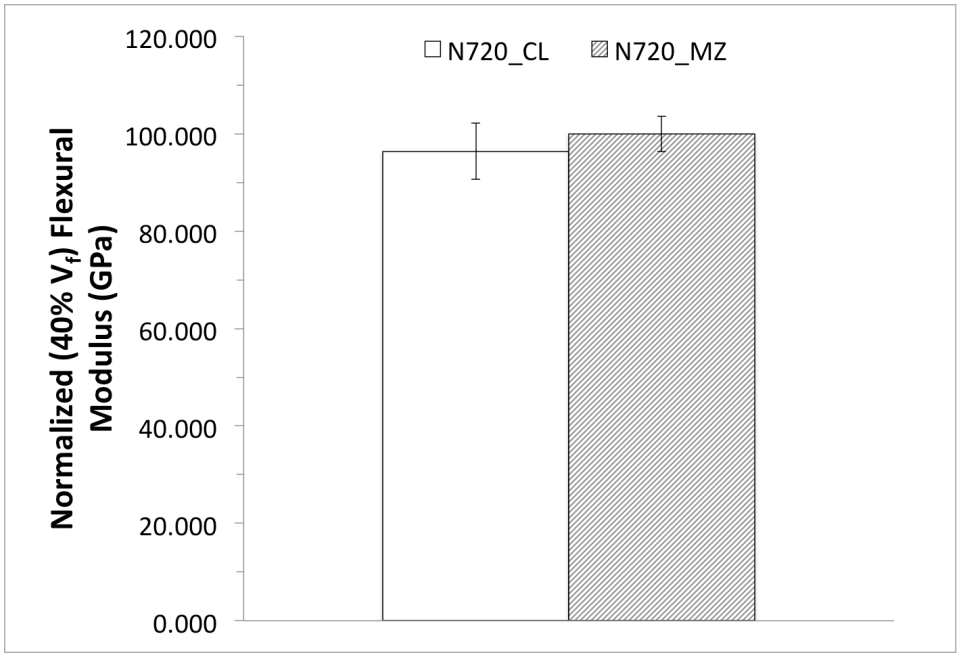

Figure 26: Flexural moduli of N720_CL and N720_MZ specimens compared (Normalized to V_f = 40%)

Figure 27 compares the average strengths of CL and MZ specimens. On average, the strength of N720 composites increased by ~26 % with the use of monazite coated fibers. Such an increase was not observed with CC samples in the cure time study. The increase suggests the interphase material is dissipating crack energy and delaying failure to fibers. Recall, this increase was also demonstrated after the composite specimen had been exposed to an oxidizing environment. This was expected based on the oxidation resistant nature of the coating. The finding is important for the application of GMCs in structures where oxidation resistance is needed.

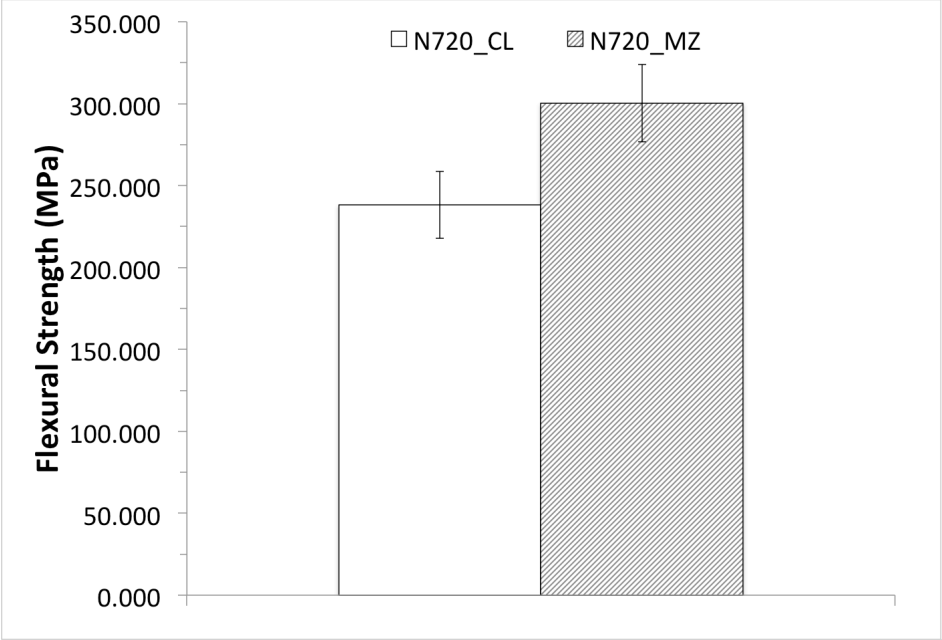

Figure 27: Flexural strengths of N720_CL and N720_MZ specimens compared

4.4.2 Monazite coating for improved toughness in GMCs

Figure 28 shows the resulting stress-strain profiles of N720 samples tested in flexure. All samples appear to display linear-elastic behavior up to failure. It was thought that MZ samples might display some inelastic behavior prior to failure like the CC specimens from the cure time study, which would be another indicator of possible crack energy dissipating mechanisms at work such as crack bridging and debonding at the interface. The obvious difference between sample curves is that the MZ samples do not fail catastrophically, but rather demonstrate an ability to maintain a greater percentage of the maximum load, relative to CL samples, after initial failure. This behavior could be the result of the MZ coating failing at the interface and thus preventing cracks from propagating through fiber bundles, but in any case, results in a greater area under the stress-strain curve, which is indicative of improved toughness. Without any change to the modulus of N720 monazite

specimens relative to clean specimens, the increased strength of monazite specimens also means increased area under the curve and thus increased toughness. Yet there seems to be only minor indications that these specimens demonstrated any inelastic deformation prior to failure. This could be due to the method of measuring mid-span displacement.

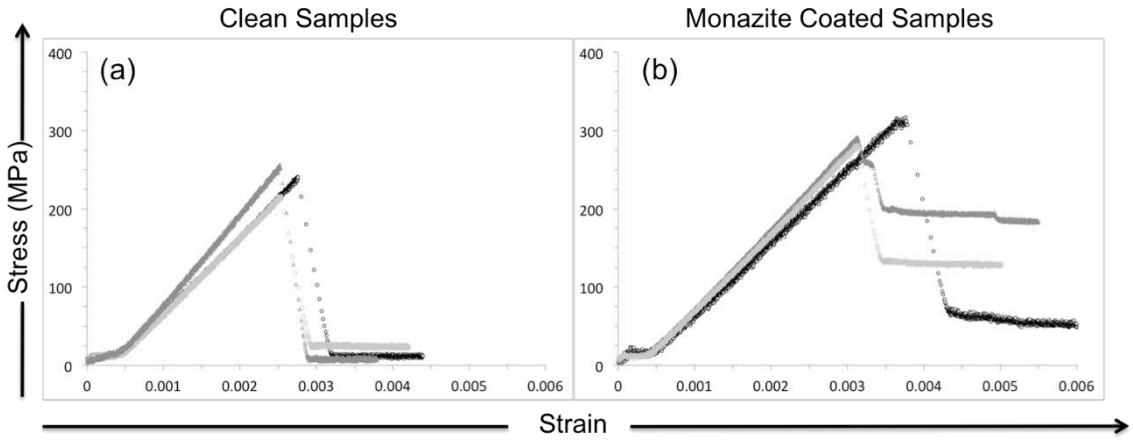

Figure 28: N720 specimen flexural stress-strain curves compared

The damage observed on the sides of both CL and MZ samples after flexure testing were very similar. In all cases, a crack appears to have originated on the tensile surface at roughly the mid-span of the specimen. The crack then seems to propagate for a short distance perpendicular to the fiber direction and then, before reaching the neutral axis, deflects along planes parallel to the fiber (see Figure 29). Since it occurred in both sample types it is uncertain if the Mode II behavior in these is suggestive of debonding at interfaces or shear failures in matrix rich regions. Additional microscopy methods are needed to discern.

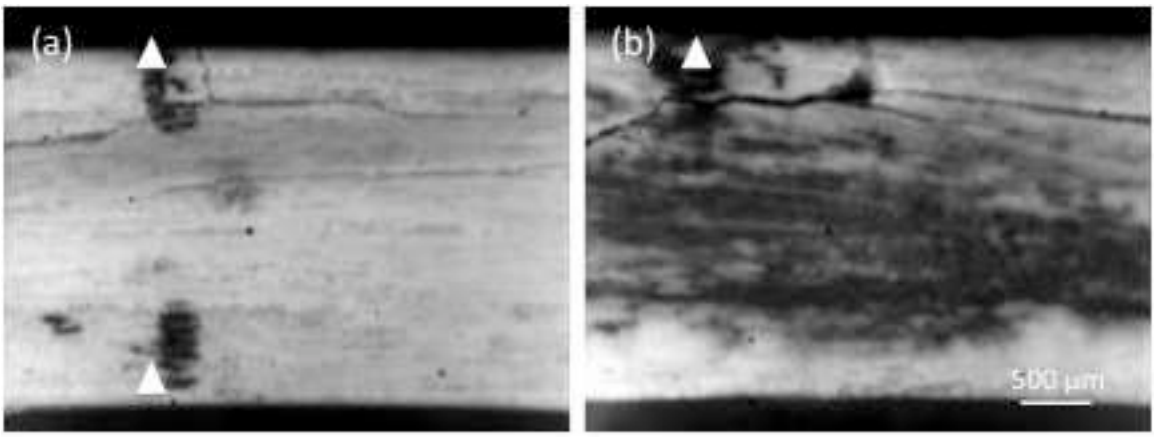

Figure 29: Typical damage observed on the sides of Nextel 720/MEYEB composite specimens after flexure testing. a) is N720_CL and b) is N720_MZ. The black marks highlighted by the white triangles are marks from a standard pencil indicating the approximate location of the mid-span of the specimens. Surfaces subjected to tensile stresses in flexure are at top of image. Fibers run left to right on the page.

MZ and CL samples were subjected to additional displacement after conclusion of the original test in order to observe for evidence of fiber pullout in samples. Figure 30 shows the fracture surfaces of CL and MZ samples as observed on the tensile side. The CL sample appears to have a more planar fracture surface than the MZ sample. It is unclear if there is actual fiber pullout, but the more tortuous fracture surface of the MZ samples would tend to indicate that crack energy absorbing mechanisms, such as crack deflection and debonding, are active.

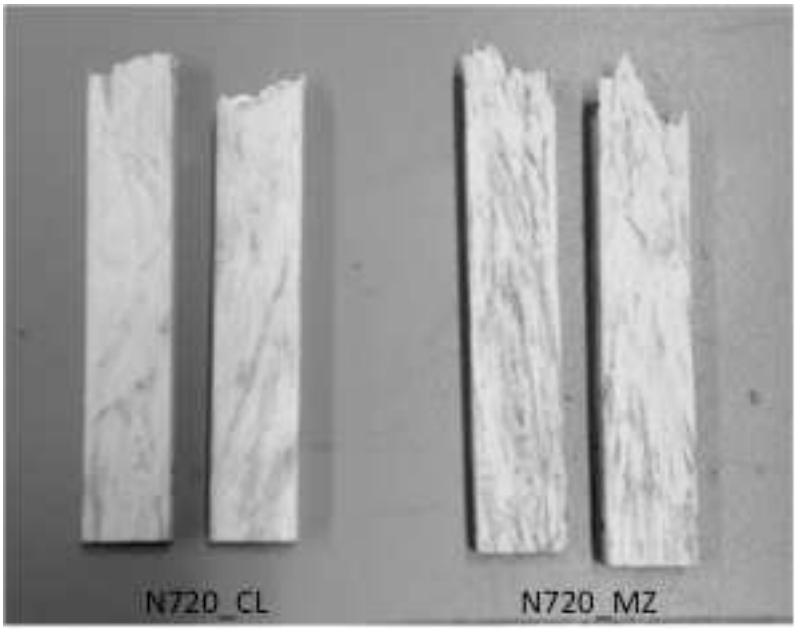

Figure 30: Fracture surfaces of Nextel 720/MEYEB composite specimens subjected to additional flexural displacement after initial failure. The tensile surfaces of samples are facing out of the page

4.5 Conclusion: Cure time and Monazite coated studies

Two separate studies were undertaken and discussed in this chapter. One, investigation observed the influence of matrix cure state on the toughness of a GMC containing a modified interface. The second study evaluated GMCs containing a monazite interphase and its effects on composite toughness and mechanical properties. The results indicate that carbon coated Nextel 610/MEYEB composites benefit from extended initial cure times. The change from a 1-hour to a 5-hour initial cure increased modulus and strength of carbon coated specimens by 60% and 150%, respectively. The CC_5hr specimens also exhibited moduli and strengths very close to the values represented by both cleaned fiber specimen types, while demonstrating superior damage tolerance. The damage tolerant

behavior coupled with the increased mechanical properties of the CC_5hr specimens resulted in superior toughness over the other sample types. These findings remove lingering concerns related to reductions in strength and modulus, given the intrinsically lower properties of the geopolymer than of a typical ceramic matrix material. In other words, doubts about the ability to utilize weak interface concepts in GMCs seem feasible. Analyzing the results appears to reveal that extended cure time improves shear resistance of the matrix and shear stress transfer within the Nextel 610/MEYEB composites containing an interphase. Therefore, this effort investigating cure time indicates that matrix cure state can severely limit the use of weak interface concepts to promote toughness in GMCs, given the large differences in constituent material properties. However, with moderate improvements to matrix properties, the use of an interphase can have a very positive effect on the toughness of GMCs.

The preliminary findings regarding the use of the oxide fiber coating, monazite, indicate that its use in geopolymer matrix composites is beneficial. Compared to samples with cleaned fiber surfaces, the results show a ~26 % increase in strength of samples that had monazite coated fibers without any loss in composite modulus. As a result of the increase, the monazite coated fiber samples demonstrate greater toughness than the cleaned fiber samples. Furthermore, improvement to composite toughness is also indicated by the more tortuous fracture surfaces of monazite samples and their ability to maintain a greater percentage of the maximum load after initial failure. These improvements were observed after exposure to elevated temperatures in an oxidizing environment suggesting that this interphase material shows stability with the geopolymer matrix. These results give greater

confidence that an acceptable degree of toughness can be developed in GMCs using longer cure times and oxide interphase coating for use in more demanding intermediate, high temperature structural applications.

Chapter 5: Physical Characterization

This chapter covers the study of various physical properties relevant to the composites used in the primary investigation of this research. Typically, the physical properties gathered were to reveal information about the microstructure of the composites to assess quality of the fabricated composites. Additionally, the physical measures obtained will aid in the interpreting the data gained in the mechanical characterization portion of this research.

5.1 Materials and Specimen Preparation

The materials and fabrication techniques for all sample types used in this study are described in Chapter 3 of this document. Any additional preparation of specimens that was necessary in order to execute the particular physical characterization technique will be described in the sections that follow.

5.2 Microstructure Evaluation

Three microstructural elements of the composite types fabricated for this research were investigated. These elements included fiber distribution, fiber volume fraction and porosity. Information obtained from all three evaluations helped assess the quality of the fabricated specimens and provided key information for interpreting each sample types mechanical response. More specifically these investigations determined whether the

analysis of mechanical properties needed to be tailored for differences observed in each composite types microstructure.

5.2.1 Fiber distribution

A common issue in the fabrication of composites is the development of matrix-rich regions caused by poor distribution of fibers [2]. These areas devoid of fiber are common sources of premature failure in composite specimens. Such failure is typical because of weakness of the matrix material and unimpeded crack growth due to the lack of fiber in these regions. Another important feature that indicates the quality of the fabricated composite, especially in unidirectional composites, is fiber alignment. High degrees of misalignment in fibers within the composite can influence strengths, modulus, and type of fracture [2]. When investigating a composite cross-section under a microscope, misalignment can be identified by irregular fiber cross-sections. In the case of fibers with a circular cross-section, the fibers often appear elliptical in shape when fibers are misaligned.

5.2.1.1 Specimen preparation

Composite cross-sections for examination were obtained by harvesting small portions of material from sample sticks. The specific details for preparation of cross-sections for observation can be found in Chapter 6, Section 6.4.1 of this document. Micrographs were obtained using an optical microscope and imaging software.

5.2.1.2 Results of investigation

Figure 31 shows a representative cross-section of the composite samples prepared for the primary investigation. The cross-section of this sample shows a random distribution of fibers. This was typical of all sample types. Additionally, there does not appear to be any

relatively large continuous regions void of fiber. In areas of tightly packed fiber, the fibers can be seen surrounded by matrix material indicating there was good wetout of the fiber bundles.

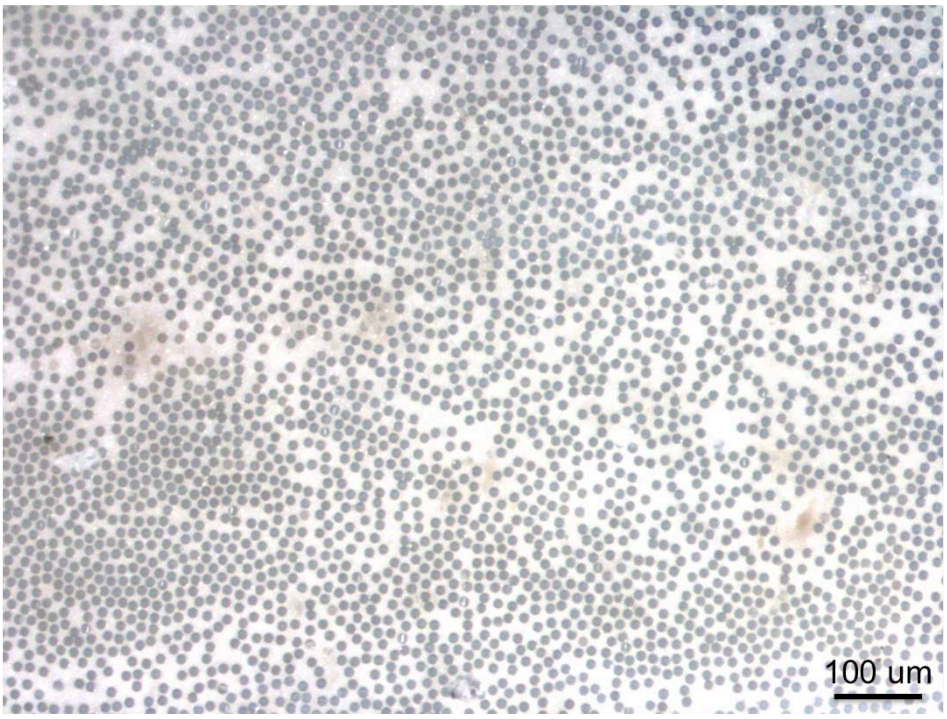

Figure 31: Microscopic view of specimen cross-section

Contained in Figure 32 are additional representative micrographs of specimen cross-sections at higher magnifications. The images were taken from composites containing the three different fiber types. The images show fiber alignment not to be an issue, as fibers composite cross-section were circular as expected. The images also show alignment of fibers did not vary based on fiber type indicating consistency of fabrication quality.

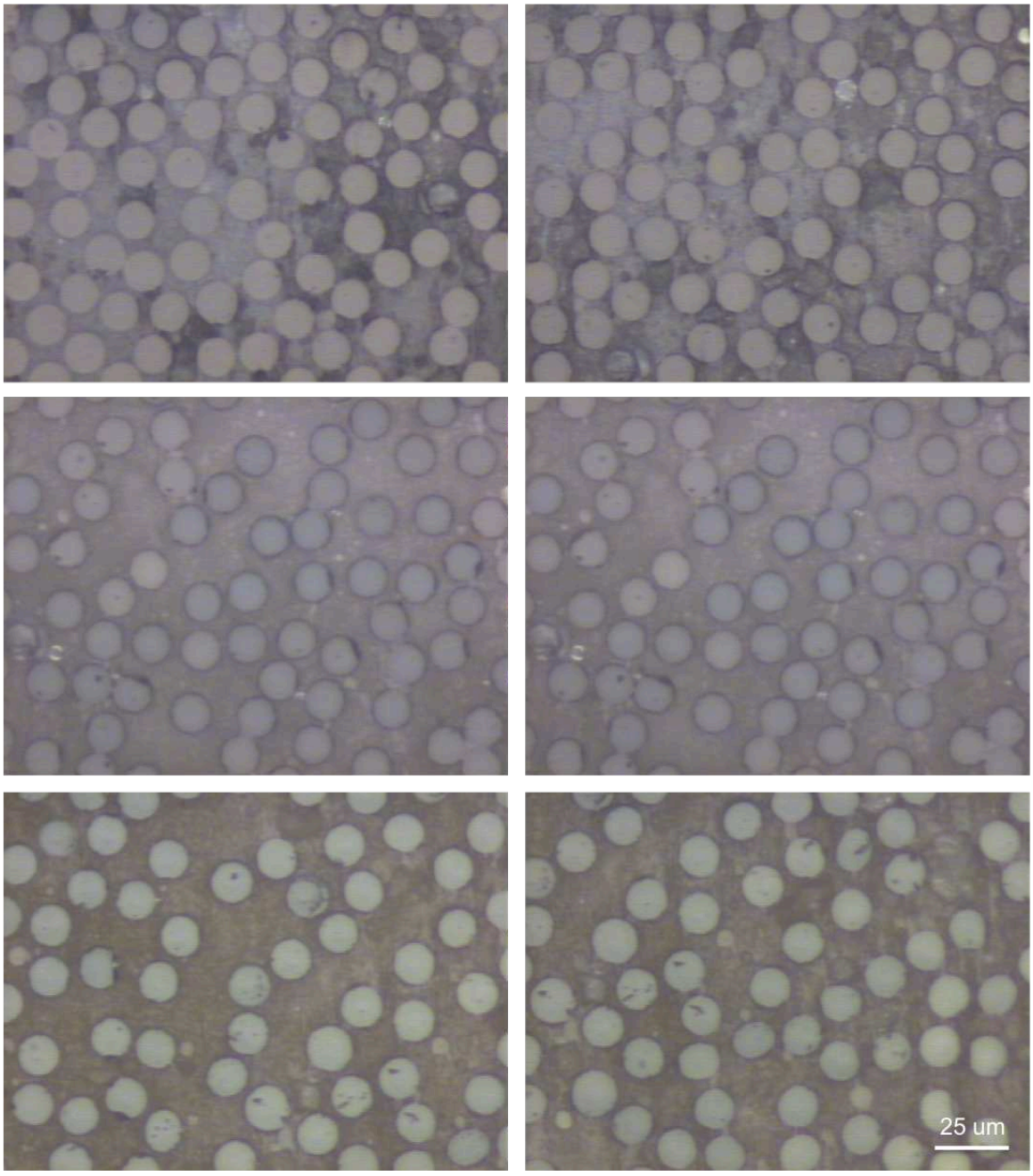

Figure 32: Images of Nextel 610/MEYEB cross-sections. From top to bottom: CL, CC, and MZ composite samples.

Also worth noting in all the images of this section is the condition of the matrix. The matrix appears free of voids and is surrounding each fiber. The color of matrix in the images varies slightly. The color appears to be associated with the fiber type used. The minor

difference in color of the images could also be to due to differences in light settings at the time the micrograph was taken.

5.2.2 Fiber volume fraction

Fiber volume fraction (V_f) was determined for each specimen tested. The main purpose for determining a fiber V_f for each specimen was for comparison of mechanical properties between sample types. The V_f has a direct effect on the mechanical properties of a composite. As such, a determination of V_f also aids in validating acquired data, such as modulus and for comparison of composite strengths.

5.2.2.1 Method for determination of V_f

To obtain a fiber volume fraction, specimens harvested from composite samples were first dimensioned. Width and thickness measurements were obtained using a micrometer with accuracy to 0.0001". Both the final width and thickness dimensions were averaged from multiple points taken on the specimen. Each specimen was measured in this way. The length of specimens was not needed in the calculation of V_f. The following equation, developed using Rule of Mixtures (RoM) principles, was used to calculate the fiber volume fraction [2]:

$$V_f = \frac{D\ N_{tows}}{9000\rho_f\ b\ d} \tag{5.1}$$

where D is the denier of the fiber, N_{tows} is the number of tows, ρ_f is the density of the fiber (*grams/cc*), b is the width of the specimen (*mm*), and d is the depth of the specimen (*mm*).

N_{tows} refers specifically to the number lengths cut from the roll of fiber that were then placed into a single cavity in the mold (refer to Chapter 3, Section 3.3.1).

A $V_{f.}$ was obtained in this way for every composite specimen. The mean $V_{f.}$ value obtained in this section was a compilation of all flexural, tensile, and short beam specimens with the exception of those specimens used in the aging study.

Additional means for evaluating $V_{f.}$ and verifying this method were considered, but the two previous studies had suggested the accuracy of the method was sufficient. That said, the calculated $V_{f.}$'s of each specimen may not be precise, but they are at least close to the true value. To be consistent and provide for a fair comparison, the method for determining V_f did not vary depending on specimen type. Finally, in processing of composite samples there was no indication of fiber loss that would be substantial enough to effect the calculation of fiber volume fraction using this method. On occasion a few single filaments were left behind during processing, but such an amount is negligible in the calculation of fiber volume fraction when considering the size of a single filament and the total number of filaments that make up a composite sample in this investigation.

5.2.2.2 Results

The average fiber volume fraction calculated from specimens for each sample type is found in Table 8 below. The table also includes the theoretical modulus of specimen types based on these average fiber volume fractions. The predicted value for composite modulus was calculated using RoM with values of modulus for both fiber and matrix given in Chapter 3 (see Table 3 andTable 4). RoM assumes perfect bonding at the interface [2]. Recall, a very

near-to-perfect bonding condition is expected for CL sample types. This may not necessarily be the case for CC and MZ samples. However, evidence provided in Chapter 4 would seem to suggest that the coatings do not influence load transfer to a large degree and therefore the moduli of CC and MZ composite samples is similar to that of CL sample types. Thus, the predicted moduli in Table 8 are expected to be close to the value of each composite sample type tested. These values can serve as comparison to the moduli determined using the data collected during flexural and tensile testing (see Chapter 6). The shorthand notation used in Table 8 to designate sample types is defined in Table 5.

Table 8: The average fiber volume fraction of the different specimen types and corresponding modulus as predicted by RoM.

Sample Type	Fiber Volume Fraction, V_f	RoM Modulus Based on V_f (GPa)
CL(A)	44.0%	172
CL(N)	46.4%	181
CC(A)	46.0%	179
CC(N)	46.0%	179
MZ(A)	40.2%	156
MZ(N)	41.5%	162

The V_f of CL and CC sample types does not differ by much more than 2%. However, MZ samples vary by sometimes almost as much as 6.5% compared to the other two sample types. It is clear from Table 8 that this has a relatively significant effect on the theoretical composite modulus of specimens. The low modulus of the matrix in comparison to that of the fiber is responsible for the significant change. Such a difference in V_f would likely also

affect the strength of samples. Generally, the relationship would be similar to that observed for the predicted modulus of samples where increasing fiber content would yield increased composite strength [2], [118]. The decrease in both strength and modulus of samples will ultimately result in a lower calculated value for toughness of the MZ specimens. However, the calculation will not be the only means to evaluate toughness of sample types. It is simply a factor to consider in the overall evaluation of toughness of sample types.

5.2.3 Porosity

Geopolymers are known to have varying levels of porosity [4], [106], [119]. It is also understood that porosity in ceramic matrix composites (CMC) can facilitate crack deflection around fibers without the need for fiber coatings [50], [120], [121]. With this understanding, one particular study that combined Nextel 610 monazite coated fibers in an alumina matrix sought a 90% density in order to consider the effects of porosity on mechanical response to be negligible [73]. It should be understood that to date no studies have looked at the influence of matrix porosity on deflecting cracks in GMCs. It's possible the influence of porosity on dissipating crack energy may vary in GMCs from CMCs because ceramic and geopolymers have dissimilar microstructure and mechanical properties. However, the premise of the studies contained here within is based on showing that the same techniques applied in CMCs to increase toughness can be applied to GMCs. Therefore in lieu of other research showing the influence of porosity on GMCs, a 90% density marker will be used as the threshold to evaluate the potential influences of porosity on the mechanical response of GMC specimens.

Porosity of individual specimens was determined using two methods. Both methods determined porosity using a theoretical value for the density of composite specimens. The theoretical density of composite specimens was determined using RoM principles and the density of the matrix and fiber (see Chapter 3). The specimens used to obtain porosities were harvested from sample sticks and were nominally 15 mm in length.

5.2.3.1 Method 1: Geometric porosity

The first method for obtaining porosity involved dimensioning rectangular specimens using a micrometer with 0.0001" accuracy. Specimen widths were measured at five points along their length. The five points were averaged to produce a nominal value for the width of the specimen. Specimen thicknesses were measured at five points along their length. At each point, along the length the thickness was also measured at three points across the width. The entire set of measurements was averaged to produce a nominal value for thickness of each specimen. Length was averaged from at least two points. The specimens were then weighed and density was calculated. Prior to weighing, specimens were subjected to drying at 100 °C for at least one hour to avoid additional mass from possible absorption of moisture [4]. Porosity was then calculated by determining the percent difference of density between the theoretical value and the measured value.

5.2.3.2 Method 2: Archimedes porosity

The second method used Archimedes' Principle to obtain the density of specimens using ASTM B962-15 as guidance [122]. For each specimen, three different mass measurements were taken to obtain the density. The mass of each specimen was recorded after drying at 100 °C referred to as the dry mass (m_d). The second mass was taken after the specimen

surface was sealed using clear liquid nail polish. This is the polished mass (m_p). Multiple coats were applied to each specimen to ensure that the specimens were sealed to prevent moisture being absorbed while obtaining the third mass. The third mass was obtained with the specimen suspended in distilled water, the submerged mass (m_s). While suspended in the distilled water no bubbles were observed on the surface of specimens suggesting the water was able to wet the surface. The three masses were then used to obtain the density using Equation 5.2 [122]:

$$\rho_c = \frac{m_d}{\frac{m_p - m_s}{\rho_w} - \frac{m_p - m_d}{\rho_n}} \tag{5.2}$$

where ρ_c is the density of the composite, ρ_w is the density of the water, ρ_n is the density of the nail polish. Temperature of the water was recorded in order to use the most accurate value for density. Once again, porosity was then calculated by determining the percent difference of density between the theoretical value and the measured value. All mass measurements were in grams and values for density in grams per cubic centimeter.

5.2.3.3 Comparison of methods

The results of using both methods (geometric and Archimedes' principle) on selected specimens to determine porosity are shown in Table 9.

Table 9: Porosity of selected specimens using two different methods

Specimen	Geometric Porosity (%)	Archimedes Porosity (%)	Absolute Difference
CL(A) – 0725A-2.3b	10.4%	11.0%	0.60%

Specimen	Geometric Porosity (%)	Archimedes Porosity (%)	Absolute Difference
CL(A) – 0922A-3.1b	7.9%	5.6%	2.30%
CC(A) – 0716A-1.1b	8.79%	5.1%	3.69%
CC(A) – 0719A-1.4b	11.24%	9.5%	1.74%
CC(A) – 0720A-2.2b	12.01%	8.5%	3.51%
CC(N) – 0714A-1.3b	10.3%	10.4%	0.10%
CC(N) – 0720A-2.4b	11.0%	10.2%	0.80%
CC(N) – 0721A-1.2b	10.8%	7.28%	3.52%
MZ(A) – 0716A-1.2b	7.9%	7.1%	0.80%
MZ(A) – 0721A-1.1b	9.9%	3.5%	6.40%
MZ(A) – 0921A-2.2b	2.9%	1.6%	1.30%
MZ(A) – 0921B-2.3b	5.1%	3.6%	1.50%
MZ(N) – 0719A-1.2b	5.1%	5.3%	0.20%
MZ(N) – 0720B-2.1b	5.61%	5.9%	0.29%
MZ(N) – 0721B-1.3b	4.0%	2.7%	1.3%

The results indicate only relatively minor differences in the methods. Regardless of specimen type, the porosity obtained using Archimedes' principle is often the lower measured value except in the cases where the geometric porosity is very similar in magnitude. Assuming limited experimental error, Archimedes' principle should be the more accurate method of obtaining specimen porosity between the two methods used. It accounts more accurately for the true volume of the specimen. Ultimately, the results suggest the geometric porosity to be in relatively good agreement with those obtained using Archimedes' principle. Differences between the two methods were generally no

more than 4%. The geometric porosity also appears on average to be the more conservative value for porosity.

Based on these results, a value for porosity was obtained for all specimen types using the geometric method. The average porosity of each sample type is listed in Table 10 below.

Table 10: Average porosity of all sample types

Sample Type	Average Porosity of Specimen Type (%)	Standard Deviation (%)	Number of Specimens
CL(A)	8.13%	1.8%	12
CL(N)	11.29%	1.4%	11
CC(A)	10.5%	1.8%	6
CC(N)	11.22%	0.6%	6
MZ(A)	6.89%	2.6%	12
MZ(N)	4.89%	0.6%	6

The measured porosities of specimens indicate greater porosity in CL and CC than in MZ specimens. MZ specimens on average meet and/or exceed the established 90% threshold. In all cases CC specimens do not, but since their measured porosities are close to that of CL specimens, the mechanical responses of these types will make for a fair comparison. Recall that the values for porosity are likely conservative based on using geometric porosity versus porosity obtained using Archimedes' principle. Therefore, it is possible that on average CC specimen porosities shown in Table 10 are slightly inflated and may meet the 90% threshold. The same might be said of CL(N) specimens as well.

The lower porosity of MZ specimens should not be of too much concern to the interpretation of mechanical data. The reason for determining porosity was to ensure minimal influence of porosity on abosorbing crack energy. The lower porosity in MZ specimens provides a little more certainty that any observed changes in mechanical behavior are more directly linked to the presence of the monazite coating. The lower porosity in these particular samples might be due to the slightly lower fiber volume fraction. It is thought the reduced amount of additional foreign surfaces amongst the geopolymer might have allowed for greater densification of the matrix.

5.3 Thermal Treatments

In Chapter 3, the processing of composite samples was discussed. Due to the fiber surface conditioning, sample types appear different in color after initial processing. Changes in color also take place after heat treatment above 400 °C in air. Such changes have been observed previously [17], [23]. The color changes are indicative of changing conditions of the fiber and likely interface. To capture these changes, the color of samples was recorded via photograph prior to and after heat treatment to draw conclusions about changes in fiber surface condition.

Recall that after initial processing, all samples were subjected to a post cure at 250 °C for five hours. Sample sticks were then subjected to a final heat treatment at 650 °C for five hours in one of two environments. Figure 33 shows the sample types prior to and after heat treatments in their respective environments.

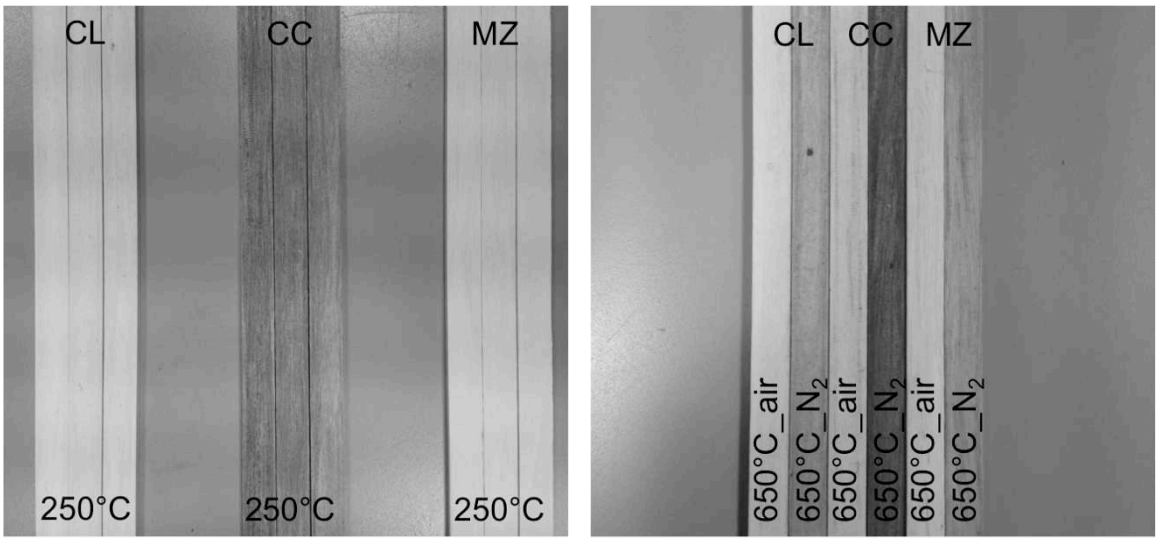

Figure 33: Color shade of specimens prior to and post-final heat treatment

After a 250 °C post cure, CL and MZ samples are a shade of white, while CC samples appear as dark gray in color. The white color of CL and MZ samples is a function of both the matrix, which is white when processed without any reinforcements and the color of the fibers (see Figure 14). The CC samples appear dark gray resulting from the mixture of the white color of the matrix and the N610 fibers that were heat cleaned in an inert environment. Recall, the heat cleaning of the N610 fibers in an inert environment resulted in a darkened fiber condition indicative of the carbon coating (see Chapter 3 and Figure 14). The dark color of the fibers transferred to the composite. As indicated in the right hand portion of Figure 33, both CL and MZ samples heat treated in air stay relatively the same color. CC samples heat treated in air, however, lose the dark gray color and become almost the same color as CL and MZ samples. The change indicates that the oxidizing environment likely degraded the carbon coated surface of these fibers. This change and apparent degradation has been documented previously [21], [23].

For samples heat treated in an inert environment all sample types became a shade darker than they were prior to heat treatment. This outcome is surprising. It was expected that all samples would experience minimal, if any, color change. The retention of the darker color for CC samples indicates that fiber surfaces likely remained unaffected after heat-treating in a non-oxidizing environment. The discussion in Chapter 4 of this document provides support for this conclusion. It is also well established that carbon coatings can withstand high temperature exposure in inert environments. Additionally, verification of the particular processes and equipment used in this study is supported by other research that has used the same [23], [38].

After observing cross-sections of specimens harvested from the sample sticks, the darkening of samples was determined to be surface contamination. The source of the surface contamination is not completely certain. It is not the purpose of this chapter to determine differences beyond the physical nature of samples. Effects such contamination may have had on the material properties, if any, will be addressed in Chapter 6.

5.4 Conclusion: Physical Characterization

The particular analyses conducted to characterize the physical aspects of composite sample types have revealed important information that will aid in the mechanical characterization portion of this research. Additionally, it has provided confidence in the quality of composites produced using the fabrication and post-processing techniques described in Chapter 3. Investigations at the microstructural level have revealed composites with satisfactory fiber distribution and alignment. Both the fiber distribution and alignment

were not biased to a particular composite sample type. Poor distribution and alignment could easily affect the results of the mechanical characterization investigation rendering the analysis of the use of interphase to improve toughness difficult or in the most extreme case, impossible. Although distribution and alignment were consistent among samples, fiber volume fraction and porosity was on average lower in MZ samples. It is not thought that fiber volume fraction should greatly affect the mechanical response of specimens in the planned characterization efforts, but it is a factor to consider when comparing strength, modulus, and calculated toughness of specimens. The porosity might have been a concern in determining the true effectiveness of monazite coatings in GMCs, but results of two techniques indicates porosity in MZ samples to be lower than 10%. 10% was determined be a threshold based on its use to examine the effectiveness of interphase for dissipating crack energy in CMCs.

Chapter 6: Mechanical Characterization

Flexure, tensile, short beam shear (SBS), and single fiber push-out testing were conducted to understand the effect of fiber surface condition on the toughness of composite specimens. In addition, mechanical properties and the interfacial characteristics of composite specimens were evaluated. This chapter addresses the methods of conducting these experiments and any special preparation of composite specimens for each type of test. The results are presented for each test and then discussed.

Each test was chosen to aid in understanding and demonstrating how fiber coating influenced composite toughness. Specifically, flexural testing was conducted in order to obtain flexural mechanical properties of composite specimens and values of toughness. Tensile testing was used as an additional means of evaluating mechanical properties and for observation of fracture surfaces. These results will be discussed in terms of effect of fiber surface on toughness of composite specimens. Finally, SBS shear and push-out testing were used to evaluate interfacial strength of each GMC. The interpretation of these results was used to understand how interfacial conditions affected the material properties and toughness of composite specimens.

6.1 Flexural Testing

6.1.1 Specimen preparation

Flexural test specimens were harvested from samples that were fabricated using the procedures discussed in Chapter 3. A total of two specimens could be obtained from a single sample stick. Table 11 provides the total number of flexural test specimens tested for the given fiber type and heat treatment environment.

Table 11. Total number of flexural specimens tested for the given conditions

Composite Type Based on Fiber Surface	Number of Specimens Tested	
	650 °C air (5 hours)	650 °C N_2 (5 hours)
Cleaned (CL)	11	8
Carbon coated (CC)	7	6
Monazite (MZ)	8	7

The flexural test specimens were nominally 80 mm (length) x 4.5 mm (width) x 1.5 mm (depth). The actual thickness of specimens produced varied within and between each specimen type, however, the MZ specimens showed the most deviation. This was due to difficulties in fabrication and not the result of dilation of the composite during post cure and heat treatments. Average thickness and standard deviation for each specimen type are shown in Table 12.

Table 12. Average specimen type thicknesses and span-to-depth ratios

Specimen Type	Thickness (mm)		Span-to-Depth	
	Average	Standard Deviation	Average	Standard Deviation
CL(A)	1.659	0.058	40.70	1.34
CL(N)	1.611	0.057	41.93	1.45
CC(A)	1.657	0.092	40.83	2.14
CC(N)	1.583	0.063	42.70	1.66
MZ(A)	1.850	0.109	36.60	2.07
MZ(N)	1.767	0.104	38.30	2.24

6.1.2 Experimental setup and calculations

Flexural testing was conducted in 4-point flexure in accordance with ASTM C1341, except as noted. Tests were conducted using an ATS uniaxial load frame. Specimens rested on two outer support rollers and force was applied via two inner rollers each located one quarter of the overall span away from its closest outer roller (see Figure 34). A fully articulating flexural test fixture was used to compensate for any taper on individual specimens. The support span of the test fixture was 67.5 mm. Support rollers were 6 mm in diameter.

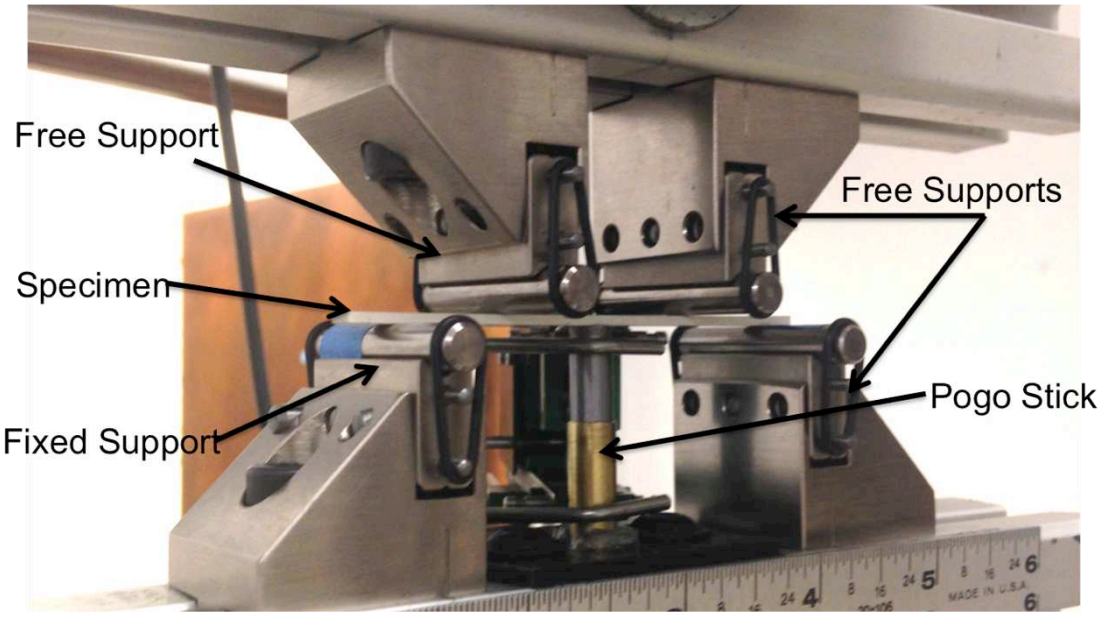

Figure 34. Fully articulating four-point flexure test fixture.

The large span was chosen in attempt to produce specimen span-to-depth ratios of 45:1. The choice of a large span-to-depth ratio for this investigation was intended to ensure failure on the tensile or compressive surface of specimens. A 32:1 ratio or higher is recommended by ASTM C 1341 for materials with low shear strength such is the case for geopolymers [113]. Ultimately, differences in thickness of specimens caused the span-to-depth to vary. The average span-to-depth ratio of each specimen type can be found in Table 12.

Specimens were tested at a displacement rate of ~0.5 mm/min. This rate is much slower then that recommended by ASTM C1341, but agrees more closely with common values reported in the literature involving flexure of brittle matrix composites [7]–[11], [16], [53], [64], [121], [123], [124]. Loading was ceased when specimens demonstrated at least a

50% drop in load or no change in load carrying capability upon further displacement. Load and displacement as a function of time, were recorded for each test. Displacement was recorded by using an extensometer mounted on a pogo stick-like device to measure mid-span displacement (see device in between outer rollers in Figure 34).

Flexural strength (S_u), flexural modulus (E), flexural strain (ϵ), and toughness (U_T) of specimens were calculated using the following relationships from ASTM C 1341 [113] except for Equation 6.4 which was found elsewhere [39]:

$$S_u = \frac{3\ P_u L}{4\ bd^2} \tag{6.1}$$

$$\epsilon = \frac{4.36\ Dd}{L^2} \tag{6.2}$$

$$E = \frac{0.17\ L^3 m}{bd^3} \tag{6.3}$$

$$U_T = \int_0^{\epsilon_f} \sigma\ d\epsilon \tag{6.4}$$

where P_u is maximum force recorded, L is the support span, b is the width of the specimen, d is the thickness of the specimen, m is the slope of the linear portion of the force-deflection curve, σ is the stress in the outer surface fibers, ϵ is the strain in the outer surface fibers, and ϵ_f is the strain at failure. Per ASTM C1341, failure was determined to be the force when test specimens split into two separate halves or when force dropped by 20% or more [113].

Measurements for strength, modulus, and toughness were averaged amongst specimens from each composite. The error bars on the charts in this section indicate one standard deviation. Values of modulus for all specimens were normalized to a 45% fiber volume fraction (V_f) for purpose of comparison. Table 8 in Chapter 5 contains the average fiber volume fraction of specimens. The strengths of the specimens were not normalized since a material's strength is sensitive to the state of the microstructure.

The choice to use 4-point flexure versus 3-point flexure was an important aspect of this research. The 3-point test configuration in combination with short test spans have generally resulted in predominantly shear failures in GMCs. According to classical beam theory, this is because under 3-point bending the absolute value of shear stresses imposed across the beam between support points is constant (see shear and moment diagrams in Figure 35).

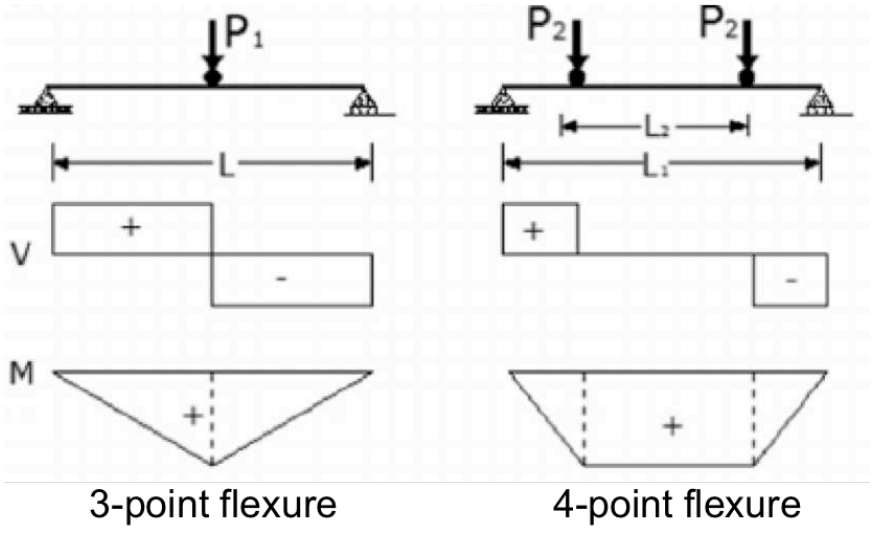

Figure 35: 3-point and4-point flexure shear and moment diagrams compared[125]

As load increases, the shear stresses experienced by the beam rise thus making it more likely for materials that have limited shear resistance to fail in shear rather than flexure as

the test intends. Given the geopolymer matrix is relatively weak in shear and the nature of research seeks to reduce interfacial shear strength 3-point flexure was exchanged for the use 4-point flexure. The intent of using 4-point flexure is to reduce the likelihood of shear failure and promote tensile failure between the loading points. The 4-point configuration achieves this by producing a constant moment between the loading points (see Figure 35). As the derivative of the bending moment, shear force is reduced to zero between loading points. Therefore, shear forces only exist between each loading and support point. The constant moment also means that between the loading points the beam experiences a constant state of stress on its outer surfaces only varying linearly through the thickness. In the case of brittle materials, this is helpful as it exposes a greater volume of material to the same force exposing potential fatal flaws in the material. In other words, a brittle material will likely fail prior to that of a tougher material because it lacks mechanisms to defeat cracks that result from the flaw.

6.1.3 Results

6.1.3.1 Mechanical properties

The average flexural moduli of composite specimens are shown in Figure 36. In Chapter 4, a Rule of Mixtures (RoM) calculation for 45% V_f determined composite modulus to be somewhere in the range 171 to 175 GPa. However, the matrix in these composites is cured for 24 hours rather than 5 hours. Using the known tensile modulus value for fiber and flexural modulus value for matrix, RoM predicts ~175 GPa for composite modulus. If the compressive modulus of the matrix is used, it could be closer to 182 GPa. The measured 4-point flexure modulus values of all specimen types lie in the predicted range or closer to

182 GPa. This is different than those values measured in 3-point flexure in Chapter 4 where modulus values were 77% to 85% of those predicted by the average RoM value of 173 GPa. The graph also indicates no definitive difference in the moduli of specimens regardless of fiber surface condition or post heat treatment environment.

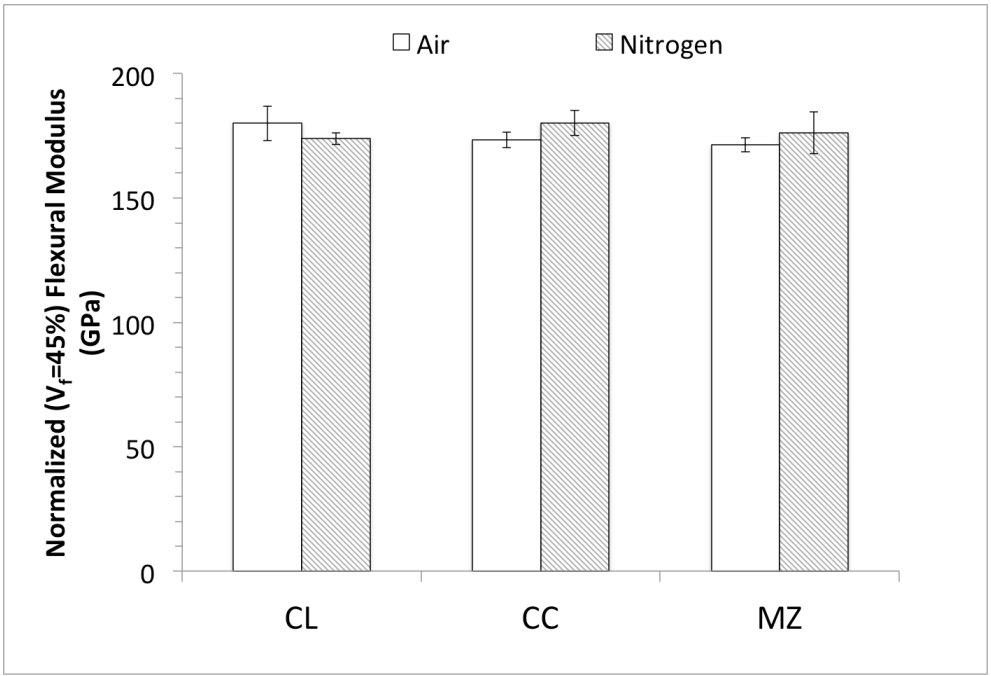

Figure 36: Normalized flexural modulus of GMCs based on a 45% fiber volume fraction

Figure 37 shows the average flexural strength of composite specimens. All specimens tested appear to fail on the tensile surface away from the support and loading pins. Despite initial tensile failure, damage produced from effects of shear was readily apparent in all composites tested regardless of fiber surface condition. This was also observed in the preliminary investigations. In this primary investigation, the degree of the shear damage varied between the specimen types. A more detailed examination of failure surfaces is addressed in Section 6.1.3.4.

The baseline cleaned fiber specimens display the lowest average strengths of all specimen types. The results seem to indicate a possible strengthening effect with the use of carbon coating, but a two-tailed t-test seems to suggest very little significance in the measured differences between the CL and CC specimen types.

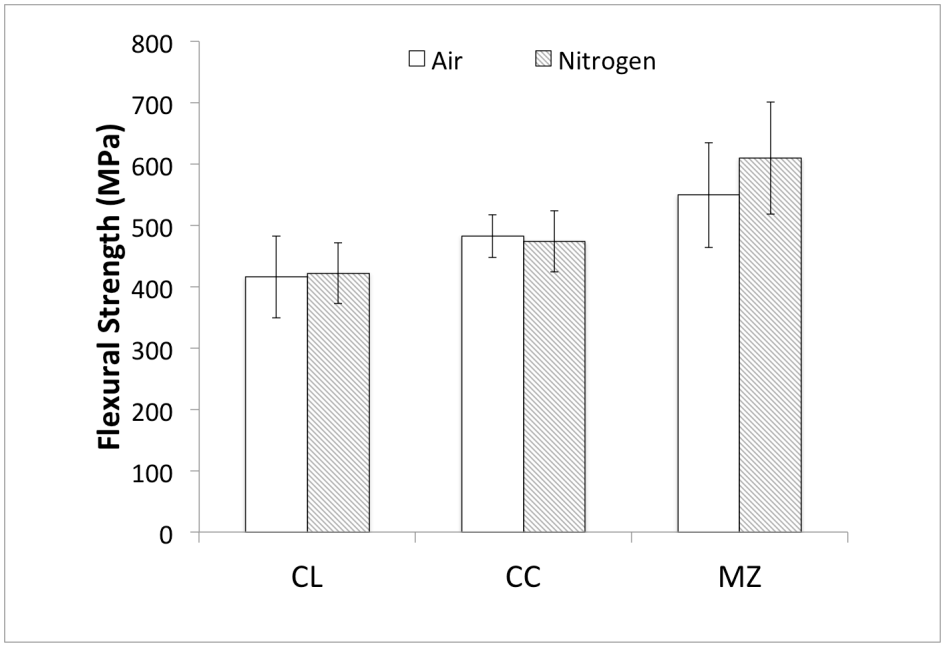

Figure 37: Flexural strength of geopolymer matrix composites

The results for cleaned and carbon coated specimen strengths are similar to those presented in the cure time investigation (see Chapter 4) excluding those specimens with the carbon coated surface only cured for one hour. The flexural strength of CL composite specimens also seems to agree with those reported in a previous study for composites with a similar V_f and tested in a 3-point configuration [23]. The flexural strength of CL specimens also agrees with those reported by Welter although a direct comparison is somewhat difficult because of the lower fiber volume fracture of the composites in that study [10]. The average strengths of CC specimen types are slightly higher than those

values measured in the preliminary investigation, but the standard deviation does not seem to suggest any great degree of significance between the two types. Any difference could be attributed to the additional 19 hours of cure time these specimens were subjected to. Given the increase in strength appears to be statistically insignificant in the CC specimens, shorter cure times should be considered in future studies involving GMCs with interphases.

In contrast, the measured strengths of MZ specimens clearly exceed those of CL and CC. The percent increase in strength of MZ over CL specimens varies based on the heat treatment environment. The percent increase is ~32% and 45% for oxidizing and non-oxidizing environments respectively. The percent increase in strength is close that measured in the monazite coated fiber study (see Chapter 4). In N610 composites with monazite coating, the percent increase is slightly higher. The differences in percent increase could easily be related to the type of reinforcing fiber, which was N720 in the case of the monazite coated fiber study.

6.1.3.2 Influence of fiber volume fraction

Within the limits of ideal fiber packing, experimentation and theory generally suggest that the strength of a composite increases with increasing fiber volume fraction (V_f) only limited by the ability to properly manufacture the composite [118]. This also assumes the role of the fiber is that of a reinforcing agent in order to improve the strength of the matrix material. However, the benefit of increasing V_f for the composite strength does have its limits and that value can be lower than expected. As such, some consideration was given to investigating whether the increase in strength of the MZ specimens was the result of

decreases to V_f. To investigate, six additional CL(A) were created in the same manner as before with one exception. The CL(A) specimens were produced with a V_f of 40% in an attempt to match the average V_f of MZ samples. The V_f of MZ samples could not be increased due to restrictions of the mold and technique for processing. CC composites were not evaluated as part of this analysis as V_f only varied for MZ specimens.

Figure 38 shows the influence of V_f on the strength of composites. For an ~6% decrease in V_f, the effect on CL composite strength appears to be only a very slight decrease, if indeed, any at all. This suggests that the strength of the CL composites is mostly insensitive to changes in fiber V_f. It seems fair at this point to conclude that the improved strength of MZ specimens has little to do with the decrease in V_f. It is also worth stating at this juncture that increased strength of MZ specimens is not provided by a greater reinforcing effect of the fiber. In other words, the fiber is not stronger with the monazite coating applied to it. Recall, if the monazite coating is applied properly to the Nextel fiber the strength of the fiber can only be retained [109]. It is possible to consider that small changes in fiber volume fraction would not affect the MZ composites in the same way as it does CL. In fact, the larger strength of MZ(N), which also has a slightly higher average V_f than MZ(A), might suggest that if MZ specimens had the same V_f as CL they would have been even stronger. This makes further sense if one considers that both the fiber and fiber coating in addition to increasing strength provide greater toughness. The more crack defeating mechanisms present the less likely cracks are to propagate unstably through the composite. Of course, at some fiber volume fraction there is likely a limited or even negative return.

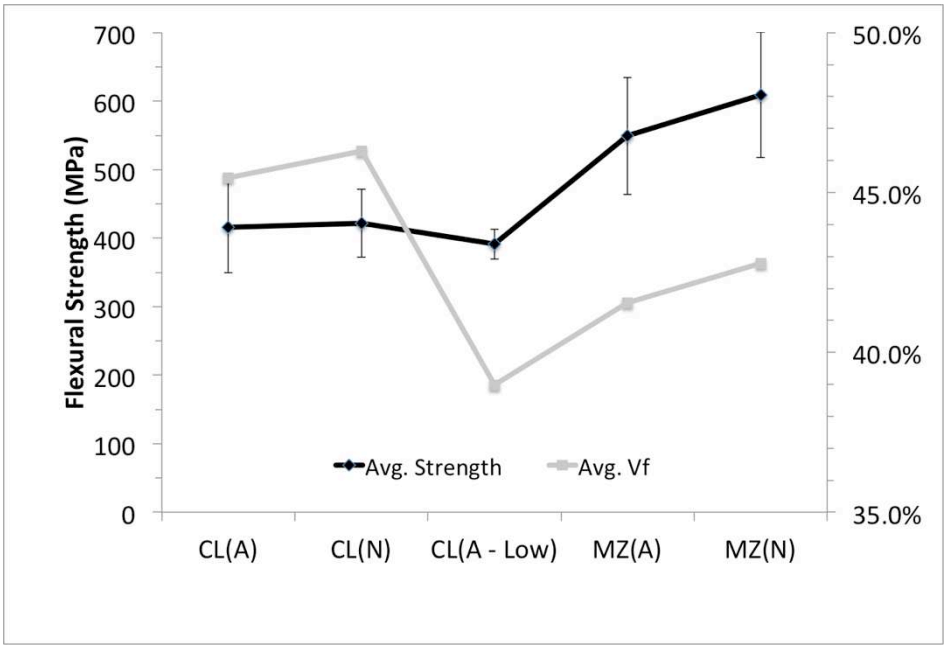

Figure 38: Flexural strength and V_f of CL and MZ composites

6.1.3.3 Toughness and damage tolerance

All specimens were tested in flexure after the final heat treatment at 650 °C in one of the two environments previously discussed. Figure 39 shows the resulting toughness of specimens as calculated from Equation 6.4. The error bars indicate one standard deviation.

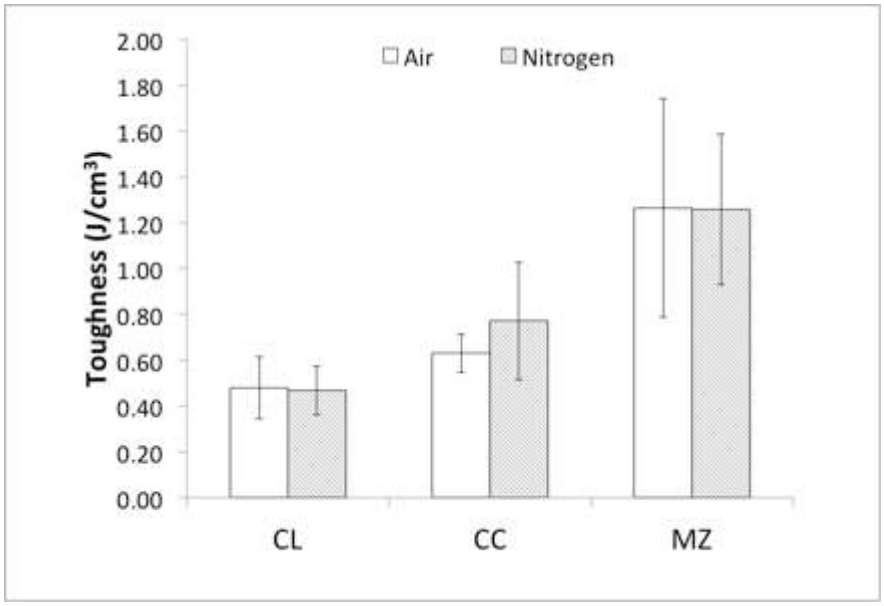

Figure 39: Calculated toughness of GMCs

The baseline CL specimens show the lowest values of toughness as expected. In fact, the results for CL specimens trend well with previous research involving N610/MEYEB composites [23]. The same study also evaluated CC(A) specimens after heat treatment beyond 650 °C. Despite some variations in processing and heat treatment temperature, the values in the previous study are fairly similar to those obtained in this current research [23].

The final heat treatment environment seems to have only influenced the toughness values of CC specimen types and not CL and MZ. Recall, heat treatment environment did not appear to have any impact on the strength and modulus of any specimen type. Such a result was expected for the GMCs that contained all-oxide constituents. A slightly higher average value of toughness was measured for CC(N) than for the CC(A) specimens. The large standard deviation for CC(N) composites would seem to statistically negate the

significance of this higher mean, but it should not be interpreted this way. The large standard deviation observed for CC(N) (and also MZ) specimens was determined to be the result of stress-strain behavior post initial failure. Figure 40 and Figure 41 show the failure of CL and CC(A) specimens was catastrophic upon the first load drop with specimens lacking the ability to carry additional load upon further displacement. In contrast, CC(N) and MZ specimens generally exhibited non-catastrophic failure after the first load drop showing varying degrees of damage tolerance upon continued displacement (see Figure 41 and Figure 42). In some cases, the initial load drop for these specimen types was greater than 20% of the max load. Recall, 20% was the cut off for determining failure per the ASTM. This standard was used in the calculation of toughness. Using this standard contributed to the larger measured standard deviation value for toughness in CC(N) and MZ specimens because some specimens experienced initial drops over 20% before demonstrating ability to continue bearing load under increasing displacement.

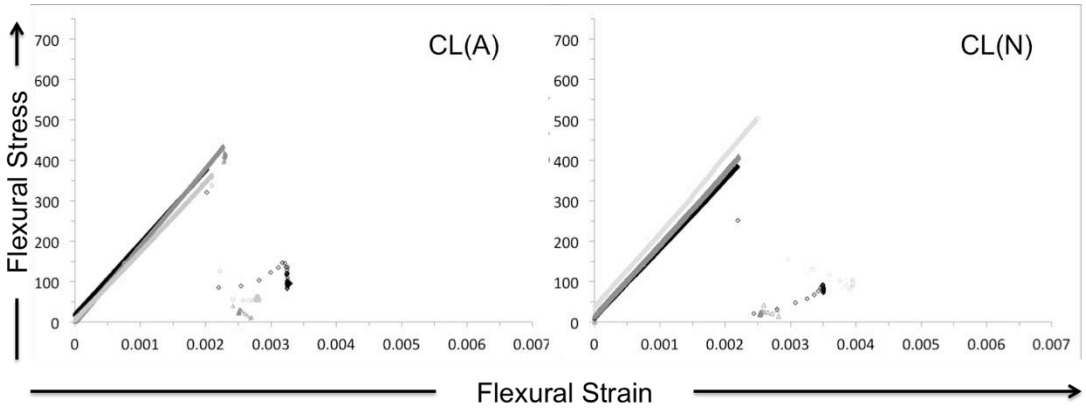

Figure 40: Typical stress-strain curves of CL(A) and CL(N) composites.

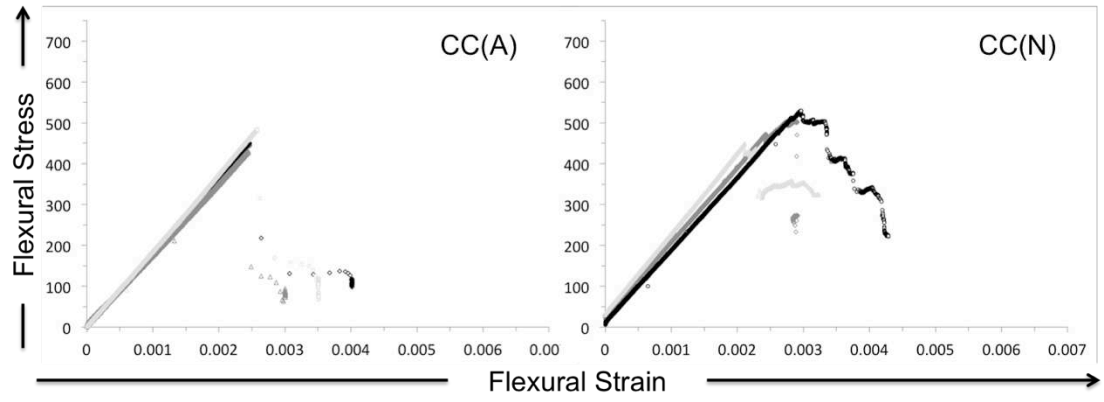

Figure 41: Typical stress-strain curves of CC(A) and CC(N) composites.

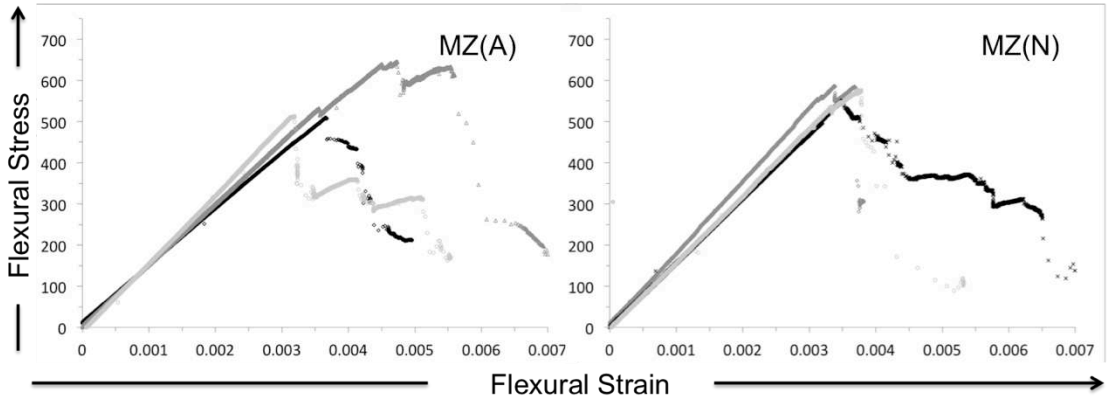

Figure 42: Typical stress-strain curves of MZ(A) and MZ(N) composites.

The greatest value of toughness was measured for MZ specimens with CC(N) specimens having the second greatest value. The toughness of MZ and CC(N) specimens increased by over 160% and 60% as compared to the baseline CL composites, respectively. The stress-strain curves of these two specimen types (Figure 41 and Figure 42), which show increased area under the curve relative to the other specimen types, coincide with the measured gains in toughness.

As already noted, the stress-strain curves in Figure 40 through Figure 42 show representative behavior of each specimen type under flexural testing. As with values of toughness, the heat treatment environment only affected the stress-strain behavior curves of those GMCs with carbon coating. While CC(A) and CC(N) specimens demonstrated no difference in their either strength or modulus values, their stress-strain behavior is altered based on the type of heat treatment environment. The carbon coated specimens heat treated in air show similar stress-strain behavior to CL specimens. CL(A), CL(N), and CC(A) all demonstrate stress-strain behavior typical of a brittle material. The stress-strain curves of CC(N) composites show a more damage tolerant behavior. The more damage tolerant behavior results in increased area under the curve, which parallels the slightly higher average calculated value of toughness relative to CL specimens. The damage tolerant behavior of CC(N) specimens in some cases is limited, especially compared to MZ specimens. Interestingly, the stress-strain curves of CC(N) specimens differ slightly from those measured in Chapter 4. It is uncertain exactly why, but there are multiple factors that could be responsible: thickness of specimens, test configuration, initial cure time, etc. Further investigation might be necessary to understand how to best prepare and test GMCs with fiber coatings, but such an undertaking is outside the scope of this research.

6.1.3.4 Failure/Fracture surfaces

The failures of specimen types in four-point flexure were all slightly unique from one another. Figure 43 shows macroscopic views of the different specimen types at the displacement where failure occurred. The heat treatment environment did not appear to affect the damage observed on CL and MZ specimens so the images in Figure 43 do not distinguish between CL(A) versus CL(N) and MZ(A) versus MZ(N). The heat treatment

environment did have a small, noticeable effect on CC specimen types. All modes of failure were present in testing these samples: tensile, shear, and compression. For the CL composites a failure on the tensile surface was usually very recognizable. Still, even with the relatively long span-to-depth ratio and 4-point flexure configuration, the specimens did not split in half upon failure. Shear damage was consistently observed in all GMCs tested. The crack in CL specimens appears to have originated on the tensile surface, traveled a short distance perpendicular to the fiber, and then diverged along planes roughly parallel to the fiber. In other cases, the shear damage was disconnected and appeared both below and above the neutral axis (see Figure 45). The observed mode of failure in CL specimens is very similar to that recorded in Chapter 4.

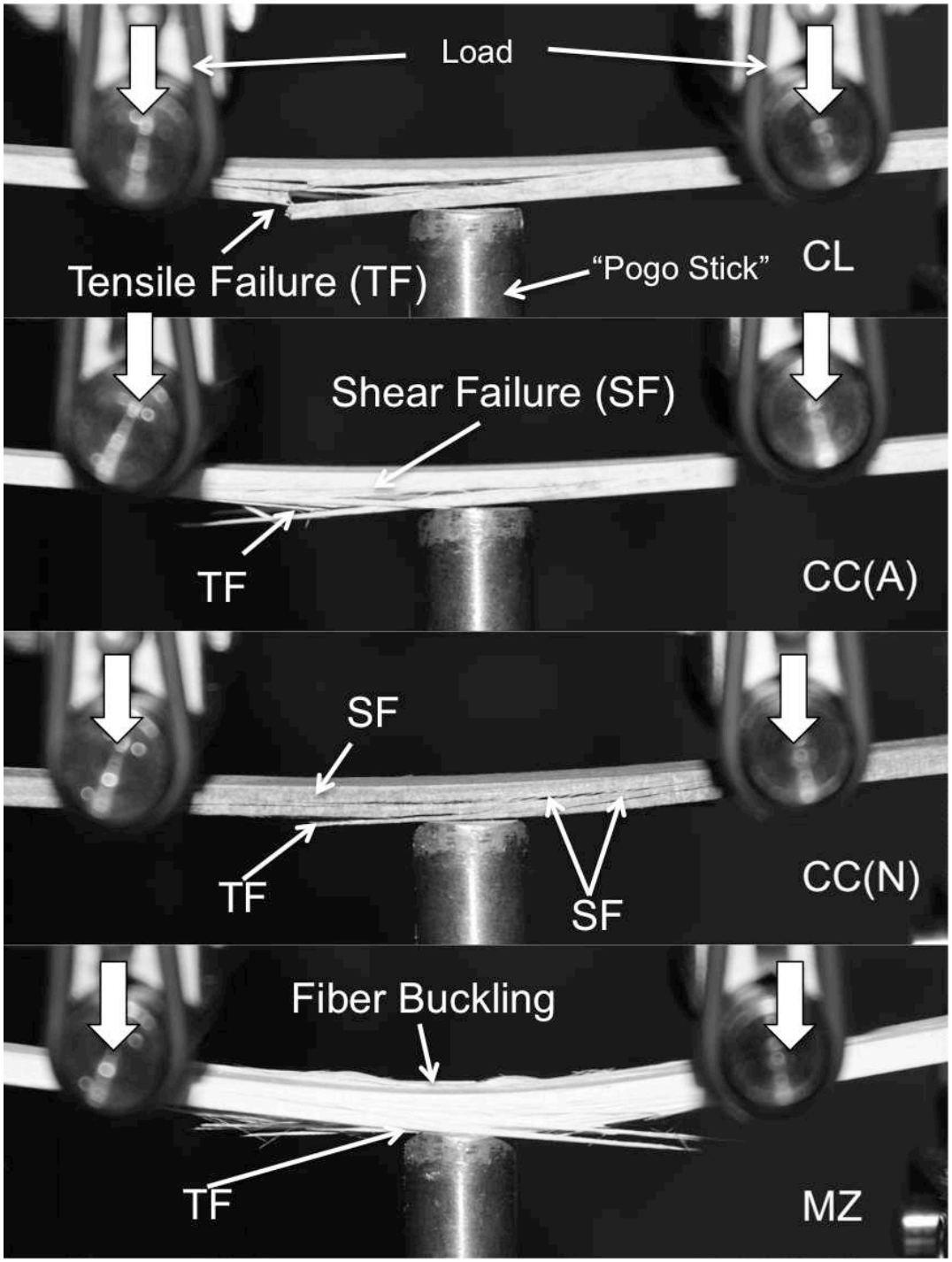

Figure 43: Representative images of each type of specimen post failure while still at full displacement.

As discussed in that chapter, the presence of shear damage in the CL specimens might be a strong indicator of the weakness of the matrix in shear. It is difficult to compare and

contrast the damage observed to other studies because of differences in the matrix (i.e. composition, initial cure, and final heat treatment), the reinforcement (type and orientation), and experimental setup. Additionally, many studies do not record failure modes. At present, only one study, as a part of doctoral thesis, has provided an adequate comparison. In that research, the failure of GMCs containing Nextel 610 fiber under three-point flexure was typified by a shear mode of failure [10]. In addition, the cure state and heat treatment of the matrix was different and discrete lamina and layers of matrix could be observed when viewing composite cross sections.

The coated specimen types were different from the CL composites in their macroscopic and microscopic failure appearance. Also in Figure 43, the damage produced on a typical CC(A) specimen after testing can be observed. The crack on the tensile surface of these specimens was less distinguishable than on the CL specimens. The crack quickly tracked diagonally towards the neutral axis of the specimen.

A crack on the tensile surface of the CC(N) specimens was even less distinguishable, almost appearing as a shear failure very near the surface of the specimen. In some cases any damage on the tensile surface of these specimens was not recognizable and failure appeared only to be the result of failure in shear like the samples measured on in Chapter 4. This result is, of course, interesting in the case of four-point flexure. Lack of tensile or compressive damage would suggest failure initially occurred at loading points or between each loading and support roller, but determining this is difficult to ascertain with certainty. Observing the tensile surfaces of specimens provide clues that specimens did fail in flexure

on the surface that was in tension. Figure 44 shows a crack meandering over the tensile surface of a CC(N) specimen.

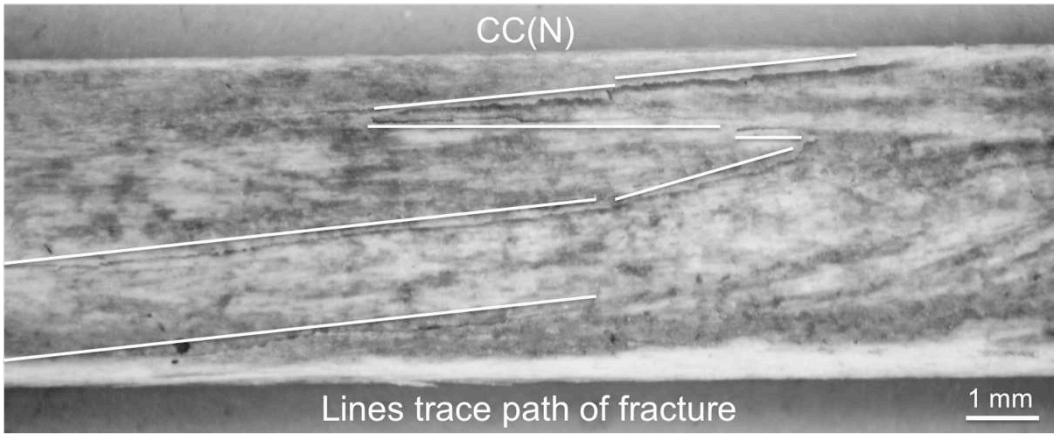

Figure 44: Micrograph of a CC(N) specimen showing a crack tracking across the surface of the composite beam. The surface shown is the surface that was subjected to tensile forces in flexure. The fibers of the composite run left to right on the page.

The image of the MZ specimen, in Figure 43, shows all three modes of failure present. The image does not depict the damage from shear very well, but shows failure on both tensile and compression surfaces as a result of fiber fracture and likely fiber buckling respectively. The presence of compression damage on some MZ specimens might also be partially due to the additional displacement that these specimens were able to endure before failure.

Figure 45 through Figure 48 are micrographs of the fractures observed in the different specimen types. The left and center images of each figure depict typical failures as observed from the sides of specimens in flexure (tensile surface of specimens shown facing top of the page). The far right image, in each figure, shows fracture surfaces of specimens after subjecting them to further displacement that caused them to split into separate halves (tensile surface of specimens shown facing out of the page).

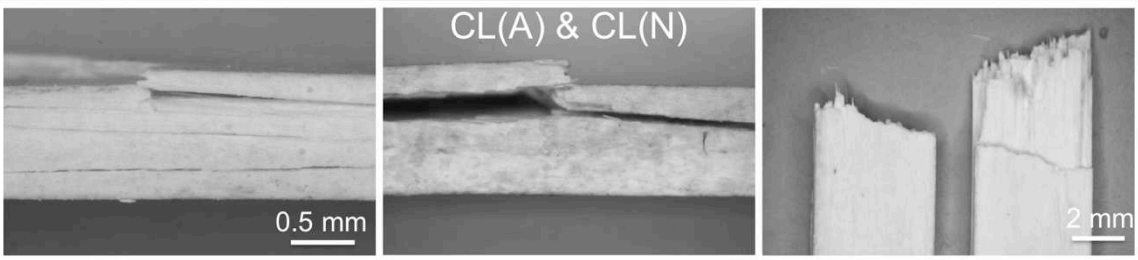

Figure 45: Typical damage in CL(A) and CL(N) composites as observed on the sides (left and center images) and fracture surfaces (far right image) after flexure. In left and center images, fibers run left to right on page, and tensile surface is facing top of page. In far right image, fibers run top to bottom of page and tensile surface is facing out of page.

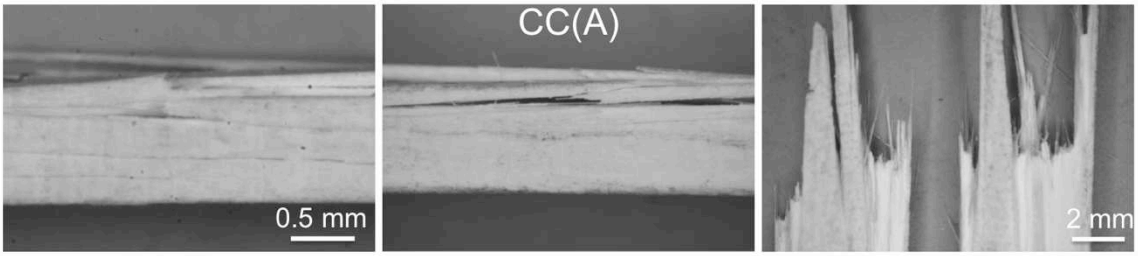

Figure 46: Typical damage in CC(A) composites as observed on the sides (left and center images) and fracture surface (far right image) after flexure

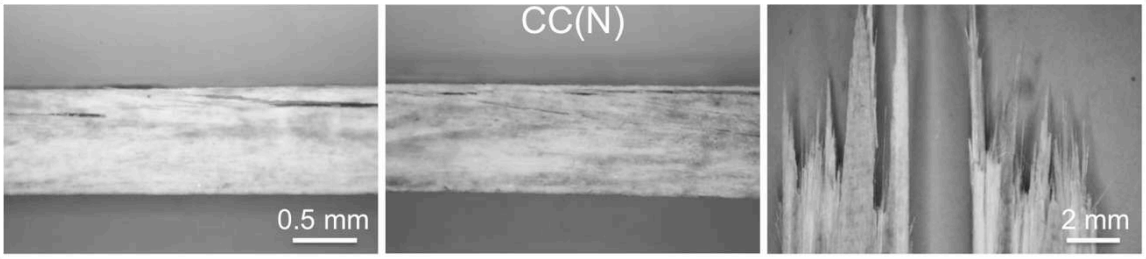

Figure 47: Typical damage in CC(N) composites as observed on the sides (left and center images) and fracture surfaces (far right image) of CC(N) specimens.

Figure 48: Typical damage in MZ(A) and MZ(N) composites as observed on the sides (left and center images) and fracture surfaces (far right image) of MZ specimens.

A failure on the tensile surface is evident in CL specimens. The same failure is present, but less distinct on CC(A) specimens. It is even less distinct for CC(N) and MZ specimens. Based on Figure 43, failure seems to have initiated on the tensile surface of these specimens, but the combined images still indicate substantial shear damage.

The damage on the sides of the CL specimens indicates brittle failure. Fiber fracture was clearly discernible on the tensile surface of these specimen types. Also, indicative of brittle failure were the fracture surfaces of CL composites, which are very planar. Recall, these specimens had the lowest measured value for toughness (see Chapter 6, Figure 39). The observed failures also agree with the catastrophic drop observed in the stress-strain curves of the CL specimens.

The stress-strain curves of CC(A) specimens were almost identical to the CL specimens, but the observed damage and fracture surfaces of the specimen types differ slightly from one another. Cracks on the tensile surface of these specimens tended to propagate diagonally or run a very short distance from the tensile surface before diverting. The shear damage seems to be very similar to that observed in CL specimens. The fracture surfaces are more tortuous than CL and show some individual or small groupings of fibers suggestive of fiber/fiber bundle pullout.

CC(N) specimens showed the same increases in strength, toughness, and damage tolerance over both CL and CC(A) composites. The failure of the CC(N) specimens appears to be shear dominated. However, Figure 44 provides evidence of a crack tracking across the

tensile surface of these beams. As already noted, this was sometimes difficult to locate in these specimens. Shear damage appears to be limited to only the halves of the specimens subjected to tensile stresses. In comparison to CL and CC(A) composites, the damage observed in these specimens does not seem to be as extensive. The resulting difference in damage between these specimen types may help explain why CC(N) specimens failed non-catastrophically. The two fracture surface halves of CC(N) specimens appear to be similar to CC(A). However, for CC(N) specimens the plane of fracture is less distinct (i.e. greater tortuosity) and what appears indicate more individual fibers present.

The failures of the MZ specimens as represented in Figure 43 and Figure 48 indicate the presence of all three failure modes. In some cases, the composite beam surfaces that were subjected to tension in flexure had a fibrous-like appearance. The damage on the sides of specimens often showed an extensive network of localized shear damage. This damage was unique to MZ specimens.

6.2 Tensile Testing

6.2.1 Specimen preparation

Composite specimens used in tensile testing were fabricated using the methods described in Chapter 3. Specimens were harvested from sample sticks using a diamond wafering blade to produce specimen dimensions of 178 mm (length) x 4.5 mm (wide) x 1.0 mm (depth).

Tensile specimens were tabbed to prevent crushing of samples in the grips (see Figure 49). Tabs were ~4.8 mm thick and ~38 mm long including the tapered section. The taper was 15°. G10 was used as the tabbing material and bonded to specimens using Epon 828 and Epikure 3140 resin system. Tabbing of specimens was done according to guidance in ASTM 1275 and a composite tabbing guide [15], [42]. Tab and specimen surfaces were sanded and cleaned prior to adhesion.

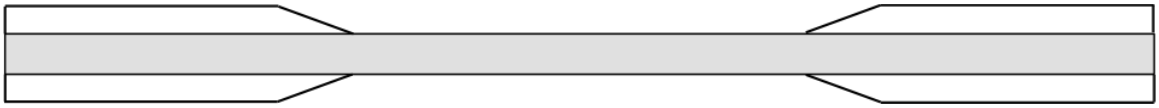

Figure 49: Depiction of specimen used for tensile testing. Tabs are shown in white. NOTE: Drawing not to scale.

6.2.2 Test Method and Calculations

Tensile testing was conducted in accordance with ASTM C 1275 [114]. Specimens were held in place by two wedge action grips (see Figure 50). The grips work by actively increasing the gripping force with increasing load in order to ensure specimens do not slip.

Figure 50: Typical configuration for tensile test of composite specimens.

Tensile specimens were tested in displacement control mode at a rate of 0.18 mm/min. Load and displacement as a function of time were recorded. Displacement was measured using a contact extensometer mounted as shown in Figure 50. The extensometer was placed with contacts on the side of specimen with greater moment of inertia to limit strain from bending. The extensometer gage length was 25.4mm. Testing was ceased after specimen fracture. Tests were considered valid if the specimens failed within approximately 25 mm of the center of the gage section. Breaking force of specimens that were non-gage section failures were only considered valid if the resulting tensile strength was within 10% of the tensile strength of specimens that broke within the gage section. A total of at least three validated tests were to be used to present average tensile strength of

each type of composite specimen. Due to the difficulty in obtaining failures within one gage length of center and effort involved in creating each individual specimen, a total of three tests for every specimen type could not be achieved. Table 13 shows the number of validated tests for each test condition.

Table 13. Total number of valid tensile tests at the given conditions

Fiber Type	Number of valid tests for each specimen type	
	650 °C in air (5 hours)	650 °C in N_2 (5 hours)
Cleaned (CL)	3	5
Carbon coated (CC)	2	3
Monazite (MZ)	2	4

Tensile strength (S_u) and strain (ϵ) of specimens were calculated using the following relationships from ASTM C 1275 [114]:

$$S_u = \frac{P_u}{A} \tag{6.5}$$

$$\epsilon = \frac{l - l_0}{l_0} \tag{6.6}$$

where, P_u is maximum force recorded, A is the original cross sectional area measured by average width and thickness where failure took place, l is the extensometer gage length at any time, and l_0 is original extensometer gage length. Modulus was calculated using a regression curve on the linear portion of the stress-strain curves.

Like the results of flexure testing, measurements for strength and modulus were averaged amongst the specimens of each type. The error bars on the chart indicate one standard deviation. Values of modulus for all specimens were normalized to a 45% fiber volume fraction (V_f) for the purpose of comparison. Strengths were not normalized for the same reasons previously discussed in Section 6.1.2.

Recall, the purpose of tensile testing was to investigate the fracture surface of specimens. The measured mechanical properties presented in this section are meant to add to the very limited amount tensile data contained in research on GMCs and support the results of flexure testing presented in the previous section.

6.2.3 Results

6.2.3.1 Mechanical properties

The Young's Modulus results are shown in Figure 51. Once again, there is no clear disparity in modulus between specimen types and their respective heat treatment environments. This result provides further assurance that the incorporation of the carbon and monazite interphases do not negatively affect the modulus of these particular GMCs.

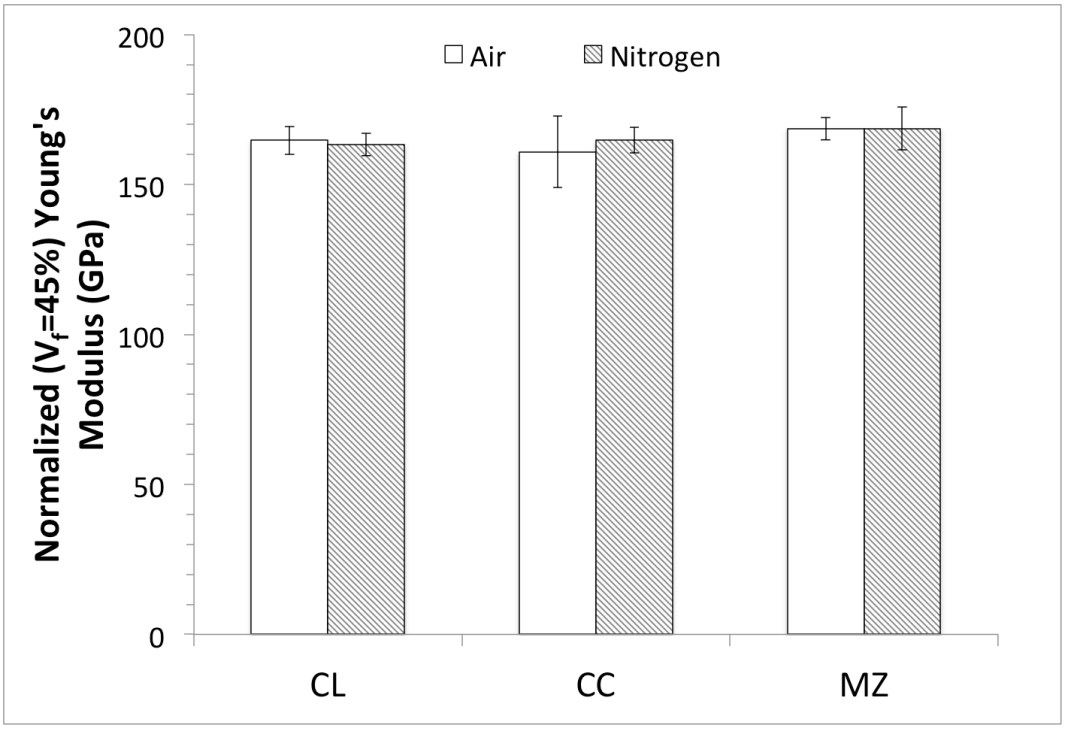

Figure 51: Normalized tensile modulus of geopolymer matrix composites based on a 45% fiber volume fraction

The measured tensile modulus appears to be a bit lower than that measured for the flexural modulus of the same specimens in Section 6.1.3.1. The values for modulus obtained from tensile testing more closely align with the predicted Rule of Mixtures (RoM) value of 175 GPa calculated for flexural testing. The measured moduli of composite specimens in tension are ~92-96% of the value predicted by RoM. However, it might be more appropriate in this case to use the higher predicted modulus value of 182 GPa for comparison. This RoM value was derived from a value of the unreinforced matrix obtained in compression rather than flexure, as described in Section 4.3.1. If this value is used, the range falls to roughly ~88-93% of that predicted by RoM and more closely parallels those values obtained in the three-point bending studies.

The tensile strengths of specimen types are shown in Figure 52. For all fiber types, the average measured composite tensile strength appeared to decrease slightly for specimens heat treated in nitrogen. This is different from the results of flexure. However, a t-test suggests that there is no statistically significant difference in strengths based on heat treatment environment. Such an outcome was expected except in the case of CC specimen types.

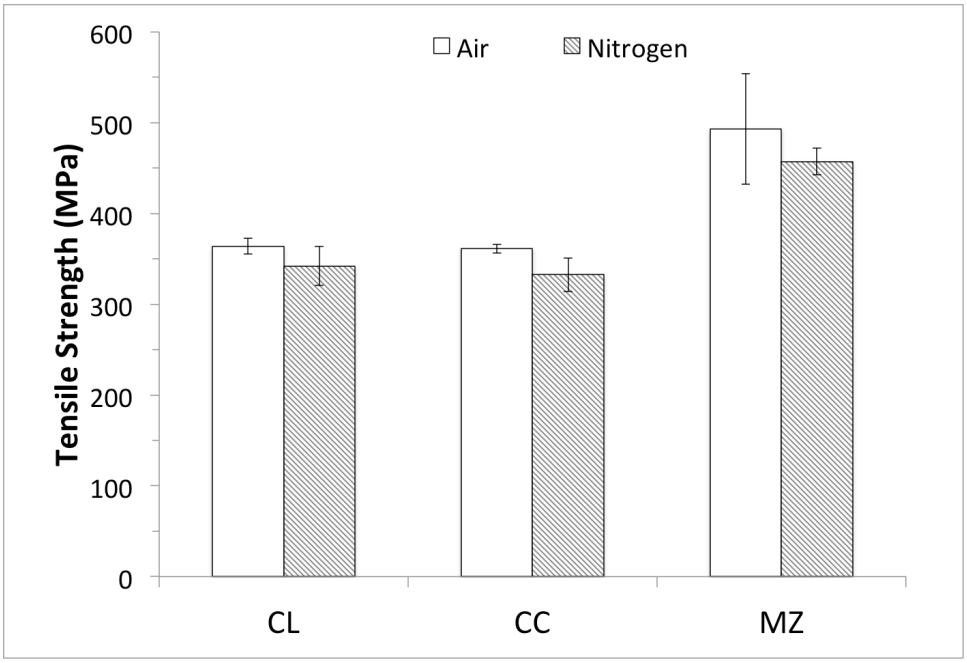

Figure 52: Tensile strength of geopolymer matrix composites

Measured tensile strengths were lower in magnitude than measured flexural strengths, yet the tests show the same trend. Samples containing monazite fiber coating have greater tensile strength than other specimens. The increase in strength MZ specimens is on the order of 34% regardless of environment as compared to CL specimens. Recall, like the MZ flexural specimens, the MZ tensile specimen types that were fabricated contained a lower fiber volume fraction than CL and CC. No additional tensile testing was conducted to

analyze the effects of a lower V_f, as was done for flexural test specimens. It was assumed the decrease in V_f did not enhance the strength of MZ tensile specimens, based on theory and the results obtained in flexure.

6.2.3.2 Toughness and damage tolerance

Calculated values of toughness and stress-strain curves are not presented for tensile specimens. The toughness of MZ specimens was superior, but only because of the measured gains in strength. The stress-strain curves of all specimens types tested in tension were linear-elastic until failure. Failure was catastrophic in all cases. No significant increase in damage tolerance was observed for any the specimen types.

6.2.3.3 Fracture Surfaces

While stress-strain curves do not reveal differences in behavior between composite types, the fracture surfaces of specimen types do differ. The fractured halves and surfaces of specimens are depicted in the micrographs of Figure 53. The baseline cleaned fiber specimens demonstrated a brittle fracture. Brittle fracture is typical of low toughness materials.

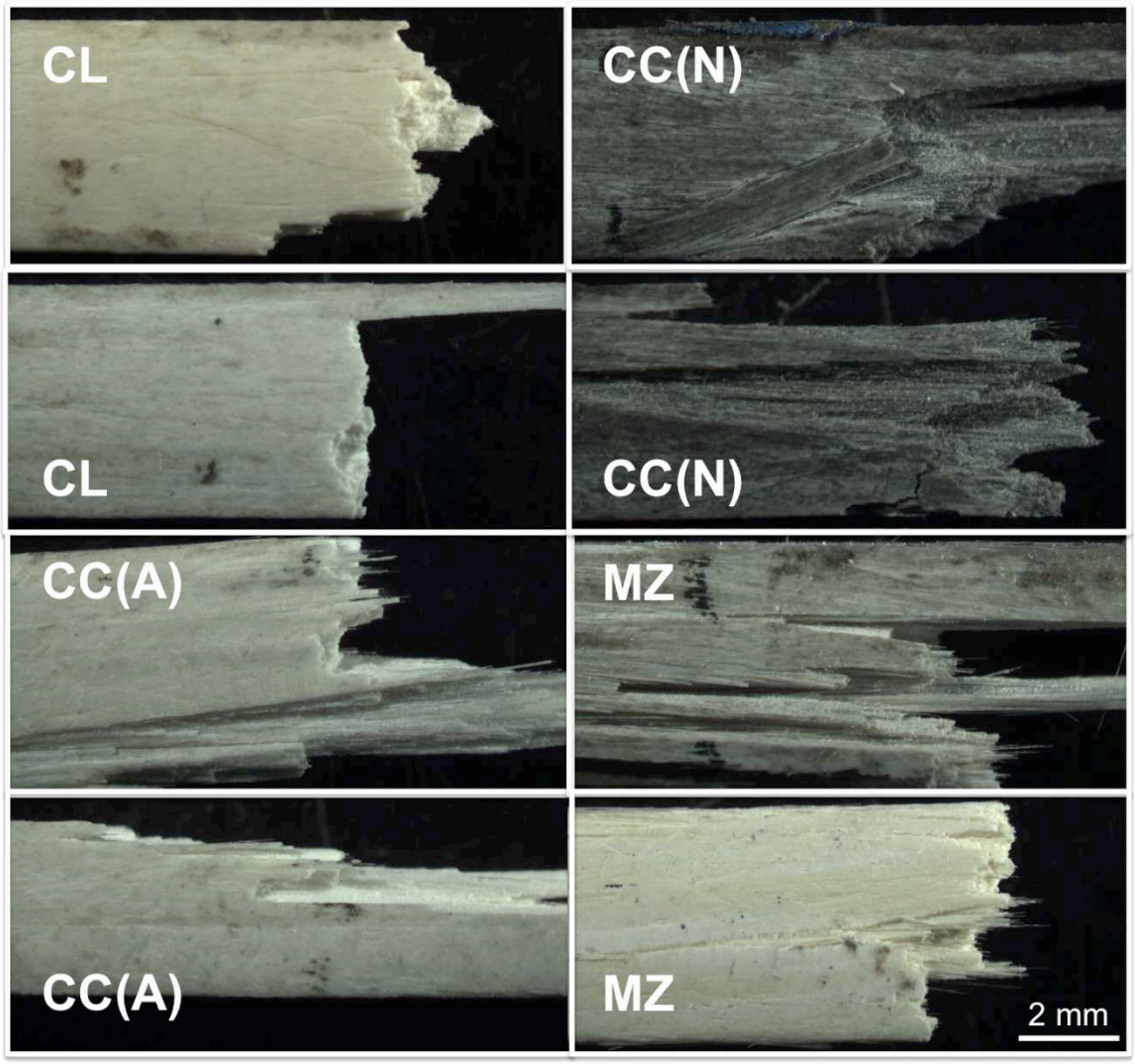

Figure 53: Fracture surfaces of GMCs tested in tension

For CC, specimen types, the fractures were not consistent, even amongst specimen types heat treated under the same environmental conditions. Some fracture surfaces of CC specimens indicated brittle behavior (not shown) like the CL specimens, while others showed fractured halves that were non-planar. Specimens that did not fail in a planar fashion often appeared very jagged with masses of fiber and matrix extending from the fracture surface suggesting the composite failed in different locations throughout the

length. Splitting of the composite was observed along directions parallel to fiber or at a slight angle to the fiber direction. This type of failure might be expected for composites with weak interfacial strength [114]. In some cases, the failures were comparable to those observed in a CMC with N610 monazite coated fiber (see Figure 54).

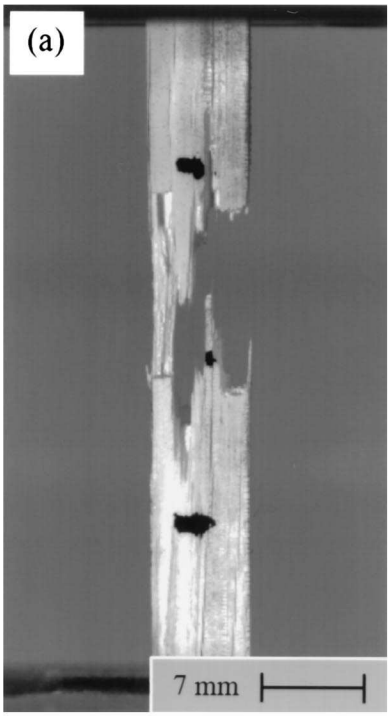

Figure 54: Broken CMC test sample containing unidirectional N610 monazite coated fiber [73].

All MZ specimens that underwent tensile testing failed in one of two different ways as represented in the lower right hand corner of Figure 53. They either split as discussed above or seem to fail along a single, slightly angled plane. In the case, where the fracture surfaces of MZ specimens were planar, there appeared to be evidence of individual fibers present, or fiber pullout. The amount of pullout present is clearly less than was observed for flexural specimens. However, even the very small amount present in MZ tensile specimens causes them to appear different from the CL tensile specimens.

6.3 Short Beam Strength

6.3.1 Specimen preparation

Short beam shear (SBS) test specimens were harvested from the samples prepared for flexure testing. The details for the preparation of composite sample sticks can be found in Chapter 3. SBS specimens were each nominally 15 mm in length and 4.5 mm in width. The thickness of SBS specimens were nominally 1.5 mm, but varied in a similar manner to the flexural specimens (see Section 6.1.1). A total of at least six specimens were prepared for testing from each of the composite types.

6.3.2 Test method and calculations

SBS testing was conducted in accordance with ASTM D2344 except as otherwise noted. Specimens were tested in a 3-point flexure configuration with a support span of 11.1 mm. The loading and support cylinders were 6 mm and 3.175 mm in diameter, respectively. The length of the support span resulted in specimen span-to-depth ratios slightly outside the recommended 4:1 ratio per ASTM D2344. The span-to-depth ratios of specimens were more on the order of 6:1 to 7:1. Beam theory encourages a larger span-to-depth ratio to reduce the likelihood of shear failure. The larger ratio produces higher tensile/compression stresses on the outer surfaces of the beams for the same applied load. That said, classical beam theory fails to describe the stress state accurately in the specimen for such short a short span [127]–[130]. It has been suggested that that a slightly higher ratio may be a more favorable configuration for SBS testing because of loading cylinder induced stresses [131].

Testing was conducted in displacement control mode at a rate of 1.27 mm/min. Load versus time was recorded for each specimen. Only peaks loads were used to calculate short-beam strength. After testing, specimens were examined to determine the mode of failure. Specimen modes of failure were categorized as shear, flexure, or mixed. Specimens that failed in flexure were noted as tensile or compressive based on the failed surface. A specimen categorized as "mixed mode" did not show a clear type of failure to warrant a distinction between shear and flexure.

Short-beam strength (F_{SBS}) was calculated using the following relationship from ASTM D2344 [127]:

$$F_{SBS} = 0.75\frac{P_u}{bd} \tag{6.7}$$

where, P_u is maximum force recorded, b the width of the specimen, and d is the thickness of specimen as previously designated in Sections 6.1 and 6.2 above. The bars on the following graph indicate one standard deviation.

6.3.3 Results

The short-beam test method is generally used to qualitatively assess similar composite types against one another and as means for a quick analysis of quality control. In most cases, short beam strength is not a clear indication of any material property due to the complexity of the stress state [127]. For this research, SBS testing was conducted as a means to evaluate the different interfacial conditions with the expectation that those composite types with coatings would show differences in their short beam strength

because of the bonds created at the fiber-matrix interface. Figure 55 shows the short-beam strengths of each specimen type. All specimen types except for CC(N) are very similar in magnitude. The disparity in values between CC(A) and CC(N) indicate an effect from the heat treatment environment. As already noted in previous sections, this was expected based on the limited oxidation resistance of carbon at temperatures above 400 °C.

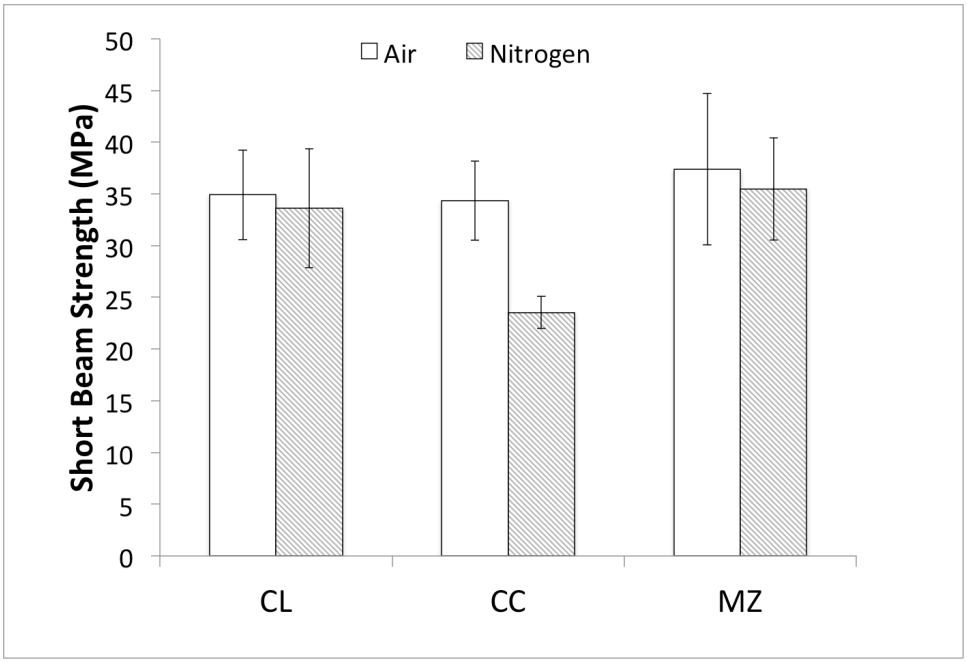

Figure 55: Short beam strengths of geopolymer matrix composites

The values of short beam strength are very similar amongst the specimen types except for CC(N). However, SBS test results should also be interpreted based on type of failure observed. The following chart, Figure 56, depicts the number of times each mode of failure was observed within a specimen type. To clarify, the word tensile in Figure 56 refers to a failure of the specimen in flexure on the tensile surface. Compressive damage was not apparent on of any of the SBS specimen types that failed in flexure.

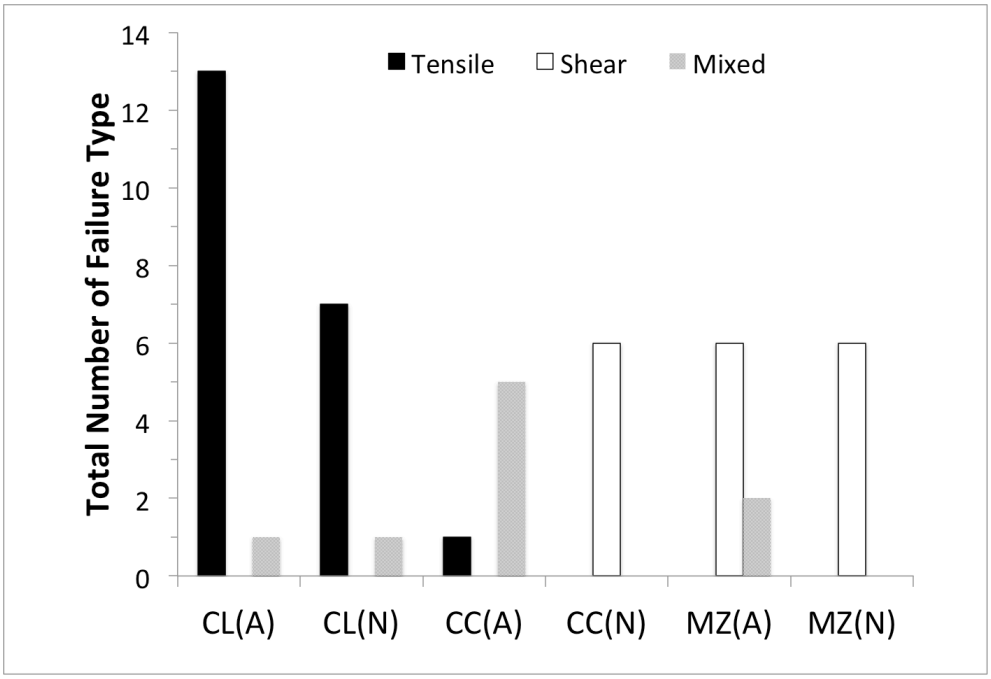

Figure 56: The number of failure type observed in SBS testing for each of the different specimen types. "Tensile" refers to failure in flexure on the tensile surface of the beam.

The chart clearly indicates the predominant failure mode in CL specimens to be flexure originating on the tensile surface. Such a failure is an invalid test according to the ASTM [127]. That is why the y-axis is labeled "Short-beam strength" in Figure 55 rather than "Short-beam shear strength." Figure 57 shows a set of three CL specimens after being tested in SBS. Once again, the similarity between CL(A) and CL(N) specimens did not warrant a distinction, so Figure 57 is representative of both types. The failure of these specimens in flexure is very apparent. The crack in these specimens traveled almost all the way through the thickness before stopping. The observed failure in CL SBS specimens is akin to the damage observed in 4-point flexure except the crack traveled a almost all the way through the thickness of the SBS specimen and there is less observable shear damage

(see Section 6.1). Considering the imposed stress states of the two flexural tests conducted in this research, the resulting damage is opposite of expectations.

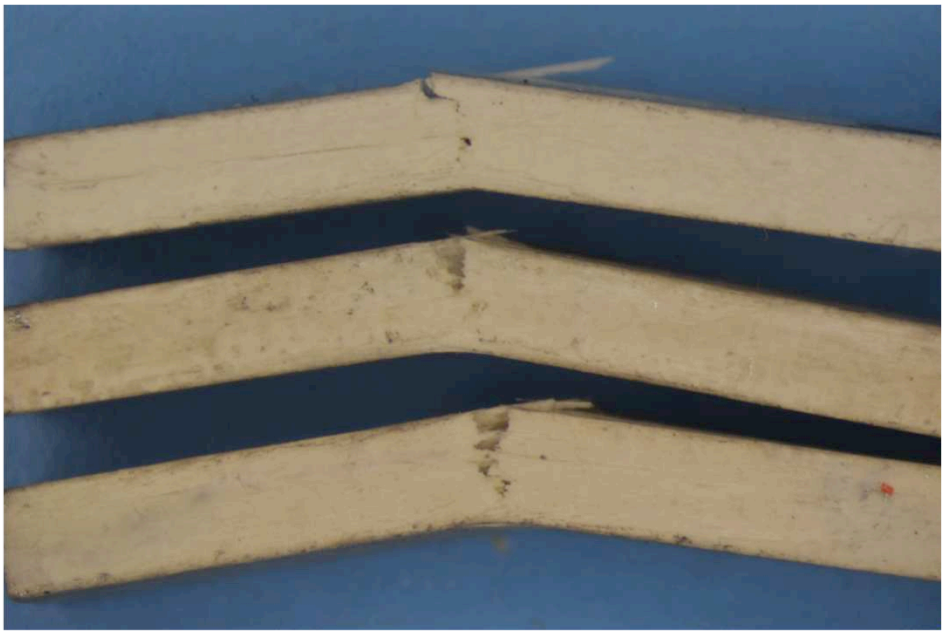

Figure 57: The damage incurred on CL specimens from SBS testing. Fibers run left to right on the page and surface of beam that was in tension is facing top of page.

The mode of failure for specimens with coated fibers is relatively different from the mode of failure noted for the CL composites. The failure mode of CC(A) specimens was not distinct, which is also an invalid test according to the ASTM[127]. Figure 58 shows both modes of failures, flexure and shear, were present in CC(A) specimens. The arrows in the figure highlight the shear damage noticed in each specimen. The arched disposition of specimens in the figure and damage on tensile surface of specimens appears to indicate failure in flexure prior to shear, however, due to the presence of both, the failures were categorized as mixed.

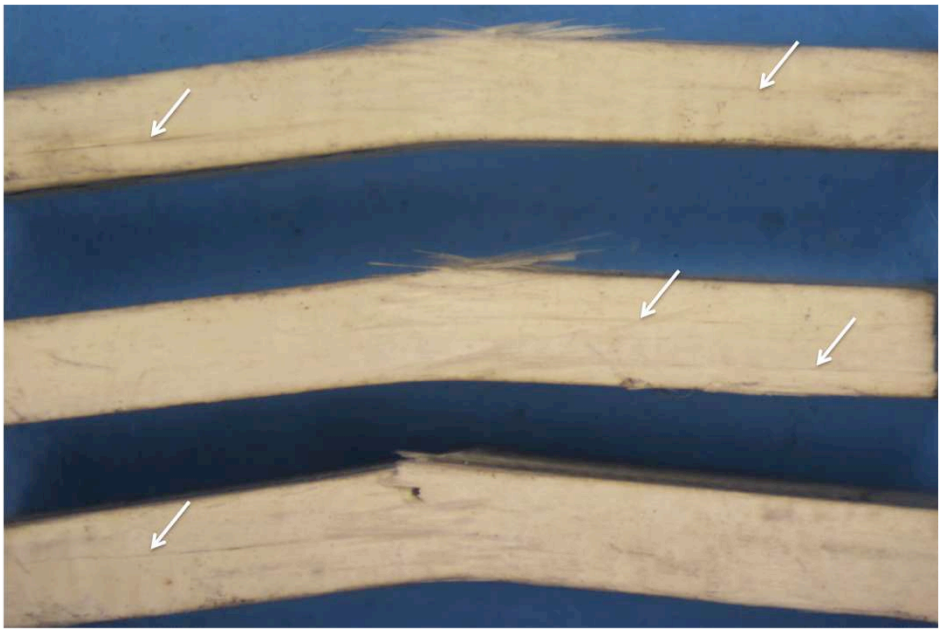

Figure 58: The damage incurred on CC(A) specimens from SBS testing. Arrows indicate lines that suggest shear failure.

An examination of damage surfaces in the CC(N) specimens after SBS testing revealed that the specimens failed in shear. This helps explain the difference in observed short beam strength of the CC(N) specimens. The strength and failure mode differences in SBS testing also corresponds to the differences previously observed in stress-strain curves of CC(A) and CC(N) flexure specimens. Figure 59 shows a set of three CC(N) specimens after undergoing a SBS test. The image shows shear as the single failure mode. This allows the short beam strength value to be interpreted as value of the shear strength. The particular methods of examination performed on SBS specimens did not allow clarity as to whether the shear failure was along the interface rather than through the matrix. However, in considering the difference between CC(N) and the CL specimens it is very likely that the difference in failure mode is the result of changes made at the interface (i.e. the presence of the fiber coating).

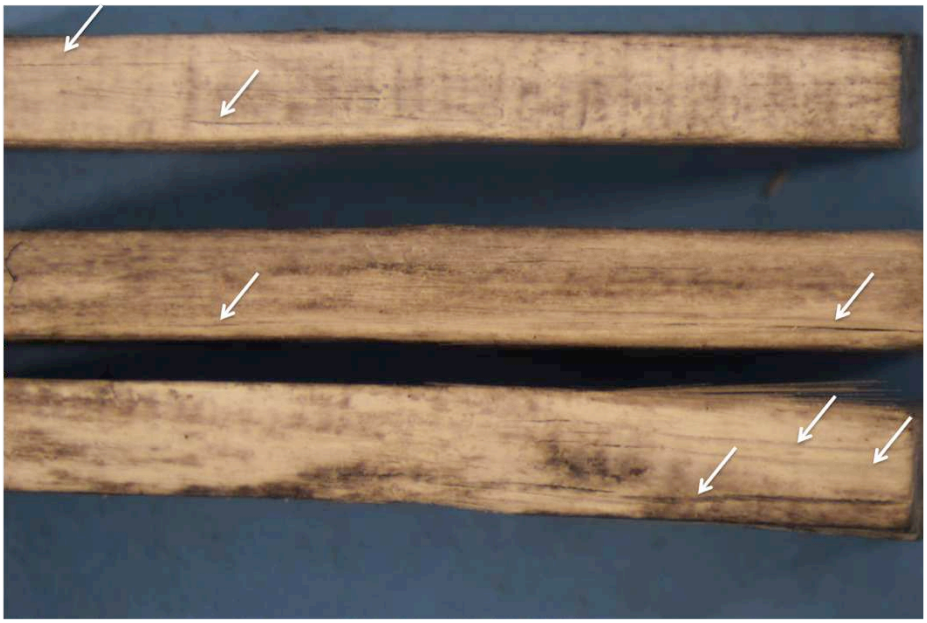

Figure 59: The damage incurred on CC(N) specimens from SBS testing. Arrows indicate lines that suggest shear failure.

The failure mode of MZ specimens was primarily shear as Figure 60 indicates. The single failure mode observed in MZ specimens means the short beam strengths of CC(N) and MZ specimens can be compared. Based on the measured values it would indicate the interfacial strength in MZ composites, as determined by SBS testing, is approximately ~34% greater than that in CC(N). What was also interesting to note about the short-beam strengths of MZ specimens was that they were similar in magnitude to CL, but the specimens did not fail in flexure. The results of flexure would lead one to expect that both composites would demonstrate failure of the fiber on the tensile surface for the same state of stress. However, this was not the case in SBS testing. It is also worth noting MZ and CC(N) being the only composites to fail predominantly in shear in SBS testing also were the only specimen types to exhibit increases in toughness and any degree of damage tolerance as measured from 4-point flexure testing.

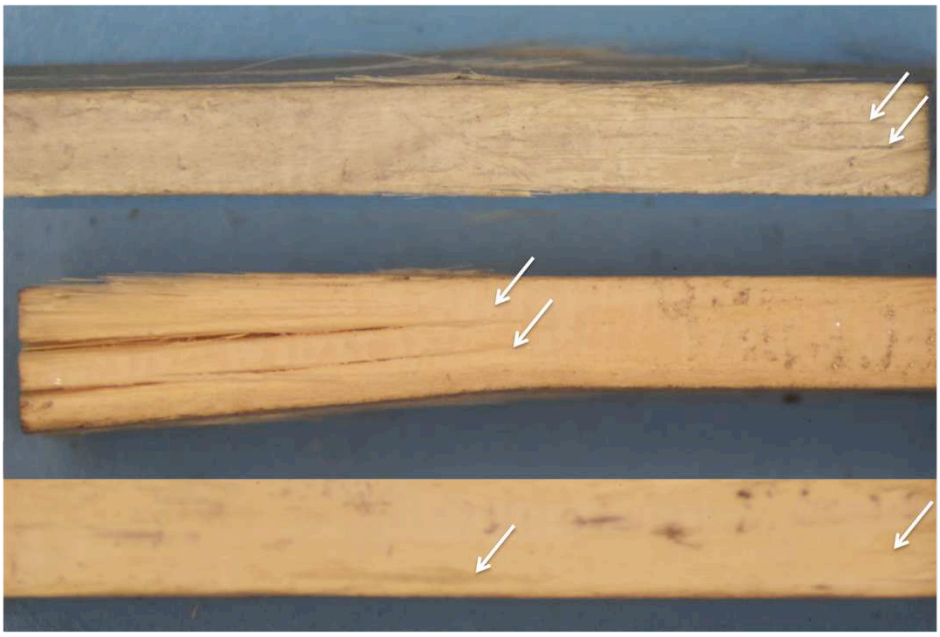

Figure 60: The damage incurred on MZ specimens from SBS testing. Arrows indicate lines that suggest shear failure.

6.4 Push-out Testing

6.4.1 Specimen preparation and experimental procedure

Fiber push-out specimens were prepared by first taking ~2 mm thin cross sections (fibers oriented perpendicular to the flat side) from each of the different sample types and embedding them in an epoxy that does not infiltrate well in order preserve the original composite nature especially the interfaces. The 2 mm thick sections were harvested from composite samples that were fabricated according to the processes prescribed in Chapter 3 including the final heat treatment. A series of grinding and polishing steps were then performed on both sides of the embedded section. Using a fine diamond embedded grinding plate, the epoxy was removed to expose the specimen surface. The specimen was

then polished using diamond lapping films starting at 15 microns and ending at 1 micron. A gentle back and forth motion was used to polish rather than a rotating wheel. The process was then repeated for the opposite side of the specimen to produce two polished surfaces for microscopic observation. A tripod jig, specifically created for polishing, was utilized to ensure flatness of specimens. The final thicknesses of push-out specimens were between 130 and 160 μm.

Fiber push-out tests were conducted at Wright-Patterson AFB. The testing apparatus shown in Figure 61, consisted of a stereo microscope connected to a monitor for viewing, an indenter, and a computer to run the test software. To push fibers, a conical, diamond flat-tipped indenter with an 8 μm diameter was used.

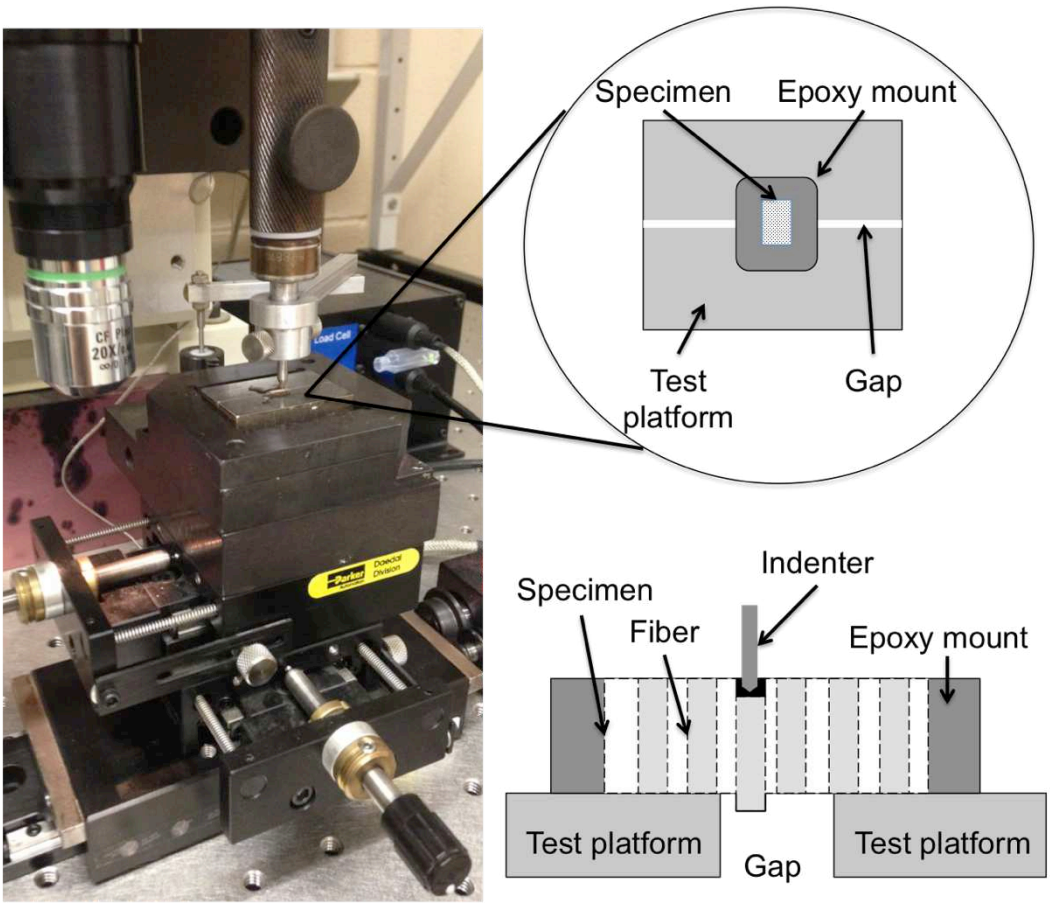

Figure 61: Push-out test apparatus and drawings of test platform setup.

Note: drawings are not to scale

Specimens were mounted over a small gap on steel test platform (see Figure 61). The gap allowed for the fiber to be pushed through the specimen (i.e. fiber push-out versus fiber push-in). To perform a push of a fiber, the test platform was set under the optical microscope. A video feed overlaid with cross-hairs allowed the designated fiber to be centered under the lens and correspondingly with the indenter probe. Once centered, the fiber diameter was measured using the push-out testing software and recorded. The test platform was then moved under the probe to perform the test. The indenter test speed was 15 μm/min. Load versus displacement was recorded for each test. Upon completion of the

test, the specimen was moved back under the microscope. An image prior to and after pushing was recorded for each fiber tested. The before and after images, as well as, the plotted data was used to draw conclusions about the validity of the test. In some cases, the indenter would shift off center resulting in poor data and/or indirect hit on the fiber. Usually, this was discovered and the test was repeated. Figure 62 shows before and after images of a pushed fiber that resulted in a valid test.

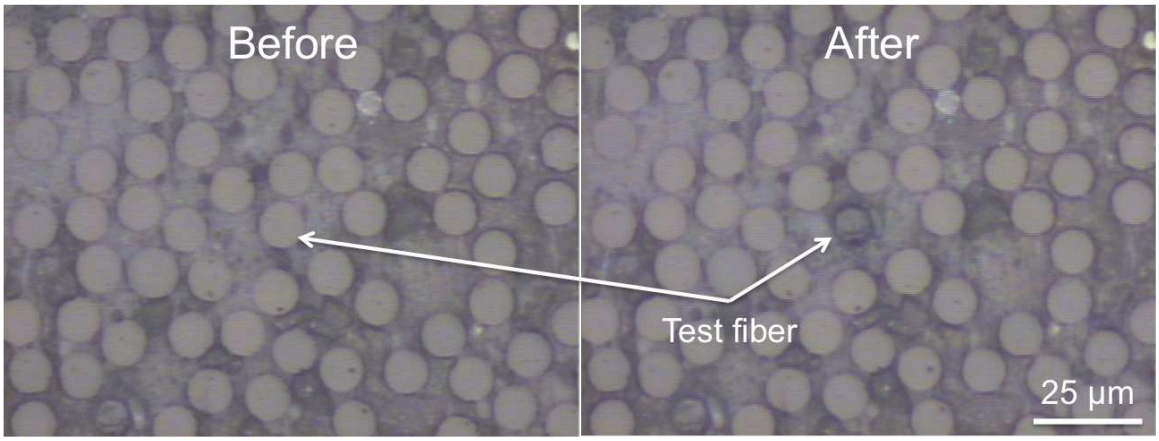

Figure 62: Before and after images showing a valid push-out test.

A total of ten fibers in each sample type were pushed and evaluated. The load-displacement traces measured during the fiber push-out test were analyzed using the model of Parthasarathy *et al* [54], [132]. The traces were corrected for machine and specimen compliances, and then fit to an analytical model, in order to extract the key interface parameters. These parameters include debonding energy, friction coefficient, interfacial roughness amplitude, and the roughness period. The residual stress was assumed to be negligible as the matrix had very low modulus compared to the fiber and coating. Values of interface toughness (debond energy) and friction stress are presented in

the following sections. In addition to these measures, Scanning Electron Microscopy (SEM) was used to observe pushed cross-sectional surfaces for evidence of pushed fibers.

6.4.2 Results

Figure 63 shows the debond energy and friction stress calculated from push-out data. The debond energies shown in the chart depict a decreasing stepwise pattern moving from CL to CC to MZ, respectively. Friction stress also varies between specimen types with CC(N) specimens having the lowest recorded values. In comparison to CMCs in other studies the values are high [53], [73].

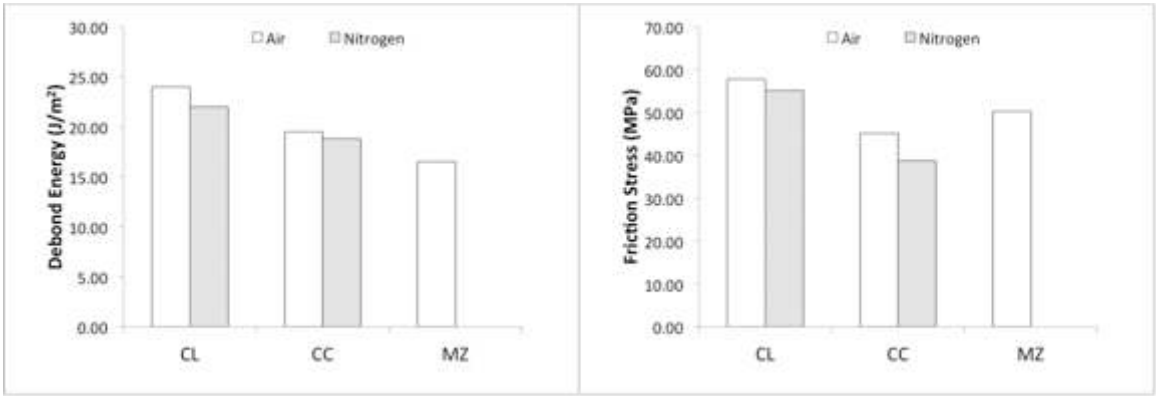

Figure 63: Debond energy and friction stress of GMCs tested in single fiber push-out

The results for MZ specimens heat treated in an inert environment are not shown because the debond energy was determined to be skewed based on observations that the indenter contacted both matrix and fiber therefore elevating the recorded load at debonding. This still resulted in a push of the fiber, but debond energies that were well above that of the CL specimens and incongruent with the MZ(A) specimens. As a result, not only are the averages higher, but the standard deviation for MZ(N) specimens was almost six times greater than for MZ(A) specimens. Figure 64 shows the debond energy for pushed fibers in

MZ(N) composites. Also shown in Figure 64 are SEM images of just a few of the fibers that had debond energies well above those of MZ(A) specimens. The arrows in the figure indicate damage around the edge of the fiber from the indenter, which are likely to be responsible for the larger measured debond energy in these specimens.

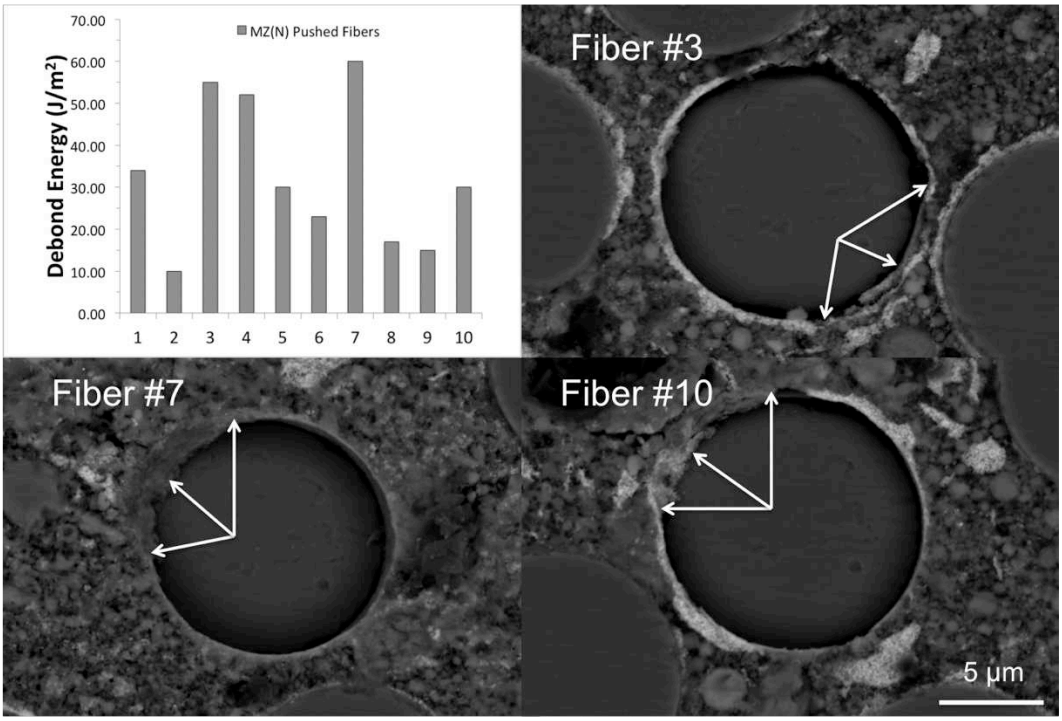

Figure 64: Debond energies of fibers in MZ(N) specimen and SEM images of select pushed fibers showing damage to matrix caused by indenter

The debond energy of specimen types are all different, but relatively close in value. The small difference, however, is significant enough to result in different push-out behavior. Using SEM with backscatter, specimen cross sections were observed after push-out. Figure 65 shows images of the pushed-in side (Figure 65a,c,e) and pushed-out sides (Figure 65b,d,f) of all specimen types heat treated in air.

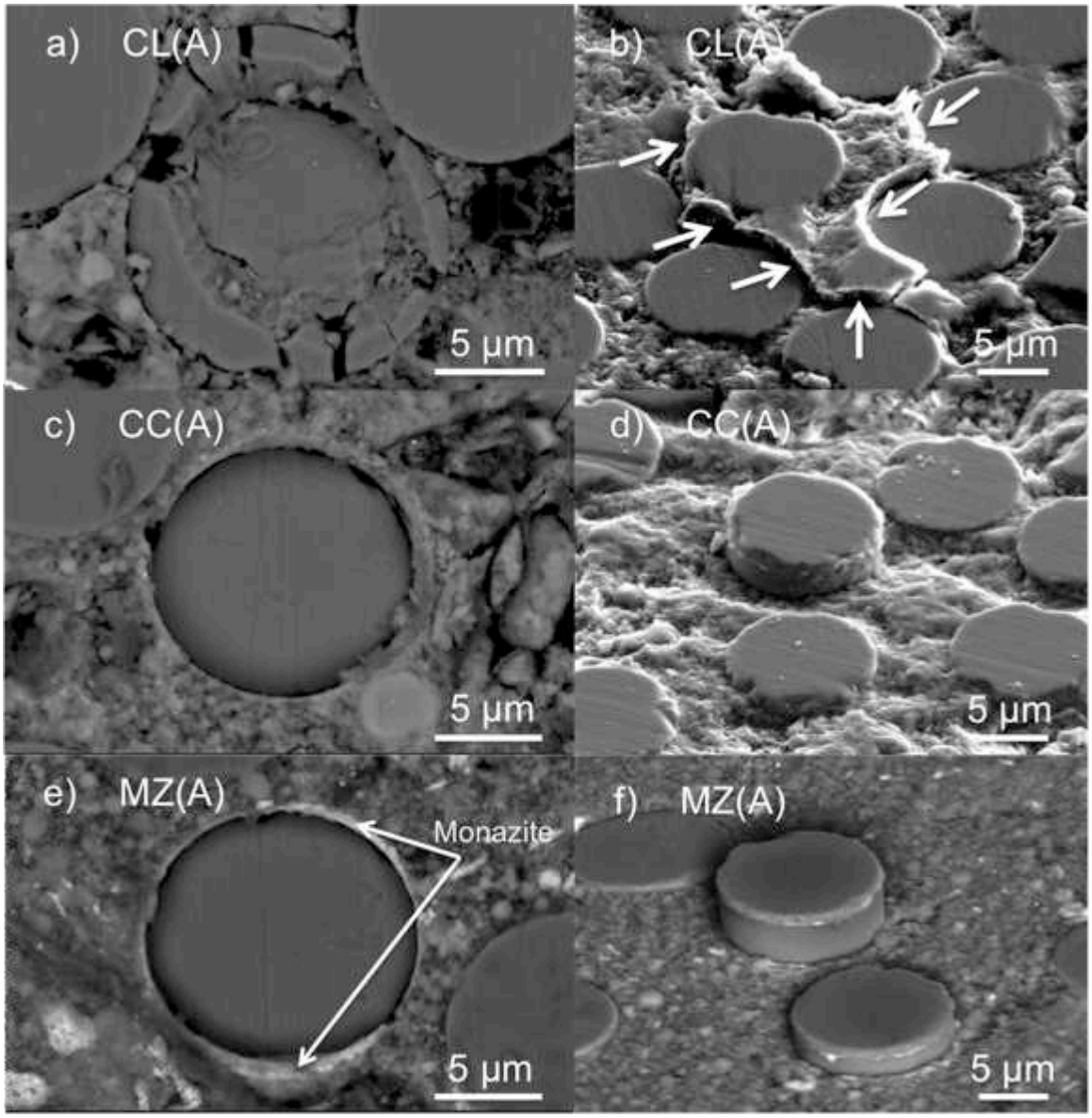

Figure 65: Representative SEM images of push-out in GMC specimens exposed to oxidizing atmosphere during heat treatment. Images a), c), & e) are taken from the side of the specimen where the fiber was pushed. Images b), d), and f) are from the opposite side. Arrows in b) were added to highlight pushed fiber and attached matrix.

Except in the case of CC(A) the images of pushed fibers are representative for specimens subject to both heat treat environments. The images of the CL specimens imply a strong bonding condition between fiber and matrix. This agrees with both the results push-out data (measures and SEM) and low values of toughness measured in section 6.1. Pushed

fibers in CL specimens were often found crushed by the indenter (see Figure 65a). On the pushed-out side of the sample, fibers either did not push or were observed with large amounts of matrix still attached to the fiber (refer to Figure 65b).

For all other specimen types, fibers pushed without the indenter damaging the fiber. Figure 65c & d shows a pushed fiber of a CC(A) specimen. The surface of the CC(A) fiber that was pushed out appears rough, especially in comparison to MZ(A) and CC(N) fiber surfaces (Figure 65d and Figure 66, respectively). In one case, CC(A) fibers that had been pushed out had a portion of the matrix still attached to it. All CC(N) fibers appeared smooth after being pushed. The difference may explain the slightly higher friction stress of CC(A) specimens versus CC(N).

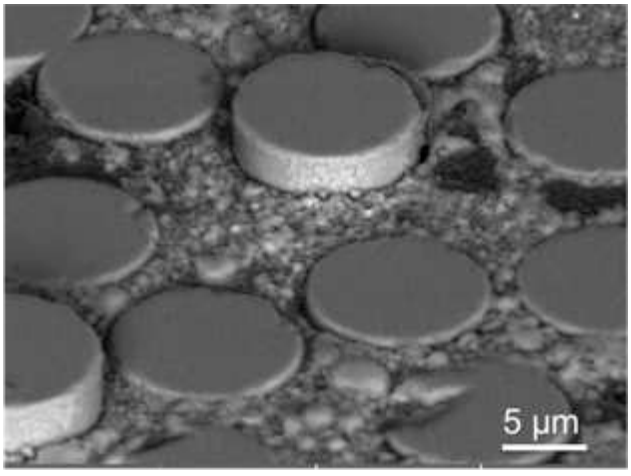

Figure 66: SEM image showing the pushed fiber of a CC(N) specimen

Pushed fibers of MZ specimens are shown in Figure 65e & f. The average debond energy of MZ(A) specimens were lower than CL and CC specimen types. Friction stress of MZ(A) specimens was higher than CC composites. They were also lower than CL specimens. Yet,

as Figure 65b indicates, the friction stress values obtained for CL specimens are not comparable. Interestingly enough, pushed fibers from MZ specimens were smooth and did not show any signs of monazite or matrix material on the fiber. Examination of the fiber socket where fibers were pushed only revealed trace amounts of the monazite coating. It may be just that it is difficult to discern. The two SEM images in Figure 67 taken from a flexural specimen shows monazite on fibers and in fiber troughs, suggesting that fracture was not preferential to one surface. This behavior was observed in another study with monazite fiber coatings [73].

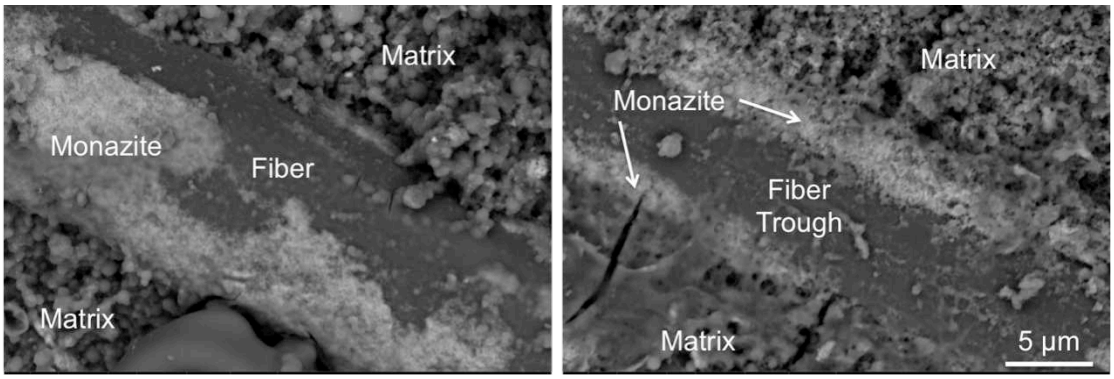

Figure 67: SEM images of a fiber and fiber trough in MZ(A) composite specimen showing monazite coating on both surfaces

6.5 Discussion

6.5.1 The influence of interface tailoring on composite modulus

The results of both flexural and tensile testing revealed that the tailored interfaces in these studies had no detrimental effect on modulus of composite specimens. Potential concerns over the negative influence of interphase on composite modulus has been highlighted many times throughout this document as result of findings in a previous study [32]. Both

preliminary studies covered in Chapter 4, the cure time investigation and study of monazite coating on Nextel 720 fibers[29], [33], had alleviated most of the concerns regarding a loss in composite modulus. In the preliminary investigation, a shift from a one-hour to a five-hour initial cure time clearly influenced composite flexural modulus of carbon coated specimens with Nextel 610 fiber. The carbon and monazite coated specimens of the primary investigation were subject to a 24 hour initial cure. It is uncertain if a 1-hour cure time would affect monazite coated Nextel 610 fiber specimens in the same way it did carbon coated fiber specimens. The cure time investigation coupled with this research does not provide sufficient evidence to make such a determination.

Improved matrix properties from an extended cure time were deemed to be only partially responsible for the improved modulus of carbon coated specimens. In addition, this research reveals that these very different coatings, especially in composition and thickness, do not necessarily always produce similar composite behavior. A study examining a breadth of initial cure times of GMCs with monazite fiber coating would be worth investigating as it could determine optimum processing times. Most importantly the similar moduli of composite specimens in this study help conclude that the incorporation of interphase materials in GMCs (carbon and monazite) can be accomplished without an unacceptable loss to composite modulus. Perhaps even more important, it also affirms that interphase materials in GMCs can be utilized for toughness improvements without a detrimental effect on the composite modulus.

While not a primary concern of this research the disparity in modulus values between the mechanical tests should be discussed. From the preliminary investigation, composite moduli under 3-point flexure were at most 85% of the value predicted by RoM. Under tensile testing, those values increased to as much as almost 96% of rule of mixtures using 175 GPa as the RoM value. The measured increase is not abnormal when moving from a flexural test setup to a tensile test. The shear deformation can cause the modulus of composites to be under reported as compared to the tensile value unless a sufficient span-to-depth ratio is used [133]. The longer span-to-depth ratio decreases the error between the two values by causing effects of shear deformation to be inconsequential. The relatively weak MEYEB matrix may have been even more susceptible to effects of shear deformation, which would account for the lower composite modulus values measured in 3-point flexure. Therefore, the values obtained in tension are probably more representative of the true modulus of composite specimens.

The increase in moduli measured from the preliminary to the primary investigation could also be the result of variations between the specimens. These variations can be compared and reviewed in more detail in specimen preparation sections of Chapters 3 and 4. A few of those variations are noted in the proceeding discussion.

The composites fabricated for the primary research were fabricated after those prepared for 3-point bending. As such, greater familiarity and working knowledge of the materials aided the more recent fabrication of composite specimens. Additionally, the specimen geometry for both tensile and those for 4-point flexure were smaller in nature. These two

factors could have improved wet out of the fibers, which in turn would have resulted in improved shear stress transfer to the fiber. Additionally, the matrix material, while still MEYEB, was prepared daily in the case of the primary research. No investigations have been conducted on the long-term cold storage of MEYEB, however, the author and fellow researchers have noticed that the material becomes more difficult to work with around ten weeks of storage time (provided it is stored at -25 °C). It was almost unusable after thirteen weeks in cold storage. The changing nature of the MEYEB might have contributed to the lower modulus of the preliminary composite specimens.

A disparity in moduli also exists between the specimens based on test method used. The moduli of specimens obtained from 3-point flexure in the preliminary investigation and tensile testing are in close agreement. However, the moduli of composite specimens from 4-point flexure were either 100% of the RoM value of 175 GPa or higher. 100%, and obviously greater, cannot be justified because RoM assumes an absolute perfect bonding condition at the interface. It is possible the flexural composite modulus used from the previous work on unreinforced MEYEB [38] is not an appropriate value to use for the composite or the fiber volume fraction of specimens might be a bit higher than calculated. As noted in the results section, it might also be that the RoM value of 182 GPa predicted by using the compressive modulus of MEYEB may be a more accurate value to use for the specimens in the primary investigation.

Still, there may be other reasons for the inflated values of modulus. The higher moduli of specimens in 4-point flexure as compared to those in 3-point may be partially attributed to

the variation in composite fabrication in each investigation as previously discussed. However, it can also be typical for modulus to differ between 3-point and 4-point flexure tests. It has been shown that due to specimen rotation at the support and loading noses the standard calculations for 4-point flexural modulus can over-estimate the actual modulus of specimens [134]. Experimental work with wooden beams (a naturally occurring composite) also produced 4-point flexure modulus values with greater values than in 3-point flexure [135]. This likely contributed to the larger modulus values observed in 4-point flexural tests. Ultimately, a more rigorous study, both on reinforced and unreinforced MEYEB is needed to qualify the exact composite modulus values. The values for modulus determined in this study are likely close, but that is not what is most important from this study. What is important is that all the types of tests demonstrated that composite moduli were similar between GMCs with and without interphase.

6.5.2 The influence of interface tailoring on composite strength

The measured strength of specimens revealed interesting and positive outcomes about the use of interphase in GMCs. Increased or even decreased strength is not a key indicator of improved toughness on its own, but it is does factor into the calculation for toughness. Thus, all other factors remaining constant, an increase in a material's strength would result in a larger calculated value of toughness.

GMCs that were fabricated with the monazite coated fibers showed superior strength to all other specimen types in both tensile and flexural and tensile tests in the primary investigation. Even in the preliminary work, the GMC specimens with monazite coated Nextel 720 fibers demonstrated increased flexural strength over uncoated fiber

specimens [33]. While of secondary importance to this investigation, this outcome suggests that this coating concept extends to other fiber types. The two fiber types, Nextel 610 and 720, have relatively different mechanical and thermal properties [107]. It can at least be surmised then that the use of this interphase in GMCs can possibly be extended to other fiber types to achieve gains in strength and potentially toughness as well.

The strength gain in composite specimens with the monazite interphase stands in contrast to the results of the other GMCs in this study. The increased strength of MZ over CL specimens can only be explained by the use of the interphase material. The increase in strength must also be the result of something preventing failure rather than any change to the fiber itself. Recall, the monazite coating does not increase the strength of fibers. Additionally, the monazite, which is expected to act as a weak interface, might limit the ability of the matrix to transfer stress to the fibers causing lower composite strength. Yet, MZ specimens are the stronger composite. Examining the fracture surfaces in flexure of MZ specimens as compared to CL support the idea that the failure was delayed. The fibrous, almost brushy, appearance of the tensile surface of beams suggests fibers did not fail in large bundles causing immediate failure of the composite. The localized and prominent shear damage also suggests cracks were diverted into weaker planes and then halted. Finally, the presence of compression damage in some MZ specimen suggests compression failure only occurred after encountering higher load levels. An examination of these results points to activation of crack defeating mechanisms, like debonding and crack bridging. These mechanisms allow for the continued transfer of stress to the fibers resulting in greater composite strength. A delay to the failure of fiber bundles caused by the interphase

was the same reason provided for the strength increase observed in the preliminary investigation covered in Chapter 4 and in one previous study [21].

Also worth highlighting is that the values of strengths measured for MZ composite specimens in both environments are consistent with expectations of an oxidation resistant coating. As already noted and of much importance to this study is that MZ specimens demonstrated these strength gains after being exposed to an oxidizing environment. For GMCs to be a viable structural component in aircraft and automobiles they must demonstrate resistance to effects of oxidation. This study confirms well-informed notions that GMCs with monazite coating would remain resistant to oxidizing effects.

In this discussion regarding strength improvements, recall also that MZ specimens had a lower fiber volume fraction on average. Potential concerns over the effect this might have had on resulting strengths were addressed in Section 6.1.3.2. The results confirm suspicions that a reduced fiber volume fraction did not improve the strength of MZ specimens. In a brittle matrix, it would be expected that a higher fractional volume of fibers would lead to higher stiffness and reduced microcracking in the matrix potentially allowing for an increase in strength [2], [136]. Regardless, changes to the fiber volume fraction in CL specimens produced the same strength and brittle behavior. However, MZ composite specimens with reduced fiber volume fraction achieved greater strength. The result is opposite of expectations. However, this research has uncovered that the reduced interfacial strength in MZ specimens aided the increase. If a higher fiber volume fraction in GMCs with monazite interphase could be achieved using different methods of processing it

is possible that these particular composites could demonstrate some of the highest strengths obtained by GMCs containing an oxidation resistant fiber. In fact, such strengths would be some of the highest reported for unidirectional GMCs containing fiber of any type.

It is not entirely clear why CC specimen types, especially CC(N), did not also demonstrate greater composite strength than CL specimens. It is possible that the method for producing the carbon coating may have degraded the strength of the Nextel 610 fibers. However, considering the carbon coating produced on Nextel 610 fibers is simply a byproduct of the original sizing, this is unlikely. The results of push-out and SBS testing would appear to indicate that the CC composites have a weak interfacial strength, and thus, the means to limit crack propagation like the MZ specimens. Other results suggest clear differences between CC and MZ composites. As previously discussed in Chapter 2 the coatings are different both chemically and physically and would be expected to cause different composite behavior. Thus, the difference comes as no surprise. The fracture in CC specimen types in flexure show less localized damage. Mode II (parallel to the fiber) cracks on these specimens are continuous and extend a greater distance on the length of the beam. Additionally, there is less evidence of fiber pullout on the tensile surface of the CC flexure specimen types. In total, the damage suggests that failure might have been more global and the cause for earlier failure of the composite.

In analyzing the reasons for CC specimen types lack of strength gain it is also best to consider those heat treated in an oxidizing environment and those heat treated in a non-oxidizing environment separately. It is understood to be that both the cleaned fiber and

the monazite coating are oxidation resistant and likely do not degrade or undergo any major changes to their microstructure at such a short time at 650 °C [73], [107], [137]. For CL and MZ fiber composites, the experimental values for strength and modulus of composites heat treated in different environment are consistent with expectations. The CC coating on the other hand should not be oxidation resistant. Thus, the lack of difference in measured strength between specimens post heat treated in air and nitrogen is somewhat surprising. The color changes in CC(A) and CC(N) specimens after post heat treatment (refer to Chapter 5) suggest removal of the coating on fiber surfaces in the case of the former and retention of the fiber coating in the case of the latter. Further evidence for the loss in carbon coating in air is confirmed by the short beam strength, the stress-strain curves, and fracture surfaces of CC(A) specimens as compared to CC(N) specimens. The higher short beam strength observed and change in failure mode in CC(A) specimens suggests changing interfacial conditions.. Also, fracture surfaces of specimens in flexure, tensile, and SBS testing more closely resembled those of CL specimens, which were brittle in nature. The combined results suggest that CC(A) specimens did not show any strength gain because of a loss in their overall ability to prevent cracks from penetrating large groups of fiber. It is a loss in the sense that the effects of oxidation made them more like CL specimens.

Still, the results of push-out would indicate that the interfacial region of CC(A) specimens is different than those in the CL specimens, which were shown to have a strong interface. It could be that a "gap," or fugitive coating (see Chapter 2, Section 2.1.5 and Chapter 3, Section 3.2.3), allows for fiber push-out to occur, but is not as effective as an actual layer of carbon.

The carbon layer may have provided an additional means of absorbing crack energy. This seems even more reasonable when actually considering that the thickness of this layer was no thicker than the original sizing applied to fibers by the manufacturer, which was likely under 100 nm. Recall, a higher value of friction stress was measured for CC(A) specimens and surfaces of these fibers appeared rough. However, the curious nature of the results produced by interfacial characteristics in CC(A) specimens could also be explained by incomplete degradation of the coating during the five hour heat treatment. Push-out of fibers was not conducted on the edges of specimens. It could be that the oxidizing environment penetrated the outer surfaces more readily than deeper interior surfaces. This would also explain both the macro- and micro- level results observed for CC(A) specimens, which exhibited some characteristics akin to both CL and CC(N) specimens on a macro and micro level, respectively.

The resulting strength of CC(A) specimens met expectations because of anticipated effects of oxidation on the interphase. However, an increase of strength was expected for CC(N) specimens. The carbon interphase was expected to provide a strengthening effect as observed before in Nextel 440 specimens [21] and anticipated to do so with additional matrix cure time in Nextel 610 specimens based on discussions in Chapter 3 and 4. As noted for MZ specimens, the strength was hypothesized to increase because of the carbon interphase dissipating crack energy and therefore preventing premature failure of fiber bundles. The resulting strengths of carbon coated specimens reveal that additional cure time of specimens does not facilitate greater strength for this composite type. In

comparison to the monazite coating, the form of carbon coating used seems to be limited in its ability to produce greater strength in N610/MEYEB composites.

There is another takeaway from the observed flexural strength of CC(N) specimens that is important to the use of interphase. Both CL and CC(N) specimens did not show a clear difference in recorded strength from the preliminary to the primary study. Such a result is important in a one of two ways. First, a change in geometry and type of flexural test did not seem to affect the flexural strength of specimens. Additionally, the 24-hour cure does not appear to improve the strength or moduli of carbon coated specimens. This suggests that faster processing times could be used for GMCs incorporating this carbon coated interphase and perhaps other interphase materials as well. This is worthy of further investigation. Extended processing times commonly used to improve matrix properties in GMCs is slightly disconcerting as they begin to lose some of their advantage over the costly and/or complicated processing procedures of ceramics. Achieving similar gains, namely strength and toughness, with shorter processing times could still make producing these GMCs with a costly interphase component economically feasible.

One final area of importance was uncovered in examining both the flexure and tensile strengths of GMCs with interphase. In both flexure and tension, measured composite strengths exhibited the same trends. The strength of CL and CC specimen was very similar and the strength of MZ specimens was the highest measured. In fact, the percent increase in strength of MZ from CL specimens in both flexure and tension were really close. Often there is difficulty in obtaining similar tensile and flexural results when testing composites.

This finding is important for the future study of fiber coatings in GMCs. It indicates that given similar test parameters, the effectiveness of fiber coatings to improve the mechanical properties of GMCs can be evaluated using flexural testing. Flexural testing is a much simpler test method than tensile testing in terms of both specimen preparation and test execution.

6.5.3 The influence of interface tailoring on composite toughness

The results indicated that GMCs with tailored interfacial characteristics demonstrated requisite features of improved toughness as compared to the baseline cleaned fiber condition. Those composites incorporating an interphase material showed higher values of toughness, evidence of non-brittle fracture and, except in the case of CC(A) specimens, non-catastrophic failure. Only in the case of tensile testing, did stress-strain curves of composites containing interphase demonstrate catastrophic failure. This could be caused by a couple factors. Despite the less complex state of stress in tension versus flexure there is still a shear stress state in tension. Evidence of splitting would suggest that the weak nature of the interface in the coated fiber composites might have caused rapid fracture of the composite along the interface resulting in a complete loss in its load carrying capability. This might have been prevented in woven or 0/90 configuration allowing for observation of more damage tolerant behavior. Additionally, it has been observed in unidirectional fiber CMCs with high interfacial friction stresses damage tolerance can be limited [138], [139]. Recall, the interfacial frictional stresses measured from push-out testing seem to be high as compared to CMCs in other studies. The higher frictional stresses, combined with the testing condition, could have prevented a more damage tolerant behavior from being observed in tension. Despite this one caveat from tensile testing, substantial evidence

exists, from this body of work, demonstrating that interfacial modifications resulted in changing composite toughness. The following entails a more detailed discussion of each type of fiber surface condition on toughness.

In flexure, the MZ specimens demonstrated the greatest increase in calculated toughness over both CC and CL composites. The larger value of toughness was influenced by two factors. The first factor, the improved strength of MZ specimens, was discussed in the previous section. The higher strength of MZ specimens, which is an integral part of the calculation for toughness, contributed to the large value of measured toughness. As discussed, the strength gains are the result of the modified interface created by the monazite coating. The incorporation of the monazite coating in GMCs absorbed crack energy as suggested by the fractures observed in specimens, thus delaying failure of fiber and fiber bundles. The delay allowed improved transfer of stress to the fibers.

The other major contribution to the larger value of toughness was the damage tolerance and graceful failure displayed by MZ specimens. The curves of MZ specimens often showed in contrast to CL specimens, some non-linear elastic behavior prior to the first initial load drop. These portions of curve indicate resistance to crack propagation [2], [41]. The successive load drops observed in some cases point to stable and unstable crack growth. With no other means of plasticity in the composite this must be the result of the coating.

As just discussed, the strength, damage tolerance, and graceful failure exhibited by MZ specimens resulted in greater area underneath the stress-strain curve, which correlates to

improved toughness. It should be noted these values of toughness are likely conservative. The calculated values of toughness do not account for the differences in fiber volume fraction. It would be expected that the increased V_f would result in greater strength and even toughness as discussed previously. Additionally, it was noted that while MZ specimens did not generally fail catastrophically in flexure after the initial load drop sometimes the initial drop was greater than 20% of the maximum load, which is the limit specified in ASTM C1341. Therefore, despite some specimens showing graceful failure, large portions of the stress-strain curves were neglected in the calculating toughness based on the definition used for failure. Regardless, the MZ specimens demonstrate superior toughness.

Observing the fracture surfaces of the different composite types supports the variations in toughness. The fracture surfaces of MZ specimens indicate a change in the damage mechanism from those of the CL specimens. The presence of fiber/fiber bundles on the tensile surface and more localized damage on MZ flexure specimens suggests progressive failure rather than sudden failure of the composite. This is in contrast to the clean specimens that generally had a very clearly defined crack that originated on the tensile surface of specimens typical of a more brittle failure. The nature of the failure relates well to the stress-strain behavior observed for CL specimens. The fracture behavior of MZ specimens is synonymous with improved toughness via activation of crack defeating mechanisms. The presence of individual fibers/fiber bundles is characteristic of a tough composite relying on deflection, crack bridging, debonding, and fiber pullout to absorb crack energy. Additionally, the fracture surfaces of CL specimens tested in the tensile

configuration were also very brittle in nature whereas MZ specimens fracture surfaces were more tortuous and did not generally fail on a discrete plane. This suggests failure of fibers in different locations throughout the composite. This likely only occurred because cracks were at least deflected or even arrested in different locations within the composite.

That both CC specimen types also showed slightly improved calculated toughness over CL composites is easily explained. The fracture surfaces from flexure and tensile testing of these composites would support such a change. However, the improvement in toughness was not nearly on the order of MZ specimens especially for CC(A) specimens. The calculated toughness of CC(A) specimens only varied from CL specimens because of their slightly higher average strength. It was noted that the slight increase in strength was statistically irrelevant, but there is rationale to not ignore the increase in strength. The fracture surfaces of CC(A) specimens would indicate that the altered interfacial condition, though likely degraded after heat treatment, might have influenced a strength increase. This is because the fracture surfaces suggest crack energy defeating mechanisms were active. In flexure, distinct fiber bundles could be observed on the fracture surface of the CC(A) specimens. In tension, the fracture surfaces of these specimens were also not generally as planar as CL specimens. Individual fibers in CC(A) specimen were also pushed successfully in push-out tests whereas fibers in CL specimens were not. As discussed in the previous section, it is uncertain whether push-out results in CC(A) specimens are from a fugitive coating or incomplete degradation of the carbon coating. Ultimately, the changes were not enough to affect the stress-strain behavior or even fracture in SBS testing. The stress-strain curves of CC(A) specimens, like CL specimens, were linear-elastic up to the

peak load. After the peak load, the curves indicated catastrophic failure. Overall, this evidence supports the possibility that the altered interface in CC(A) specimens did indeed affect toughness by delaying failure of the fiber.

This relatively minor effect could be considered somewhat significant for GMCs in general. Assuming the particular increase in toughness is the result of a fugitive coating it is possible that the effectiveness of such a coating could be improved by increasing the initial thickness of the carbon layer on fibers. In research, a fugitive carbon interphase (see Chapter 2, Section 2.1.5) has proved to be just as effective as the carbon interphase itself [64], and with increased thickness, greater strength has been reported in ceramic matrix composites [24]. The larger thickness might promote lower debond energies and lower friction stress allowing for more crack deflection and fiber pullout. Preparing fiber tows and weaves with a layer of carbon is relatively common. The process can easily be extended to many fiber types and would be much easier to implement than that of the application of monazite. A GMC with a fugitive coating may be an economical way of producing toughness in GMCs.

A clear improvement in toughness is less difficult to argue for CC(N) specimens. The improvement in the calculated toughness was not just the result of a minor strength increase. The increase in the calculated value of toughness for CC(N) specimens also arises from the non-linear elastic portions in the stress-strain curve and damage tolerant behavior displayed after failure. In addition, distinct fiber and fiber bundles are present on the fracture surfaces of CC(N) specimens in flexure. The fracture surfaces of CC(N)

specimens in both flexure and tension also appear more tortuous than CL specimens. As already noted, the particular damage and shape of fracture surfaces is very indicative of crack defeating mechanisms being active. The end result being delayed failure of the composite and gains in toughness.

6.5.4 Source of improved toughness

6.5.4.1 Indications from push-out

As discussed, previous work and even the preliminary studies of this research revealed the potential effectiveness of coatings in GMCs [21], [23], [29], [33]. Weaker interfacial conditions were presumed to be responsible for the behavior. Fracture surfaces and evidence of fiber pullout had indicated that this was the case. However, a direct examination of the interfacial conditions in GMCs containing interphase had been lacking until this research. Both push-out and the SBS testing conducted in this work provide an evaluation of interfacial conditions in these GMCs with interphase on a micro and macro level. The results clearly established differences in the interfacial properties between each type of GMC tested in this study.

Most telling of the different interfacial conditions between specimens were the SEM images of composites revealing pushed out fibers. Only those specimens with an interphase, carbon or monazite, showed fibers cleanly pushed out. On the "pushed" side, the fibers of CL specimens were damaged. The "pushed out" side of CL specimens also revealed that fibers that did push, pushed with matrix attached to them. The results reveal the geopolymer matrix bonds strongly to the clean fiber surface condition as compared to

those specimens with carbon and monazite fiber surfaces. This was expected based on the similarity of the chemical composition of the two primary constituent materials and validates postulations of this investigation and previous research.

CC(A) specimens, unlike CL specimens, were abled to be pushed yet both specimen types exhibited relatively similar mechanical behavior and failure in a brittle manner. Given these results, examination of push-out results could lead to a false positive for toughness in a GMC if parameters, such as debond energy and friction stress, are neglected for only observing whether fibers were pushed using microscopic methods. Until a greater library of push-out parameters are developed for GMCs, mechanical tests should accompany any push-out testing to confirm that any altered interfacial conditions improve toughness.

The calculated debond energies and SEM of pushed surfaces confirms that a stronger interfacial condition exists in CL specimens as compared to CC and MZ specimens. This renders CL specimens incapable of absorbing much crack energy. Interestingly, the debond energy of specimen types is relatively close in value. However, the SEM images confirm that the small differences in values resulted in a change in push-out behavior and ultimately toughness of the GMCs. The stronger interfacial bond translated into brittle failure for CL specimens. The fractures in CL specimens further confirm that mechanisms were not activated to absorb crack energy.

To the authors' knowledge this work is the first of its kind for geopolymer composites, as no other push-out data on GMCs currently exists. Comparing this study to research on

CMCs containing Nextel fibers, the debond energies presented for GMCs are higher. For studies conducted with CMCs, debond energies for strong interface materials were on the order of 8 and 15 J/m^2 and debond energies for those containing interphase materials including monazite, were in the range of 1-5 J/m^2 [73], [140]. In all cases, GMCs with and without interphase revealed much higher interfacial properties. Values obtained from push-out would be expected to differ between GMCs and CMCs. Each composite type varies a great deal from one another especially in regards to the mechanical properties of the matrix, matrix shrinkage, and thermally induced stresses created during processing. To speculate, the higher debond energy in GMCs might be a result of the much larger disparity between matrix and fiber modulus because the equations used [75] dictate that as matrix modulus tends away from fiber modulus interface toughness increases. That said, the equation also suggests the effect to could be rather minor. Other factors might also include the lower processing temperatures and cure shrinkage of the geopolymer matrix. Regardless, what is important is the lower interfacial strength in specimens is directly associated to gains in strength and toughness in GMCs.

6.5.4.2 Using SBS to understand differences in interfacial strength

Alone the values of short beam strength do not provide clarity about the interfacial conditions, but coupled with the types of failures observed in SBS specimens a distinct difference could be noted. CC(N) and MZ specimens, which showed the most toughness and damage tolerant behavior were the only specimen types to fail generally in shear. Other evidence has established the failure of these specimens in shear as the result of

weaker interfacial conditions. The push-out behavior of these specimens clearly indicates weaker interfacial conditions exist.

However, push-out also revealed a weaker interfacial bond in CC(A) specimens. Measured short beam strengths did not clearly indicate a weaker interfacial strength in CC(A) specimens. This could simply be the result of testing the composite on a micro versus macro level. Indeed, it could also have a lot to do with state of the degraded interphase. The CC(A) SBS specimens generally indicated both shear and flexure failure on the tensile surface. This was different than CL specimens which showed flexure on the tensile surface as the predominate mode of failure in SBS testing with basically no sign of shear failure. The failure in flexure helps support suspicions that carbon coating in the CC(A) specimens was compromised from the heat treatment creating a stronger bonding condition. However, it is not entirely certain why results from CC(A) specimen testing reveals evidence of both a strong and weak interface an i.e. SBS result versus push-out, respectively. As proposed earlier, it could be that the coating was not fully degraded or only degraded on or near edges of the composites. It could also be the coating has completely disappeared and the "gap" is producing some of the results associated with a weaker interfacial condition. The results of push-out seem to suggest it could be either. The debond energies of CC(A) and CC(N) specimens are similar suggesting the carbon coating may have not be degraded in the central portion of the specimens where testing was conducted. However, the slightly elevated friction stresses of CC(A) to CC(N) specimens would suggest that interfacial conditions have changed slightly. The rough nature of CC(A) fiber surfaces, which was indicative of matrix attached to surface, would

tend to support the idea that the bond may have been enhanced via diffusion at the fiber matrix interface. The higher frictional stress in CC(A) might also explain the higher short beam strength and failure type of these specimens in SBS testing.

Also, interesting from the results of SBS testing was the short beam strength measured for CC(N) specimens. The short beam strength of CC(N) specimens was the lower than all the other specimen types. However, only CC(N) and MZ specimens can truly be compared because these specimens failed in shear. -This finding from SBS testing implies improved toughness does not necessarily mean achieving lower short beam strengths. In fact, the higher shear performance of MZ specimens results in a better balance of properties and a better GMC, combining improved strength and reduced brittleness. It is likely the higher short beam strength of MZ specimens is linked to the properties measured in push-out; the other singular or additional contributing factor could be the nature of the coating itself. Further experimentation would be needed to confirm. With only two data points, CC(N) and MZ composites, it is uncertain whether the optimum short beam strength lies above or below the value measured for MZ assuming shear is the dominant failure mode. However, the data does suggest that if GMCs do not fail in shear in SBS testing, they will likely not demonstrate tough behavior as indicated by the measures of toughness for CL and CC(A) specimens already presented and discussed

In light of this, SBS testing appears to be a very adequate way of conducting an initial evaluation of fiber coatings in GMCs. It is even possible that given a little more data, SBS testing could prove to stand alone without requiring supporting flexural and tensile tests.

GMCs containing a coating or interfacial modification could immediately be screened for their potential to achieve gains in toughness by evaluating the failure mode. This is an important finding because SBS testing is very easy and inexpensive to conduct and requires very limited amounts of material. That said, both flexural and push-out testing would be invaluable for evaluating the effectiveness of the coating on mechanical behavior and identifying the specific interfacial parameters that give rise to the greatest gains in toughness.

6.6 Conclusion

The results and the discussion of the primary investigation involving GMCs with tailored interfaces were presented in this chapter. The different fiber surface conditions – cleaned, carbon coated, and monazite – allowed for the evaluation of three different interfaces. The CL specimens served as the baseline for comparison of the other two types. The results included data collected from flexure testing and tensile testing of composite specimens. These tests were conducted to obtain mechanical properties and for observation of mechanical behavior. Modulus and strength data were presented for each along with photos of damage incurred during testing and fracture surfaces. Additionally, stress-strain curves and values of toughness were presented to provide an evaluation of the effect of each fiber surface condition on damage tolerance. Interfacial characteristics were evaluated for each fiber surface condition using SBS testing and single fiber push-out. Short beam strengths and failure surfaces were presented. Also presented were debond energies and friction stress values of each specimen type obtained from push-out testing along with images of pushed fibers.

The results of flexure and tensile testing revealed no significant differences between the modulus of composite specimens. The testing with and without interphase revealed the greatest gains in strength and toughness were achieved by the incorporation of monazite fiber coating in the GMC. Gains in toughness were the result of higher strengths and more damage tolerant behavior of MZ specimens. The strength and toughness of MZ specimens increased by ~35% and ~165% respectively as compared to the CL composites. Fracture surfaces of MZ specimens appeared to contain the presence of discrete fiber and fiber bundles and best described as tortuous in nature. The flexural and tensile strengths of all other specimen types, CL and CC, were similar. The fracture surfaces of CL and CC(A) specimens displayed a brittle type failure. The toughness of CC(N) specimens did greater than that of clean specimen. Graceful failure was also distinguishing mark of CC(N) specimens unlike CL specimens, which failed in a brittle, catastrophic manner. This finding aligns with expectations that composites anticipated to have un-degraded coatings after heat treatment were the only ones to show improved damage tolerance.

The results of SBS testing and push-out testing demonstrated differences between each type of surface condition investigated in this study. CL and CC(A) specimens tested under short beam conditions failed in flexure and/or demonstrated a mixed failure of both flexure and shear. This was expected of specimens with high interfacial strength. However, shear failure was the predominate mode observed in CC(N) and MZ specimens. CC(N) short beam strengths were the lowest of all specimen types. All other specimen types had similar short beam strengths. In push-out, debond energies decreased slightly from CL to CC to MZ specimens. Friction stresses were highest for CL composites, but observing images of

pushed fibers revealed that fibers were damaged from the indenter and either not pushed or pushed with lots of attached matrix material. All other specimen types generally could be pushed without damage to the fiber. The friction stress of MZ specimens was roughly 10 and 5 MPa higher than CC(N) and CC(A) specimens, respectively. The slightly higher friction stress, but lower debond energy of MZ specimens compared to the other specimen types appears to have resulted in the better balance of interfacial properties for promoting toughness in GMCs.

The interpretation of the results points to the effectiveness of a weaker interfacial coating for producing improved strength and toughness in GMCs. The improved strength of MZ specimens was attributed to monazite coatings preventing the early failure of fiber bundles by activating crack defeating mechanisms such as deflection and debonding at the interface. Confirmations that such mechanisms could be active were confirmed from push-out testing. Additional validation that such mechanisms were active became apparent from the observation of fiber/fiber bundles on fracture surfaces and extensive, localized shear damage on the sides of specimens. The damage suggested that cracks were not propagating through fibers, but instead being deflected at the surface of fibers as would be expected if the interface was weakened.

SBS and push-out testing confirmed that a difference in the mechanical response of composite specimens was the result of differing interfacial conditions. The improved damage tolerance of CC(N) and MZ specimens was attributed to weaker interfacial conditions than specimens from the baseline CL composites. Thus, applying the weak

interface concept to GMCs is an acceptable means of promoting toughness even after elevated temperature exposure. In oxidizing environments, this requires a thermally stable fiber coating.

Chapter 7: Thermal Aging

The effect to geopolymers or GMCs after long-term elevated temperature exposure is not well researched. To investigate these effects, composite specimens that were thermally aged in air were subjected to flexural and short beam shear testing for mechanical characterization. Aged unreinforced MEYEB specimens were also tested in flexure and compression to observe how long term exposure affected the geopolymer. The results of this testing are compared and presented with the results discussed in Chapter 6. Only CL and MZ composite specimens were subjected to thermal aging in an oxidizing environment. Results of the tests are briefly discussed to provide insight for use of GMCs under long term service conditions and for future research.

7.1 Composite Specimen Testing

7.1.1 Specimen preparation, experimental, and calculations

The procedure for aging composite specimens was discussed in Chapter 3. Recall, the total aging time for specimens included the original 5 hour treatment at 650 °C. For example, specimens designated as aged for 50 hours were subjected to 45 more hours at 650 °C in addition to the original 5 hours. All aged composite specimens were subject to the same fabrication, test procedures, and calculations discussed in Sections 6.1.1 & 6.1.2 and 6.3.1 & 6.3.2 for flexural and short beam shear testing respectively. That said, the MZ specimens prepared for 50 and 500 hour heat treatments were on average thicker and as a result had

a lower fiber volume fraction than the MZ specimens only treated for 5 hours. This was due to some difficulties encountered in manufacturing MZ specimens. As a consequence of the larger thickness, they also had a lower V_f than CL specimens.

7.1.2 Results of aged composites specimens in flexure

7.1.2.1 Mechanical properties

Thermal aging did not appear to have any effect on the flexural moduli of CL or MZ specimens. The average normalized moduli of aged specimens were well within the error of those values presented for 4-point flexure in Chapter 6. The lack of difference between specimen moduli precluded the need for a chart depicting the measurement of each type of specimen.

Figure 68 shows that thermal aging may have had an effect on composite strength. Both CL and MZ specimens show a small decrease in the strength with additional time at temperature. The decrease between 5 and 500 hours is roughly 10% and 15% for CL and MZ specimens respectively. Except for the case of MZ specimens aged for 500 hours the decrease seems to be within the standard error shown. After aging, the average strength of MZ specimens does remain higher than CL specimens with or without aging. After 5 hours the MZ specimens were roughly 32% stronger than the CL specimens. After 500 hours of aging the strength of MZ specimens is only 21% greater than the CL specimens aged for the same amount of time. The small loss in both composite types does not come as a surprise. In a study, using a GMC referred to as PyroSiC (also developed by Pyromeral, the manufacturers of MEYEB), a loss in the tensile and flexural strength was observed after

elevated temperature exposure despite noting the thermal stability of the SiC fiber up to 1000 °C [141]. The authors reported a ~23% loss in strength in both cases after aging the GMC for 500 hours at 650 °C [17].

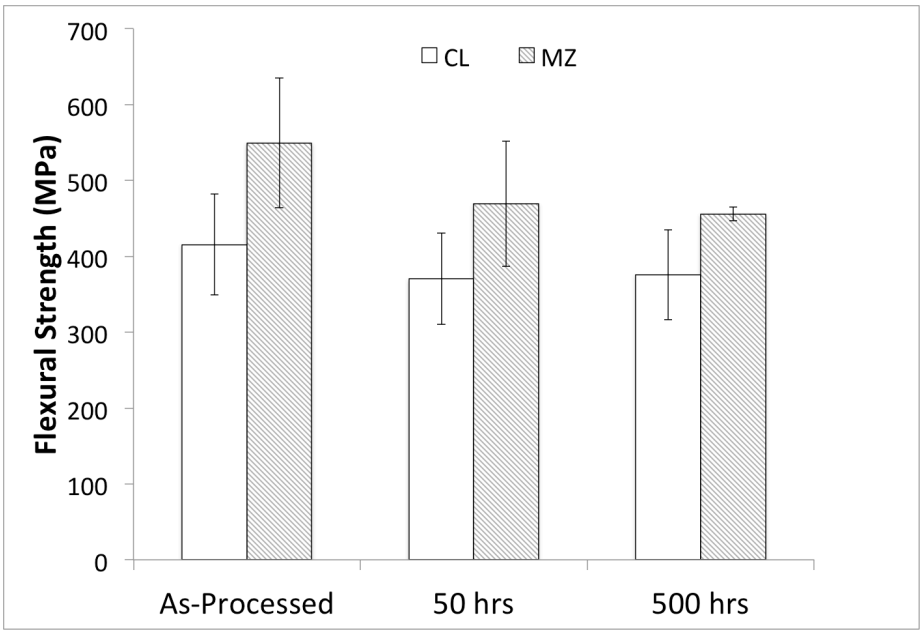

Figure 68: Flexural strength of CL and MZ aged specimens compared

7.1.2.2 Influence of fiber volume fraction on strengths

As before, the strength results should be interpreted in light of differing composite fiber volume fractions (V_f), which occurred as a result of difficulties controlling the final thickness of specimens during processing. Figure 69 shows the strengths of aged composite specimens in relation to fiber volume fraction. All CL specimens have similar V_f. The average V_f of 50 and 500-hour MZ specimens was around ~36%. This is roughly 5% lower than MZ specimens heat treated for only 5 hours. This is also 8% to 9% less than any of the CL specimens. As noted in the previous section, the strength of MZ specimens decreased with aging. The decrease in strength also corresponds to the decreased volume

fraction in the aged specimens. As discussed in Chapter 6 (see Section 6.1.3.2), a decrease in strength would generally be expected for composites of a lower volume fraction as is observed here. Also worth noting here is that average strength of MZ specimens are all higher than CL specimens with or without any aging.

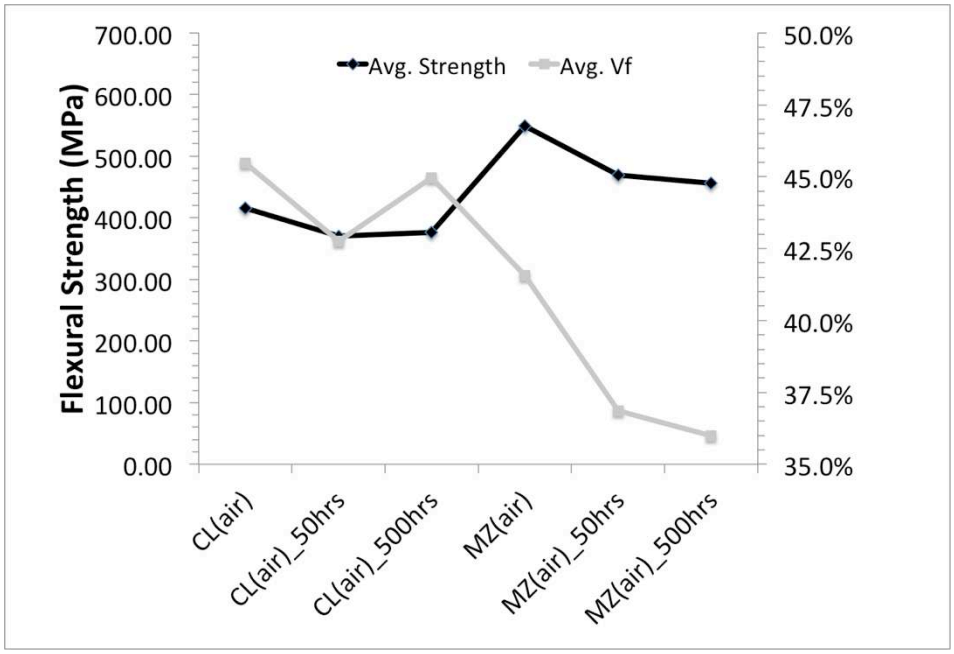

Figure 69: Flexural strength of aged specimens in relation to V_f

7.1.2.3 Damage tolerance

The stress-strain behavior of aged composite specimens was evaluated. The curves of CL specimens are shown in Figure 70. As expected CL specimens exhibited no change in damage tolerance with respect to time at temperature. For specimens aged for 50 and 500 hours, the stress-strain response is linear-elastic until failure with failure being catastrophic in nature. This is the same behavior observed after only 5 hours at 650 °C (see Figure 40 for comparison).

Aging does appear to have some effect on the stress-strain response of MZ specimens (see Figure 71). The curves indicate differences in composite modulus. This can be explained by the variation in fiber volume fraction between each individual specimen. After 50 hours, there does not appear to be a clear change in the behavior of specimens. Only in a small number of cases was failure catastrophic for MZ specimens aged for 50 hours. The stress-strain curves show some inelastic deformation prior to first failure. However, after 500 hours, the damage tolerant behavior that was common to MZ specimens aged for 5 and 50 hours was virtually absent. Only in few cases did MZ specimens aged for 500 hours not fail catastrophically. Clearly, the stress-strain curves of MZ specimens after any amount of aging still include more area under the curve than CL specimens.

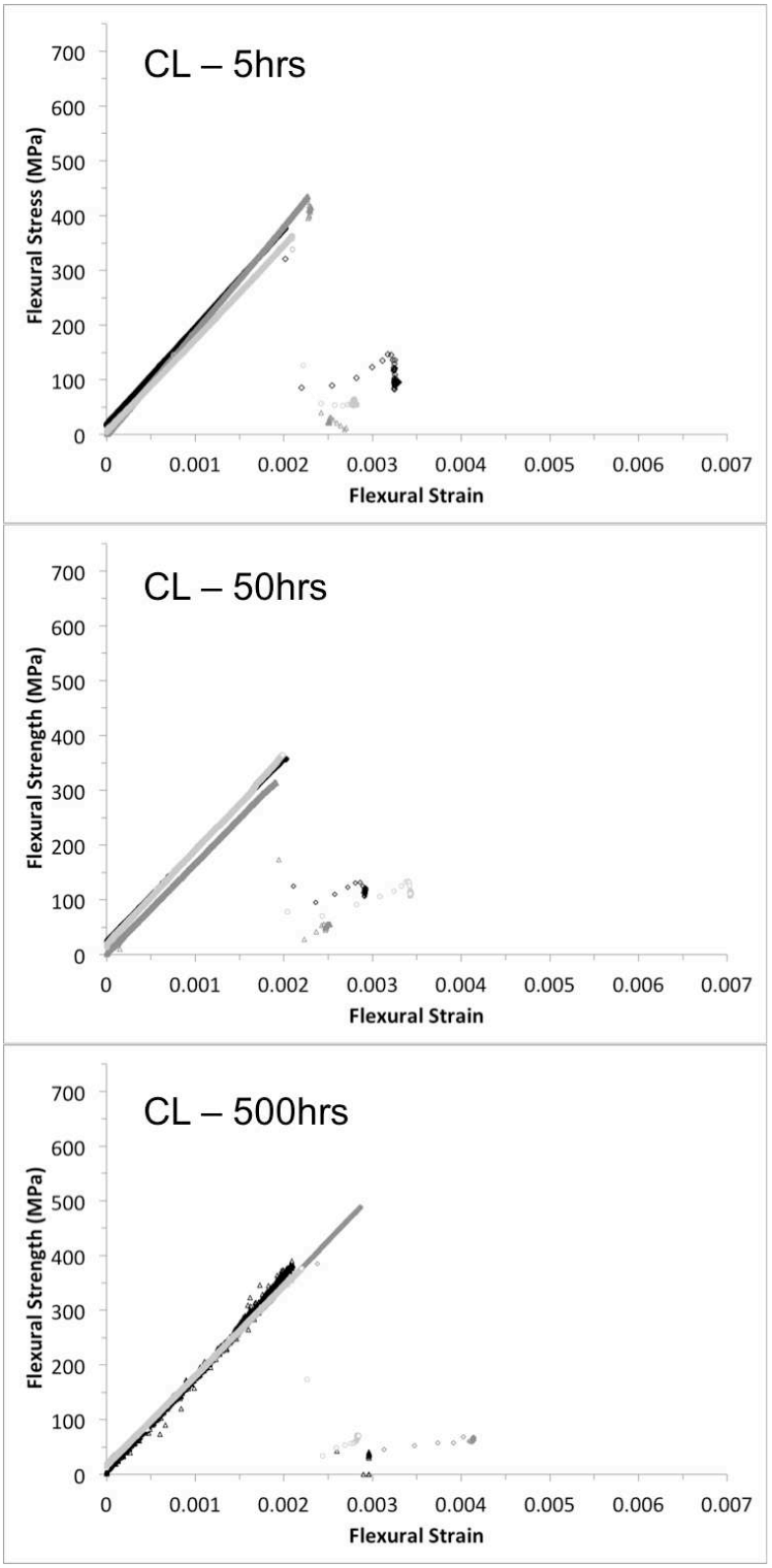

Figure 70: Stress-strain curves of aged CL specimens: 5, 50, and 500 hours at 650 °C

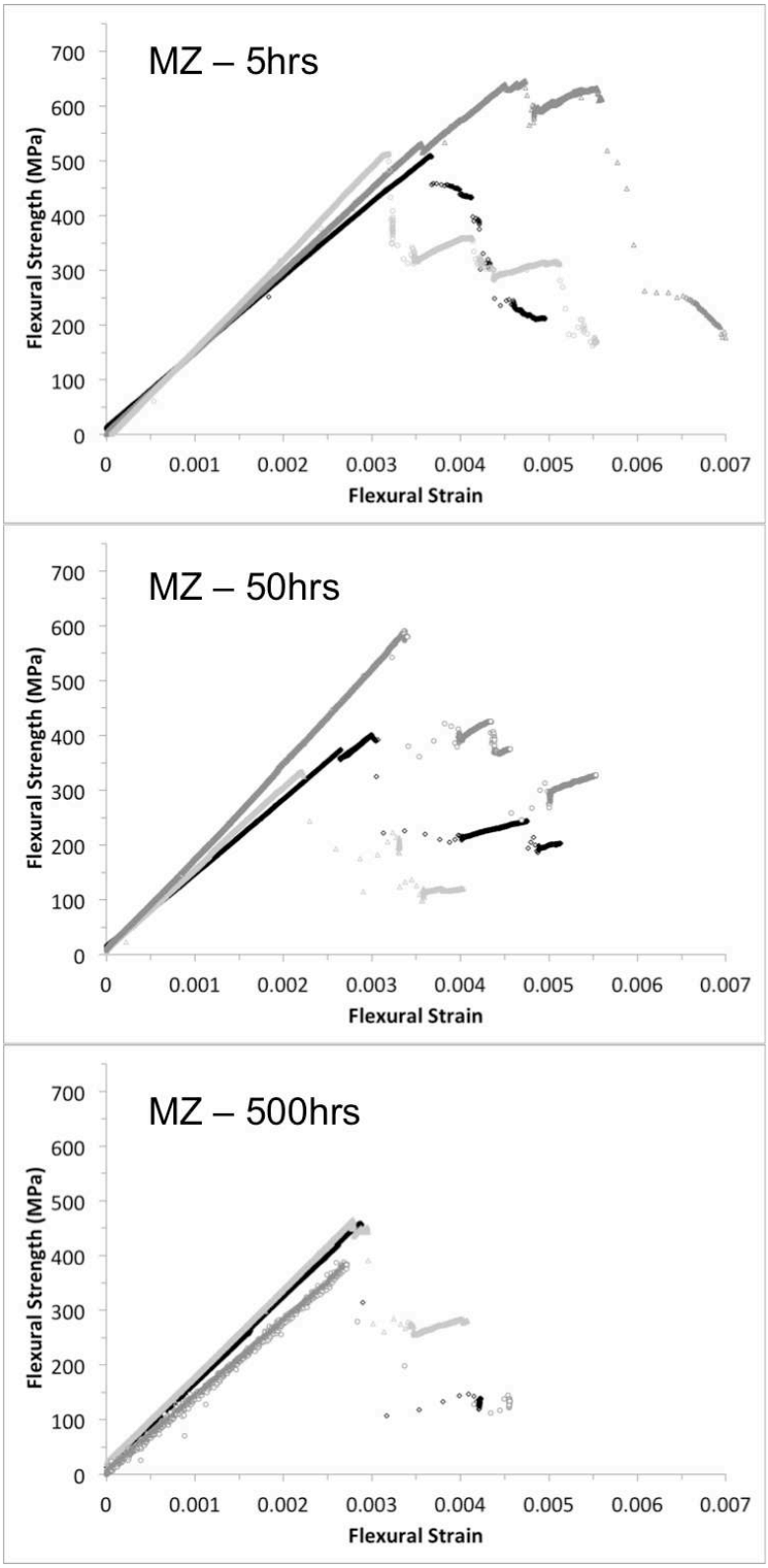

Figure 71: Stress-strain curves of aged MZ specimens: 5, 50, and 500 hours at 650C

7.1.2.4 Fracture in specimens

The nature of fracture in aged CL and MZ specimens can be seen Figure 72 and Figure 73. The images on the left of each of these two figures show a side view of the damage incurred after initial failure. The images on the right show fracture surfaces after the beam is subjected to additional displacement causing the beam to split apart into two sections. The CL specimens regardless of time at temperature do not vary in their appearance. The beams are characterized by a distinct Mode I crack originating from the tensile surfaces, which quickly diverts in both directions along the plane of the fibers. The fracture surfaces are planar and the layer exposed from the Mode II failure appears to be relatively ordered and smooth.

Unlike the CL specimens it appears that aging may have had an influence on the fracture behavior of MZ specimens. At 50 hours and 500 hours, a distinct crack on the tensile surface of beams can be seen. This is similar to the CL specimens, but shear damage is still more prominent in MZ specimens than in the CL. The fracture surfaces do not appear to change much until 500 hours of exposure time. The fracture surfaces of the 5 and 50-hour MZ specimens are very uneven and complex. Fiber bundles and even what appear to be individual fibers can be observed. It could be argued that the image of the 50-hour MZ specimens shows these features to a lesser degree marking a possible transition point. The fracture surfaces of 500-hour MZ specimens, while still not quite like CL specimens, definitely seem less complex and lack the presence of fiber/fiber bundle pullout as compared to the other 5 and 50-hour MZ specimens.

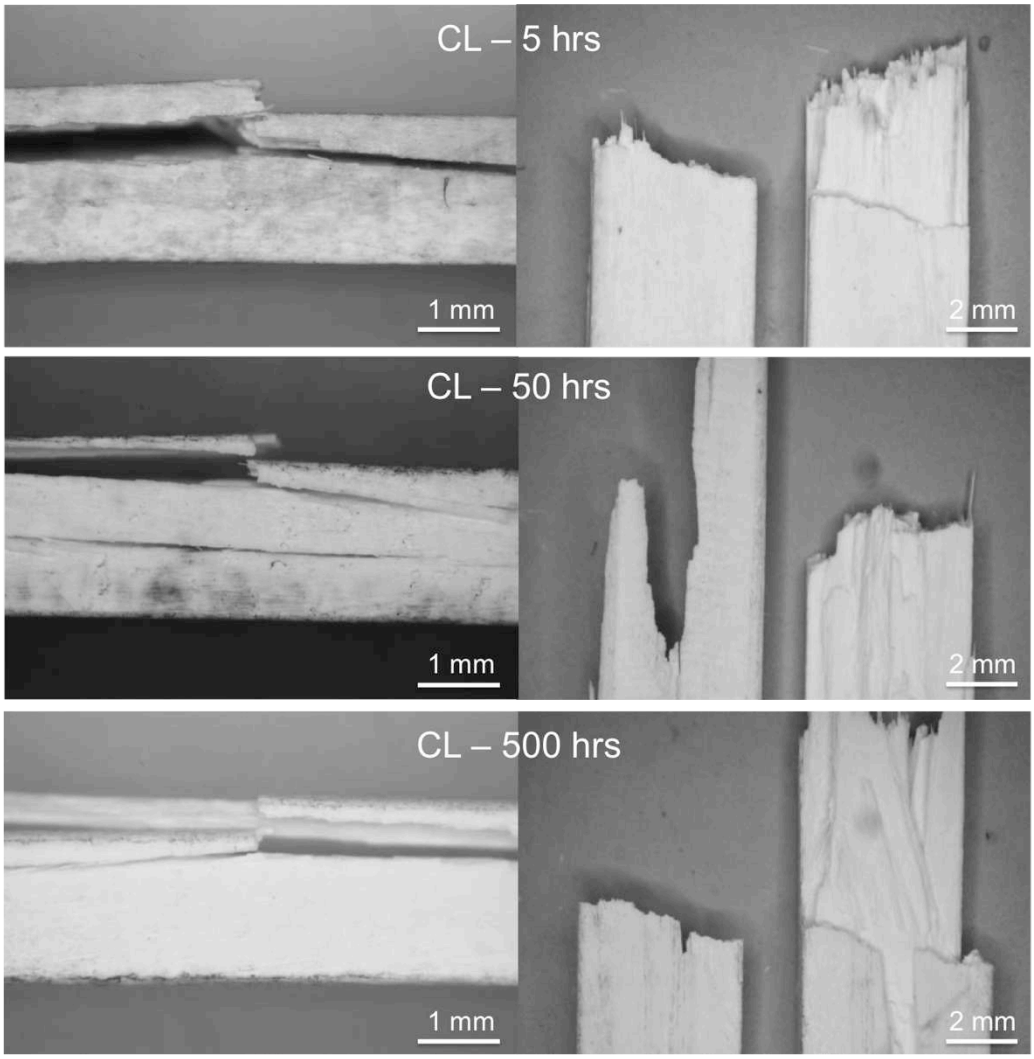

Figure 72: Damage and fracture surfaces typical of aged CL specimens. The surface of the beam subjected to tensile forces face top of page in the set of images on the left and out of the page in the set of images on the right

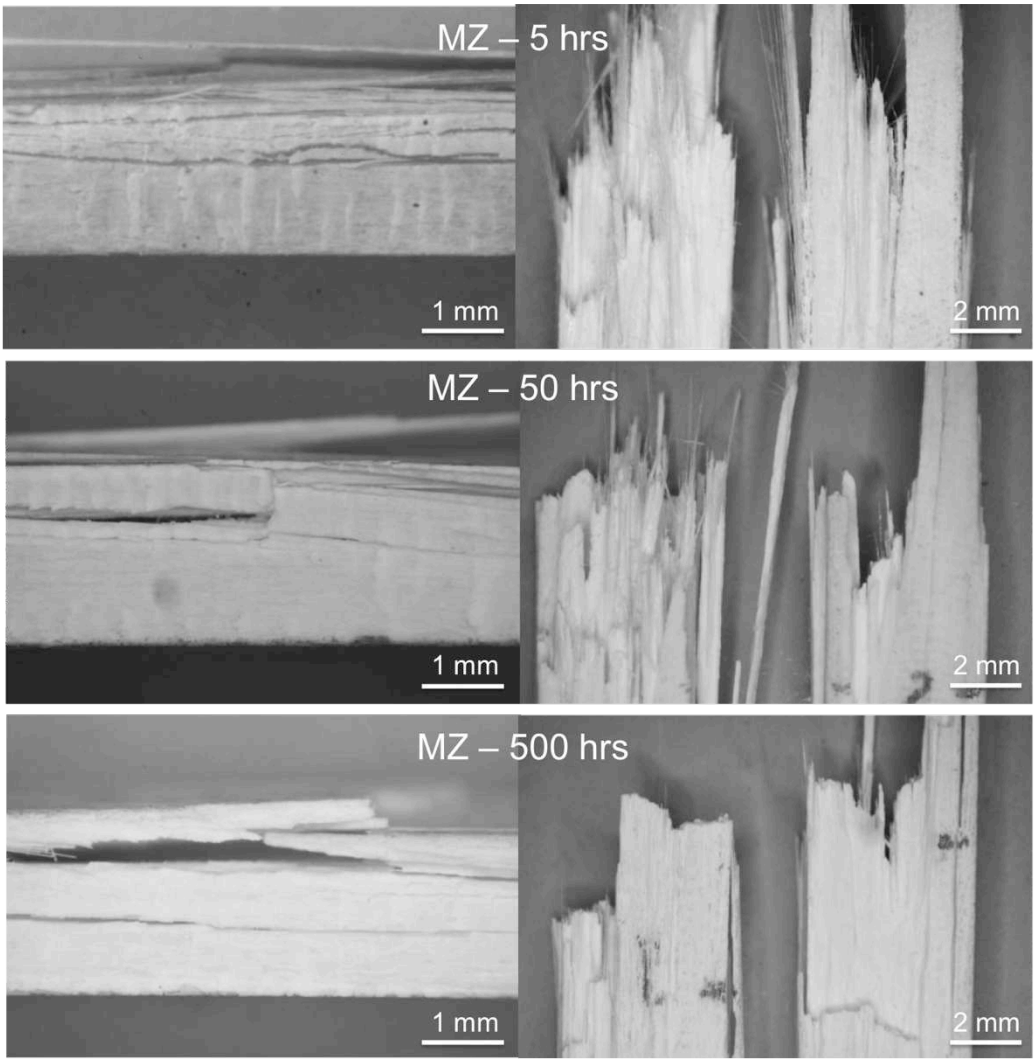

Figure 73: Damage and fracture surfaces typical of aged MZ specimens. The surface of the beam subjected to tensile forces face top of page in the set of images on the left and out of the page in the set of images on the right

7.1.3 Results of aged composites specimens in short beam shear

7.1.3.1 Short beam strength

The short beam strengths of unaged versus aged specimens are shown in Figure 74. As discussed in Chapter 6, it is also important to interpret resulting short beam strength values in light of how specimens failed in short beam shear. Figure 75 shows the type and

frequency of failures in each specimen. The results indicate that short beam strength of CL specimens declines with at least 50 hours of thermal aging, albeit only very slightly. All except one CL specimen at the 5-hour condition exhibited failure in flexure on the tensile surface. Considering the type of failure, the slight decrease in CL specimen short beam strength correlates with a decrease in flexural strength. Recall, a slight decrease in flexural strength of aged CL specimens was noted in section 7.1.2.1 (see Figure 68).

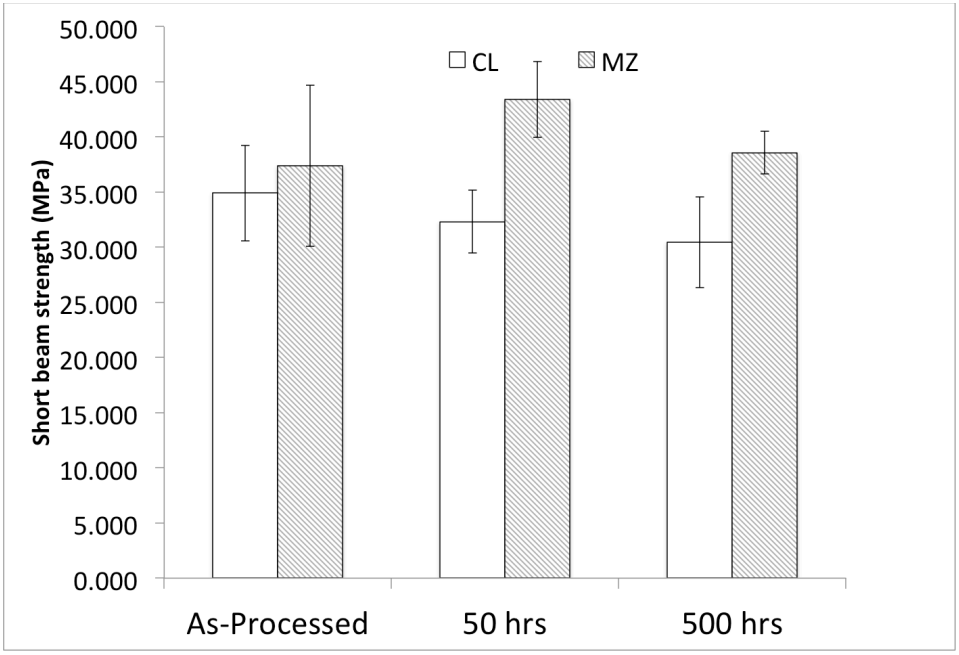

Figure 74: Short beam strengths of aged specimens compared

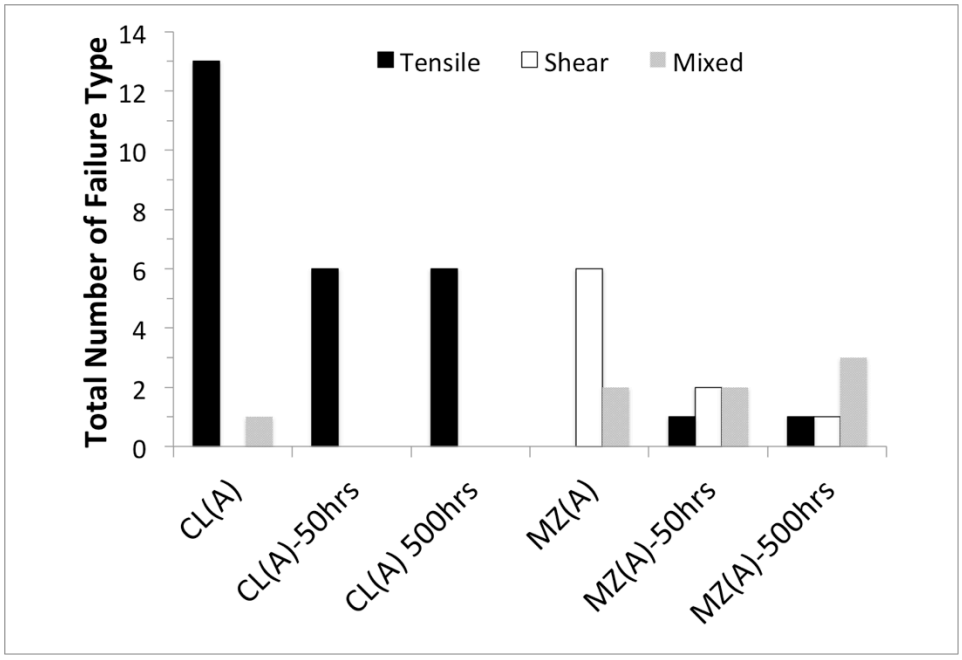

Figure 75: Type and frequency of failure observed in SBS testing of aged specimens

The short beam strength of MZ specimens was on average consistently higher than CL with the differential increasing with thermal aging. That said, the differential seems to be a result of decreasing CL short beam strength rather than a significant changes in the short beam strength of MZ specimens with increased exposure time.

The type of failure exhibited by MZ specimens does change with thermal aging. The change in failure based on frequency in Figure 75 can be compared visually with the images in Figure 76. The additional exposure time at temperature resulted in fewer failures in MZ specimens where shear was the only mode of failure. The results indicate the mode of failure in short beam shear changes with as little as 50 hours at 650 °C for MZ specimens.

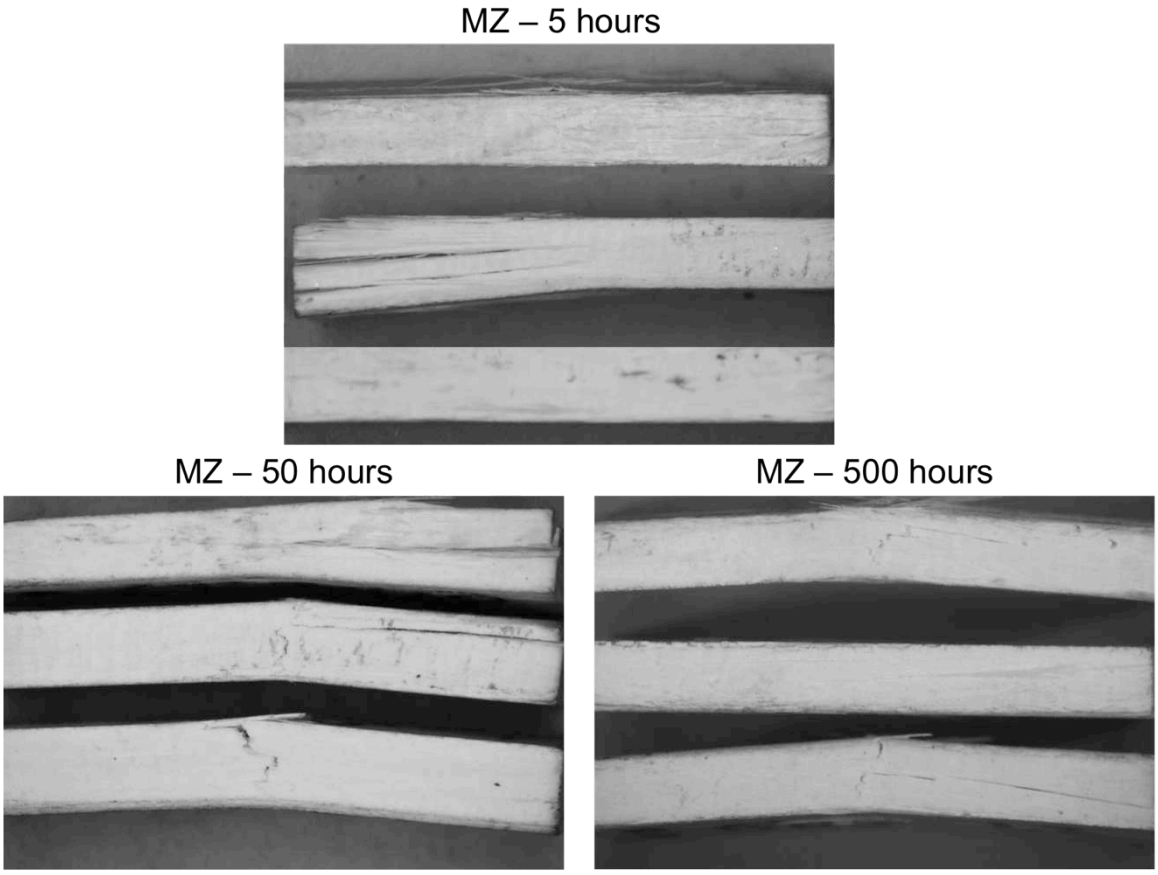

Figure 76: Fracture in aged and unaged MZ specimens produced during SBS testing

7.2 Unreinforced Specimen Testing

7.2.1 Specimen preparation

As already discussed, the cylindrical and prismatic samples prepared in section 3.3.2 were not altered much from their fabricated form to produce both compression and flexural test specimens, respectively (see Figure 17). Only light sanding techniques were applied to produce the final dimension of specimens. The final dimensions of specimens were intended to replicate the specimens used in previous research with unreinforced

MEYEB [38]. The compression specimens were 6 mm in diameter and varied in length from ~15.5 to 19.5 mm. Flexural specimens were nominally 4.25 mm (depth) x 4.25 mm (width) x 45 mm (length).

A total of ten compression specimens were prepared for testing. Five of the specimens received the standard 5-hour heat treatment at 650 °C and the other five were aged for maximum 500 hours of exposure at this same temperature. For flexural testing, a total of 18 specimens were prepared. Nine of those 18 specimens were aged for 500 hours, while the other specimens were heat treated for only 5 hours at 650 °C. No unreinforced specimens were prepared for the intermediate exposure time of 50 hours.

7.2.2 Experimental setup and calculations

7.2.2.1 Compression testing

Compression testing was conducted in accordance with testing that was part of a recent doctoral work [38]. The testing was conducted in the same Applied Test System screw driven load frame used to test specimens in 4-point flexure. Specimens were placed in an aluminum compression cage (see Figure 77). The crosshead speed was 0.5 mm/min. Testing was ceased upon failure of specimens. Load as a function of time was recorded for each test. The compression strength (C_u) of specimens was calculated using the following relationship also used in the previous work [38]:

$$C_u = \frac{P_u}{A} \tag{7.1}$$

Where P_u is the load at failure and A is the cross-sectional area of the specimen.

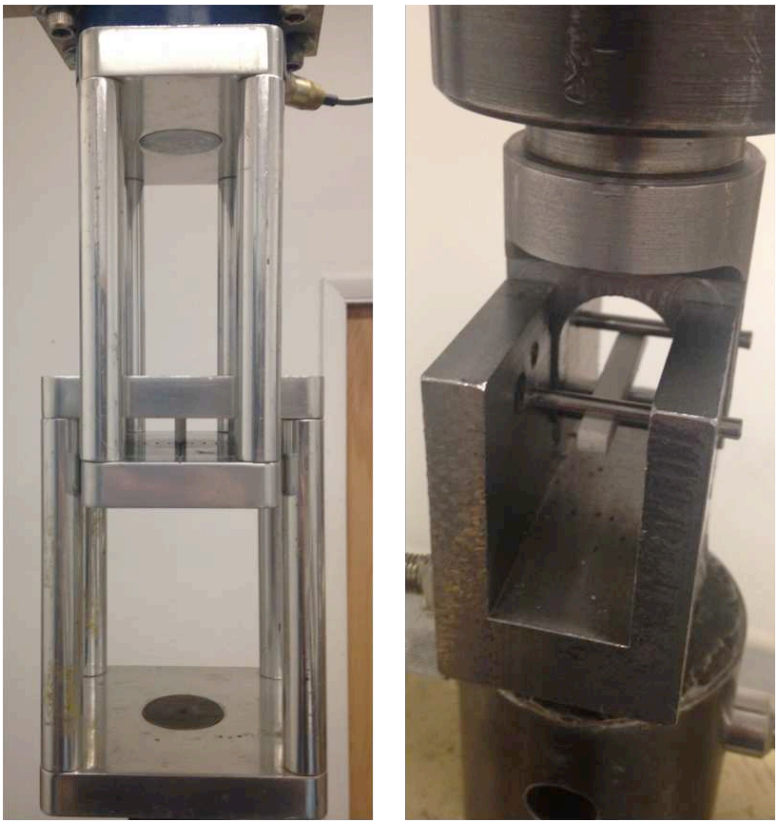

Figure 77: Test fixtures and setups used for unreinforced samples: compression (left image) and 3-point flexure (right image)

7.2.2.2 Flexural testing

Flexural testing was conducted in accordance with the research that tested unreinforced MEYEB beams [38] and with ASTM C1341 [113]. The testing utilized a 3-point configuration. This is unlike the 4-point set up used for composite specimens. The testing also utilized a different test fixture from that used in Chapter 6 (see Figure 77). The choice of a different flexure configuration and fixture were necessary in order to establish a direct comparison to previously reported data on the mechanical properties of the unreinforced MEYEB matrix. The only differences between the flexure tests of this investigation and the previous study was that they were performed in different load frames. The loading nose and support pins were 6 mm and 3.175 mm in diameter respectively. The support span of

the test fixture was 30 mm making the span-to-depth ratio roughly 7:1. It is a short span, but the very brittle nature of the MEYEB geopolymer makes it exceptionally easy to produce failures in flexure. Specimens were tested in displacement control mode at a rate of ~0.5 mm/min. Load as a function of time was recorded for each test. The flexural strength (S_u) of specimens was calculated using the following equation [113]:

$$S_u = \frac{3\ P_u L}{2\ bd^2} \tag{7.2}$$

where P_u is maximum force recorded, L is the support span, b is the width of the specimen, and d is the thickness of the specimen.

7.2.3 Results: Aged unreinforced specimens

7.2.3.1 Mechanical properties in compression

Figure 78 shows the compression strength of the unreinforced MEYEB matrix and the influence of aging. Five specimens were tested from each condition, but two specimens were rejected from the un-aged specimens due to test setup issues and final length to circumference ratio. Of the five aged specimens one specimen was rejected based on the resulting low failure load, which occurred much earlier than other samples.

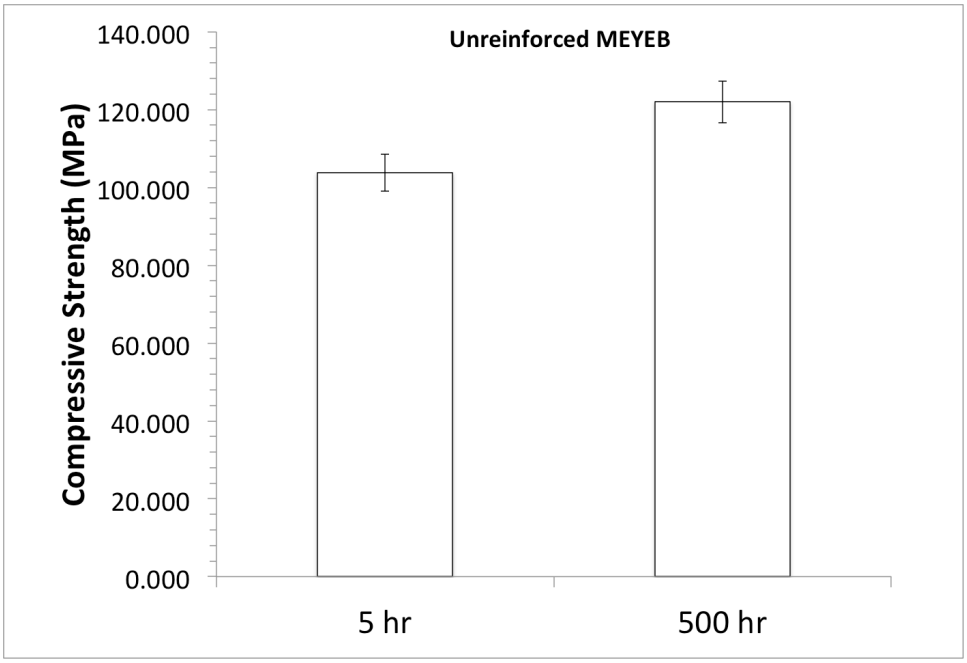

Figure 78: Compressive strength of aged unreinforced MEYEB specimens compared

The compression strength of the 5-hour specimens agree well with values already for unreinforced MEYEB heat treated at this temperature [38]. (Refer to Table 2 for comparison.) After 500 hours, the compression strength of the MEYEB appears to rise. The increase is roughly 17%. The failure of specimens was catastrophic. Only small portions of each specimen could be recovered because specimens broke into small pieces and were ejected with substantial velocity in all directions from the aluminum cage. The strength increase is consistent with increased density of the matrix.

7.2.3.2 Mechanical properties in flexure

The flexural strength of aged, unreinforced MEYEB specimens is shown in Figure 79. In previous research, the flexural strength of unreinforced MEYEB was reported to be ~11 MPa for specimens heat treated at 650 °C for five hours. The results of this investigation

show a ~300% increase in strength of specimens of the same type. Other research would agree with the lower value and suggest the value obtained from this investigation might be inflated [8], [9], [88], [95], [142]. As such, the magnitude of the flexural strengths obtained from this investigation should be treated with caution. Considering the resulting compression strength values of MEYEB in this investigation were similar to values previously reported it is uncertain why there is such a disparity in the flexural strengths.

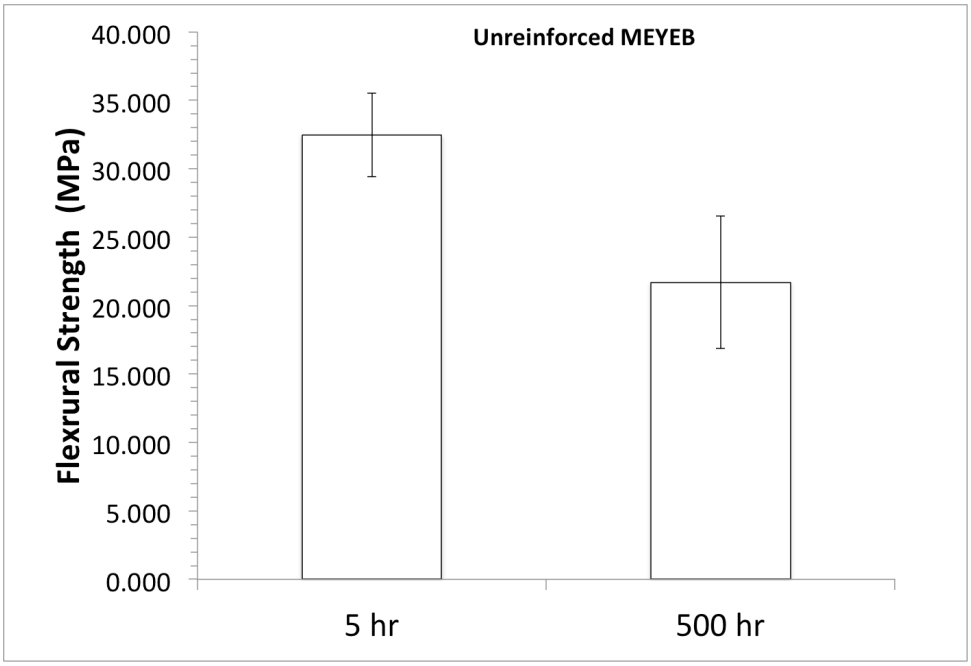

Figure 79: Compressive strength of aged unreinforced MEYEB specimens compared

While magnitudes should be observed with a note of caution, it's possible the flexural strengths of specimens can be evaluated in a qualitative manner. Unlike in compression, the flexural strength of MEYEB specimens decreases with aging. According to the data, the decrease is ~33%. All specimens failed catastrophically breaking into two halves. As anticipated, the fracture surfaces all specimens indicated a brittle failure (see Figure 80)

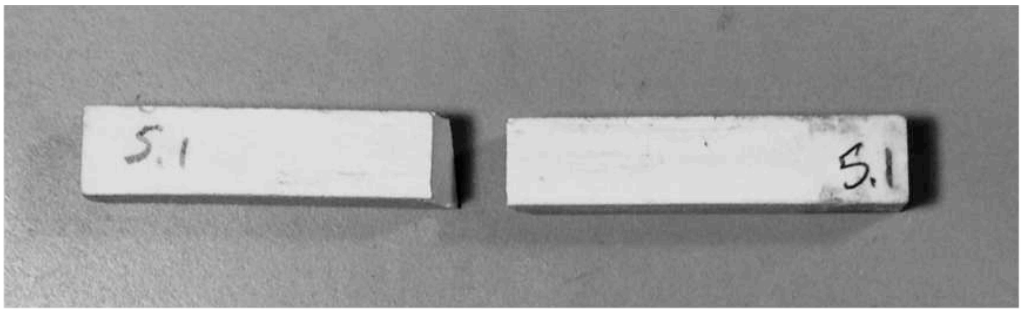

Figure 80: Fracture of unreinforced MEYEB specimens in flexure

7.3 Microstructural Changes

The resulting changes in mechanical behavior of both composite and unreinforced specimens prompted an examination of changes at the microstructural level of the materials. The microstructure of composite and unreinforced specimens aged for 5 and 500 hours were examined using SEM. Figure 81 and Figure 82 compare the effects of aging on the composite microstructures of CL and MZ specimens, respectively. (The foreign matter, as labeled in Figure 82, was determined to be so by EDS and appears to be a contaminant introduced during preparation of samples for observation.) The images in these figures reveal little difference between composite microstructures regardless of aging or fiber surface condition. Despite the similarity depicted in these images the overall examination was deemed inconclusive. A degree of variation in the microstructure throughout specimens and presence of fiber made it difficult to determine if actual differences in the microstructure did exist.

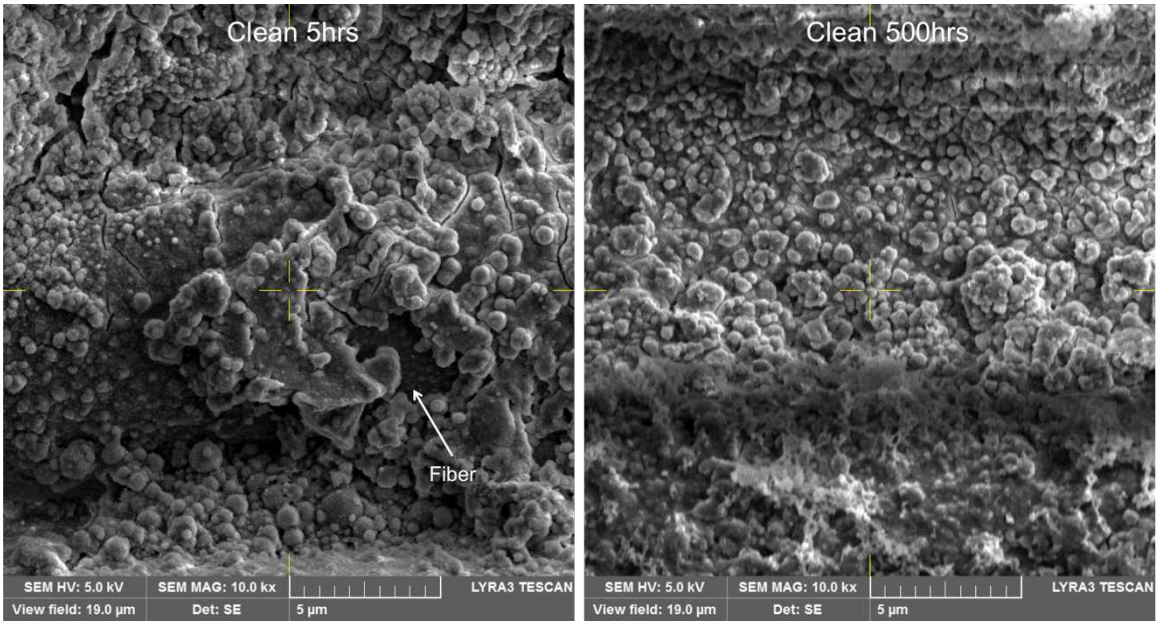

Figure 81: Aged and unaged microstructure of CL specimens compared

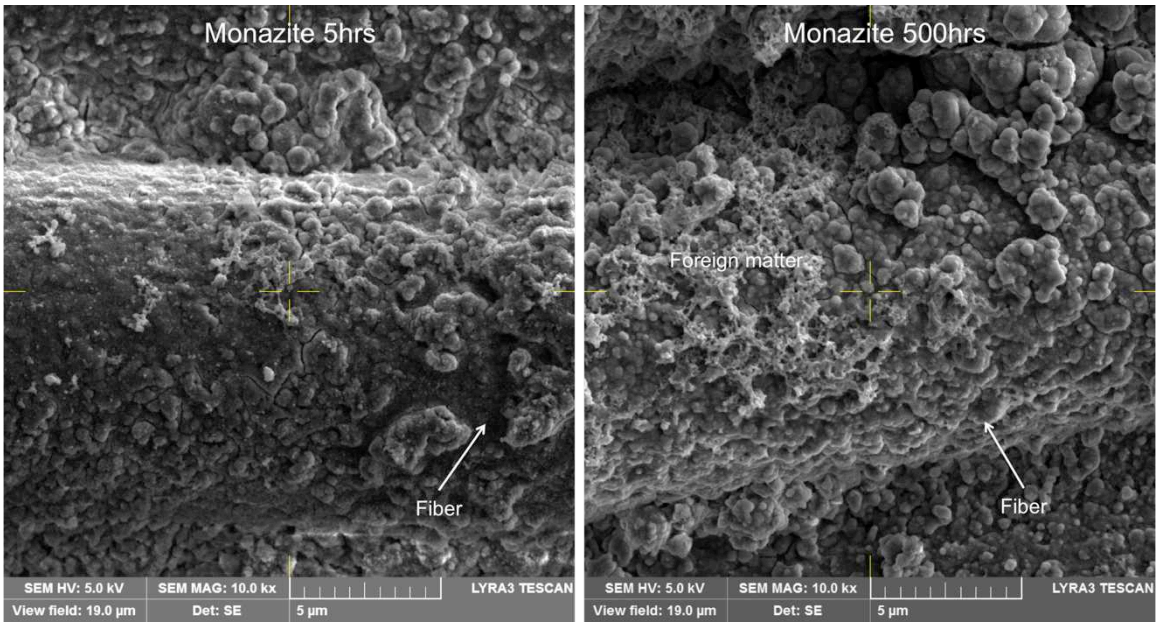

Figure 82: Aged and unaged microstructure of MZ specimens compared

The effect of aging on the unreinforced specimens is shown in Figure 83. Even at a lower magnification these unreinforced specimens do exhibit a noticeable change in the

appearance of their microstructure after 500 hours at 650 °C. Those specimens heat treated for 500 hours reveal a structure that is more interconnected. In a previous study, a small reduction in the particle nature of the MEYEB was noted after 5 hours at 650 °C with a complete loss of the particle nature of the MEYEB after 5 hours at 870 °C [38]. It appears that with the maximum exposure time of 500 hours at 650 °C the structure of the material transforms. In other geopolymer potassium-based geopolymers, a similar coalescing effect has been observed after elevated temperature exposure and attributed to effects of dehyrdroxylation and sintering [34].

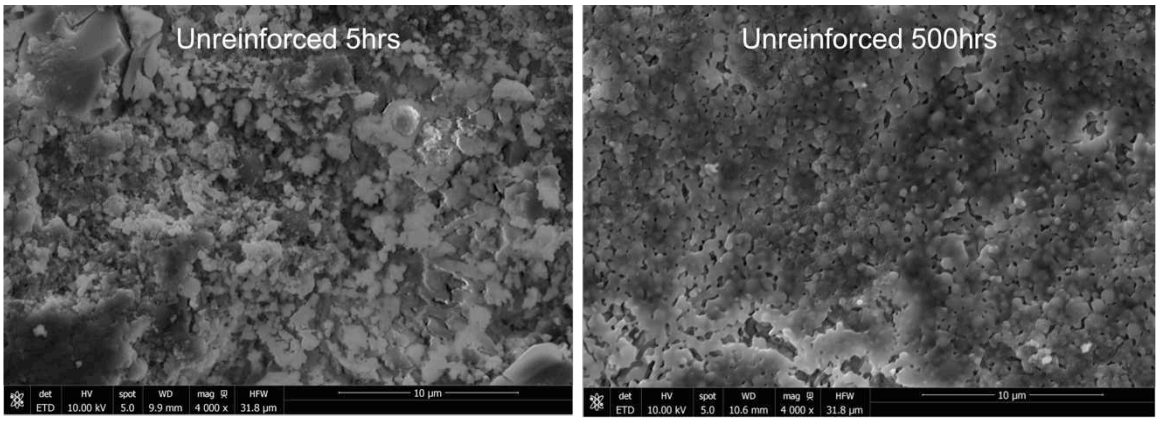

Figure 83: Aged and unaged microstructure of unreinforced specimens compared

Comparing the microstructure of reinforced and unreinforced specimens a difference appears to exist. It would seem the fiber may have influenced the final form of the geopolymer matrix structure or it simply altered its appearance because of its presence

7.4 Discussion

7.4.1 Influence of thermal aging on mechanical strength

Thermal aging of the unreinforced, geopolymer resulted in increased compressive strength and decreased flexural strength of specimens. SEM of the microstructure revealed the particle structure of the geopolymer had coalesced after aging. This is similar to what had been observed before in MEYEB with higher temperature exposure [38]. It has been reported that exposure of geopolymers and MEYEB to temperatures beyond 600 °C, usually near 800 °C, results in microstructural changes that reduce open porosity and increase density of the geopolymer [34], [38], [103], [143]. The microstructure of the MEYEB after thermal aging seems to suggest a similar effect of high temperature exposure. It was reported that the compressive strength of MEYEB increased after exposure to 760 °C, but at the same temperature no change in the flexural strength of the specimen occurred [38]. Assuming only densification and not an actual phase change of the material at these temperatures, it would be suspected that the reduced porosity would aid the geopolymer in compression because of the reduction in flaws. The significant loss in flexural strength of MEYEB after thermal aging might be explained by same effect. The more particle and porous nature of MEYEB prior to aging may have had a slight crack mitigating effect under tensile loads. With a loss of these features, the MEYEB maybe acting more like a weak monolithic material and as such its flexural strength would be reduced. Studies have noted increases in the flexural strength of certain types of geopolymers after exposure to temperatures above 650 °C (800 °C and higher) [101], [103]. In each, the rise is linked to a

sharp decrease in the porosity from sintering. This may suggest the changes observed in the microstructure are not complete even after the maximum exposure time of 500 hours.

A complete understanding of the effects of thermal aging on unreinforced MEYEB was out of the scope of this research. In addition, minimal attention has been given to thermal aging within the geopolymer community of researchers, so not much can be said at this time without further investigation. What is understood is that after thermal aging the nature of MEYEB changes, which affects its mechanical strength and also alters its appearance at the microstructural level. The results of aging also call into question the thermal stability of geopolymer despite previous data suggesting 5 hours at 650 °C had produced a stable condition for the geopolymer [38], [84]. The changes in MEYEB associated with thermal aging are likely related to sintering of the material, which were previously noted to occur in geopolymers exposed to slightly higher temperatures than 650 °C.

The effect of thermal aging on composite specimen strength seems to be less clear, but the changes could be closely related to the effects that were noted in the unreinforced material. Flexural testing only showed a slight decrease in flexural strength of CL and MZ specimens after the minimum amount of thermal aging. Significant losses were not observed with continued aging. The loss, albeit small, was somewhat of surprise. No changes were expected in the fiber and/or monazite interphase material based on original coating temperatures and stability in other composites at higher temperatures [53], [108]. Little is known about the long-term exposure of the combined constituents at temperatures of

650 °C. Unfortunately, observation of the microstructure did not provide any clues and in fact suggested the changes observed in the unreinforced matrix might have been retarded by the presence of the Nextel fiber. An associated effect on the thermal evolution of geopolymers has been observed in geopolymers with added alumina particle filler [103]. It is possible the Nextel fiber, which is mostly alumina, may have had the same effect on the microstructure of the geopolymer.

A reduction in flexural strength of MZ specimens could be related to the changing structure of the matrix. However, the reduced strength may be explained by the reduced fiber volume fraction in these specimens. The fiber volume fraction of the aged MZ versus unaged MZ specimens was reduced on the order of 5%. Recall, this was due to difficulty controlling the final thickness of specimens during manufacture and not a thickness increase due to heat treatment. The difference in V_f is small so it is not entirely certain this would have an effect. Additionally, the same percent difference was investigated for CL specimens, which indicated no change (see Chapter 6, Figure 38). The lack of change in CL specimens despite a decreased V_f could be because of their brittle nature. The same figure in Chapter 6 did show that small changes in the fiber volume fraction of MZ specimens resulted in changes to the strength of specimens. Considering the mechanism for increased strength in MZ specimens has been demonstrated to be the result of the interphase, it is possible that any reduction in V_f in MZ specimens has a greater effect on its strength.

7.4.2 Influence of thermal aging on damage tolerance

Stress-strain curves would indicate MZ specimens to have a reduced ability to provide the same degree of damage tolerance after thermal aging and therefore demonstrate reduced

toughness. The effect seems to be more pronounced after 500 hours, but it appears that changes possibly start as early as 50 hours of thermal aging. Fracture in these specimens also supports the change, as the MZ specimens seem to exhibit a less damage tolerance. Once, again this reduced toughness is more evident in those specimens aged for 500 hours. The changes in the failure mode of MZ specimens in SBS testing also indicate that the shear properties changed after aging. It is possible based on these results the interphase may be degraded by the long-term temperature exposure. However, the thermal properties of MZ [67] do not support the notion of degradation under the thermal conditions these composites were exposed to. However, its chemical stability with the geopolymer is unknown. Despite the possibility of a degraded interphase, it is still effective at producing a higher degree of toughness in the geopolymer composite as compared to aged or unaged CL specimens after 500 hours at 650 °C.

As just noted, changes were not expected to occur in the fiber or the monazite interphase from thermal aging at these temperatures. Furthermore, SEM of the composites prior to and after aging did not reveal obvious changes in the fiber or microstructure. Based on this, it could be that the reduced fiber content might be responsible for the changes observed in the stress-strain curves and fracture surfaces. The reduction in fiber content would mean fewer crack energy dissipating mechanisms present. This too would explain the less tortuous fracture appearance of aged MZ specimens in flexure and the change in SBS failure modes.

Additionally, the slightly less damage tolerant behavior of MZ specimens could be explained by changes taking place in the microstructure of the geopolymer as was observed in the unreinforced material. The sum total of evidence gathered within this investigation and also from outside sources might suggest increased densification and thus shrinkage of the matrix. This could have increased the interfacial bond strength of the composite. Increased interfacial bond strength could explain the SBS fracture surfaces and the reduced toughness of specimens. However, the lack of evidence for any microstructural change occurring in the composite specimens containing the monazite interphase does not offer enough support for this idea at this time. Still, it is a factor worth considering to explain the reduced the toughness in MZ specimens aged for 500 hours.

Additional work is definitely needed to truly understand how aging effects the toughness of composite MZ specimens. Push-out experiments, which were unfortunately not originally scheduled as part of this investigation, would be helpful in determining if any changes occurred at the interface. Clearly, the effect of thermal aging on toughness of specimens would also be better understood if fiber volume fraction was not a variable. Regardless, results do still indicate that MZ specimens aged for the maximum amount of time retain an interphase capable of producing greater toughness than that observed in CL specimens.

7.5 Conclusion: Thermal Aging

Another set of CL and MZ composites specimens were fabricated in addition to those created for the primary study in Chapter 6 and subjected to thermal aging to simulate long-term service conditions. The additional composite specimens were subjected to either an

intermediate an aging time of either 50 or 500 hours at 650 °C. Specifically, the testing and examination of composite specimens were conducted to investigate changes in the toughness of composite specimens. Four-point flexure testing was conducted along with short beam shear tests to compare with data presented and discussed in Chapter 6 of this document. Additionally, the fracture surfaces of specimens were examined for possible indications of changes to composite toughness.

To aid in understanding of how the mechanical strength and microstructure was altered by thermal aging, unreinforced specimens were also created. Sets of these specimens were subjected to either 5 or 500 hours at 650 °C for comparison. Compression and three-point flexural testing were conducted on these specimens in accordance with procedures used in prior research with MEYEB. In both reinforced and unreinforced specimens, SEM was used to observe changes in the microstructure of specimens prior to, and after, the maximum thermal exposure time of 500 hours.

The observations of microstructure in unreinforced specimens exposed to 650 °C for 500 hours indicated the material had coalesced, which was the likely the result of sintering. Additionally, the compression strength and flexural strength of unreinforced specimens were altered by extended thermal exposure. The changes in the nature of the MEYEB matrix may have contributed to the composite performance after longer thermal exposure.

Aged MZ composite specimens at both thermal exposure times remained damage tolerant and still exhibited greater strength than CL specimens before and after aging. Both CL and

MZ specimens did indicate very slight decreases in strength of 10% and 15% after maximum thermal exposure time, respectively. Short beam shear testing and fracture surfaces of MZ specimens after 500 hours of aging suggested that the interphase might have been compromised and potentially resulted in the less damage tolerant behavior observed in the stress-strain curves of aged MZ specimens as compared to aged. The change was a surprise because of the thermal stability of the monazite interphase. Possible explanations included the reduced V_f in the MZ specimens fabricated for aging as compared to the specimens created for the primary study or microstructural changes in the matrix that might have altered the interfacial conditions. Still, the changes were not substantial enough to render the monazite interphase ineffective in providing improved composite toughness as compared to CL composite specimens.

Chapter 8: Summary & Conclusions

8.1 General conclusions

The main objective of this research was to demonstrate improved toughness of brittle geopolymer matrix composites through the use of fiber coatings. The use of fiber coatings, which are generally used to toughen advanced ceramic matrix composites (CMC) by establishing a weak interfacial condition, was expected to do the same in GMCs. However, the application of the fiber coatings in GMCs becomes a unique problem to solve because of the different mechanical properties of the matrix and processing conditions compared to those of CMCs. As such, it was also important to demonstrate that fiber coatings could be used to improve toughness and maintain acceptable composite mechanical properties, which are highly influenced by the strength of the bond at the interface. Additionally, the application of GMCs for use as a structural components will likely expose them to oxidizing environments with temperatures in the range of ~400 to 800 °C. As such, the hypothesis of this research as proposed was that through the use of fiber coatings, continuous fiber reinforced geopolymer matrix composites can demonstrate improved toughness, while still retaining a high degree of strength and modulus even after exposure to elevated temperatures.

The research revealed that processing conditions of the geopolymer, which cause variations in its final properties, can have significant influence on GMCs using interfacial

modifiers. In cases where the fiber-matrix bond is much stronger, the relatively poor properties of an incompletely cured geopolymer matrix did not negatively influence the modulus or the strength of the overall composite as the type of reinforcement appeared to dictate the final mechanical properties of the composite. This is consistent with experience gained in the study of polymer matrix composites, where the matrix also has lower mechanical properties than the reinforcing fibers, and achieving favorable composite rely on a strong bond at the fiber-matrix interface. Unfortunately, when the fiber-matrix bond strength was reduced through the use of an interface coating, the poor mechanical properties of an incompletely cured geopolymer matrix had negative effects on the ability of the composite to load the fibers and resulting significant drop in mechanical properties was observed. However, a full recovery of composite modulus and strength were witnessed when a small increase in the mechanical properties of the matrix were achieved by subjecting the GMC with the weaker interfacial condition to an extended cure time. This finding alleviates original concerns surrounding the use of interphase in GMCs. The recovery is attributed to increased shear resistance of the matrix and shear stress transfer from matrix to fiber. For the MEYEB geopolymer, there appears to be a sufficient increase in properties of the matrix when curing for at least 5 hours versus only 1 hour. There may be little observed benefit to the mechanical properties of GMCs with weak interfaces when the initial cure exceeds 5 hours. In order to capitalize on more economical production methods for GMCs with weak interfaces this should be explored in future investigations.

The incorporation a tailored interphase in GMCs was beneficial to composite toughness in all cases except where the fiber coating was degraded by the oxidizing environment.

Toughness in GMCs with the uncoated Nextel 610 fiber was limited due to the strong bonding condition created at the interface. SEM of corresponding fiber push-out specimens revealed damaged fibers on the "pushed-in" side of specimens and chunks of matrix still attached to fibers on the "pushed-out" side. These specimens demonstrated no damage tolerance and failed catastrophically in flexure and in tension. This has revealed what was originally only theorized: a stronger bonding condition between fiber and matrix in GMCs results in a low toughness composite.

Specimens that contained the carbon coated fiber condition heat treated in an oxidizing environment demonstrated similar toughness to the uncoated GMC specimens. SEM from push-out testing, short beam shear tests, and evaluation of fracture surfaces suggest the bond between fiber and matrix was enhanced possibly due to diffusion of similar species in the fiber and the matrix. This appeared to be confirmed by the rougher surface of pushed fibers in these specimens and higher friction stress measured during push-out. Despite an enhanced bonding condition, the results of these tests also suggested these specimens had a slightly weaker bonding condition than uncoated specimens. This means diffusion was not uniform throughout the specimen or that a narrow gap may have existed at the interface. If a gap, it is possible fugitive coatings may be used in lieu of more expensive oxide coatings for producing greater toughness in GMCs and is worth further investigation.

Although GMCs with carbon coated fiber, heat treated in a non-oxidizing environment demonstrated improved toughness over the cleaned fiber surface condition, the toughness of GMCs containing the monazite coated fiber was superior to all other specimen types

regardless of heat treatment environment. The larger measured value of toughness for monazite coated fiber specimens was the result of increased area under the stress-strain curve from inelastic deformation and non-catastrophic failure and also from increased strength as compared to the baseline cleaned fiber specimens, which did not incorporate a fiber coating. Analysis of push-out and short beam shear testing provided clarity that the interfacial strength in the GMCs containing interphase had been reduced as compared to uncoated fiber composites. While carbon coated specimens did exhibit similar stress-strain behavior to the monazite coated specimens, the strength of the specimens did not increase and measured value of toughness was lower. The amassed data suggests interfacial tailoring to improve toughness requires more than a simple reduction in the interfacial properties of the composite. The particular interfacial properties of monazite coated specimens produced superior toughness as compared to carbon coated GMCs. Additionally, extremely poor shear stress transfer caused by properties of the matrix, as was case for GMCs with interphase cured for one hour, resulted in a composite with poor mechanical properties and limited toughness. Therefore, only a carefully tailored interfacial strength in GMCs can produce tough behavior while still retaining elevated mechanical properties.

The push-out tests were the first known tests of this type to ever be conducted on GMCs. Two measures, debond energy and friction stress, were presented for each GMC, which differed based on fiber surface condition. The measurements, together with SEM of push-out specimen surfaces, revealed key differences between the interfacial characteristics of each type of GMC. Of the two specimen types that demonstrated improved toughness,

monazite fiber coated specimens had the lowest debond energy, but higher friction stresses than that of the carbon coated specimens heat treated in an inert environment. The higher friction stress of monazite specimens, which appears to be from the coating failing internally, may be responsible for the greater toughness measured for these specimens as compared to carbon coated specimens. The results have become the only known direct examination of interfacial properties in GMCs. The analysis of push-out testing in conjunction with mechanical testing have revealed that push-out testing can be extended to determine the potential of GMCs to demonstrate toughness much in the same way it has for CMCs.

Short beam shear tests, which aided characterization of the interfacial strength also appear to be an acceptable means of initially qualifying coatings for use in GMCs. The results of this simple, cost effective technique that involves a small investment of material demonstrates ability to link failure in short beam testing to the potential of the composite to demonstrate enhanced toughness.

In addition to demonstrating increased toughness after elevated temperature exposure at 650 °C, monazite coated fiber GMCs remained tougher than specimens without coating after thermal aging. Thermal aging was intended to simulate the GMC under service conditions. Toughness appeared to be reduced, but it is possible the reduction was the result of variability in fiber volume fraction of specimens subjected to aging. The results also revealed the changes could be the result of thermal instability of the matrix, which may have altered interfacial properties of monazite coated specimens. This effort involving

thermal aging is only one of two known studies that exists in the literature on GMCs or even geopolymers adding to limited knowledge on the acceptable service conditions for geopolymers. The effort points to the potential thermal instability of the geopolymer after long-term elevated exposure at temperatures.

However, and more importantly, GMCs with fiber coatings subjected to limited or long-term thermal aging, despite changes occurring in the matrix, can continue to demonstrate relatively higher degrees of toughness than GMCs without fiber coatings. The interfacial conditions appear to be a key parameter dictating toughness and also for maintaining, or even improving upon, the mechanical properties of the composite. This technique of using fiber coatings to improve toughness in CMCs has been demonstrated now for GMCs, which contain a matrix much different than that of typical advanced ceramics. This research has laid the groundwork for future investigations that involve tailoring the interfacial bond in GMCs. Additionally, it has demonstrated greater potential of GMCs to be used in high temperature, structural applications.

8.2 Future Work

The efforts of this study have demonstrated even greater potential for using GMCs in high temperature structural applications. However, as were studies prior to this one, this is only a launching point for future investigations in this area. The following provides some recommendations for future work:

- The relatively simple procedures associated with fabricating GMCs provide the opportunity for a low-cost, hi-temperature material. Time necessary for the

fabrication of components directly affects the final cost of the component and therefore the economical feasibility for larger scale production. Unfortunately, research has revealed that longer cure times in geopolymers allow for full reaction of species and greater mechanical properties. This research revealed the length of initial cure time also effects composite properties for those GMCs containing weakened interfacial conditions. The increased cure time in coated GMCs appeared to improve shear resistance and shear stress transfer to fibers. However, comparing the results of the preliminary examinations of Chapter 4 with the results in Chapter 6 reveals little difference in toughness and mechanical properties in GMCs with coatings even though the cure times varied by as much as 19 hours. This may mean there is an opportunity to reduce the processing time for GMCs with fiber coatings and still achieve tough behavior and relatively good mechanical properties. Therefore, future studies should be used to identify the least amount of cure time necessary in GMCs with fiber coatings that produces the same mechanical behavior as those produced using the optimal initial cure condition time of 24 hours.

- Within the past few years, some attention has been given to using geopolymers as precursors to ceramics. The transformation of the geopolymer to a ceramic is a result of high temperature exposure (well above the designated use temperature), which produces a phase change. The same concept has been employed to produce CMCs from GMCs. Some of the difficulty in incorporating fiber coatings in CMCs to produce greater toughness is the result of the high temperature processing, which creates undesirable thermal residual stresses at the interface after returning to room temperature and changes that occur in the coating itself. Since GMCs are

processed at much lower temperatures this may create an opportunity to overcome some of these effects. An informative study would be to determine the effectiveness of fiber coatings in promoting toughness in GMCs converted to CMCs.

- It was revealed by this research that the monazite fiber coating was effective at producing greater toughness in GMCs after elevated temperature exposure. However, it is unlikely such GMCs will be subjected to loading only after thermal exposure. For consideration, as a high temperature, structural component high temperature mechanical testing should be performed. High temperature will likely effect the interface because of thermal expansion effects. Such testing will reveal the effectiveness of the monazite coating to provide improved toughness under service-like conditions. Predictions on how the thermal environment might effect toughness and interfacial parameters can be made by understanding the coefficient of the thermal expansion of the different constituents.
- The use of carbon fiber and SiC fiber in GMCs generally results in favorable composite mechanical properties: strength and relative degrees of toughness. An informative future effort could evaluate the interface and toughness in these composite types along side a GMCs similar to that used in this research. This would aid in understanding the interfacial conditions that promote toughness in GMCs containing carbon and SiC fibers that do not necessarily always need a coating and the more oxidation resistant fibers, like Nextel 610, that do. Furthermore, it will provide a way to more directly compare the improvement in mechanical behavior offered by the monazite coating applied to an alumina based fiber to these other fiber types.

- This research revealed that weak interface concepts commonly used in CMCs is applicable to GMCs. This was demonstrated only using two different coating types. The evidence clearly indicated a difference in resulting toughness between the two coating types because of the unique interfacial conditions created by each. In addition, these coating types varied in thickness. Both of these parameters, coating type and thickness, can greatly influence composite behavior. As such, further efforts should focus on analyzing the effect of altering these two parameters. This could include either numerical/modeling methods, similar experimentation to that employed by this research, or some combination of both. If numerical and modeling studies are conducted, it should be noted that the methods developed to characterize the interfaces in CMCs may be inadequate for addressing GMCs because of the large disparity in properties of the matrix materials. It should also be noted that any model developed for a coating type may be restricted to that particular coating as the material make-up (composition, structure, and fracture behavior) can also influence the overall mechanical behavior of the composite.
- The Nextel 610 fibers used in this study are very robust fiber type from a thermal and mechanical property standpoint. However, the properties come at a cost. The Nextel 610 fibers, and most of the fibers in the Nextel series, are relatively expensive. Applying coatings to fibers also adds an additional production step and can very costly. Incorporating coatings on fibers that are less expensive yet still offer the necessary thermal and mechanical properties, like basalt fibers, should also be explored. This is important for maintaining the cost savings associated with using GMCs in the intermediate temperature range of 400 °C to 900 °C versus CMCs

and metal matrix composites which generally require more costly materials and processing steps.

Bibliography

[1] K. Pielichowski and J. Njuguna, *Thermal Degradation of Polymeric Materials*. iSmithers Rapra Publishing, 2005.

[2] K. K. Chawla, *Composite materials science and engineering*, 3rd ed. Springer, 2012.

[3] R. J. Kerans, R. S. Hay, T. A. Parthasarathy, and M. K. Cinibulk, "Interface Design for Oxidation-Resistant Ceramic Composites," *J. Am. Ceram. Soc.*, vol. 85, no. 11, pp. 2599–2632, Dec. 2004.

[4] J. Davidovits, *Geopolymer Chemistry and Applications*. Geopolymer Institute, 2008.

[5] J. Davidovits, "Geopolymers and geopolymeric materials," *J. Therm. Anal.*, vol. 35, no. 2, pp. 429–441, 1989.

[6] R. E. Lyon, P. N. Balaguru, A. Foden, U. Sorathia, J. Davidovits, and M. Davidovics, "Fire-resistant aluminosilicate composites," *Fire Mater.*, vol. 21, no. 2, pp. 67–73, 1997.

[7] Q. Zhao, B. Nair, T. Rahimian, and P. Balaguru, "Novel geopolymer based composites with enhanced ductility," *J. Mater. Sci.*, vol. 42, no. 9, pp. 3131–3137, May 2007.

[8] A. J. Foden, "Mechanical properties and material characterization of polysialate structural composites," Ph.D., Rutgers The State University of New Jersey - New Brunswick, United States -- New Jersey, 1999.

[9] P. He, D. Jia, T. Lin, M. Wang, and Y. Zhou, "Effects of high-temperature heat treatment on the mechanical properties of unidirectional carbon fiber reinforced geopolymer composites," *Ceram. Int.*, vol. 36, no. 4, pp. 1447–1453, May 2010.

[10] M. Welter, "Unidirectional fibre reinforced geopolymer matrix composites," 2013.

[11] M. Alzeer and K. MacKenzie, "Synthesis and mechanical properties of novel composites of inorganic polymers (geopolymers) with unidirectional natural flax fibres (phormium tenax)," *Appl. Clay Sci.*, vol. 75–76, pp. 148–152, May 2013.

[12] K. D. Tran D. H, "Effect of curing temperature on flexural properties of silica-based geopolymer-carbon reinforced composite," *J. Achiev. Mater. Manuf. Eng.*, 2009.

[13] J. A. Hammell, "The influence of matrix composition and reinforcement type on the properties of polysialate composites," Ph.D., Rutgers The State University of New Jersey - New Brunswick, United States -- New Jersey, 2000.

[14] J. Mills-Brown, K. Potter, S. Foster, and T. Batho, "Thermal and tensile properties of polysialate composites," *Ceram. Int.*, vol. 39, no. 8, pp. 8917–8924, Dec. 2013.

[15] J. Mills-Brown, "High temperature composite materials and structures," Ph.D., University of Bristol, 2013.

[16] P. He *et al.*, "SiC fiber reinforced geopolymer composites, part 2: Continuous SiC fiber," *Ceram. Int.*

[17] D. W. Radford, C. Bulcher, M. Rollin, and T. Nivala, Peter, "Elevated Temperature Structural Properties Evaluation of SiC Reinforced Polysialate Matrix Composite." Society for the Advancement of Material and Process Engineering, 2013.

[18] S. Yan *et al.*, "Preparation and in-situ high-temperature mechanical properties of Cf-SiCf reinforced geopolymer composites," *Ceram. Int.*, vol. 43, no. 1, Part A, pp. 549–555, Jan. 2017.
[19] "Technical Data MEYEB™ resin for composite materials." Institut Geopolymere, May-2007.
[20] C. G. Papakonstantinou, P. Balaguru, and R. E. Lyon, "Comparative study of high temperature composites," *Compos. Part B Eng.*, vol. 32, no. 8, pp. 637–649, Dec. 2001.
[21] D. W. Radford, A. Grabher, and J. Bridge, "Inorganic Polymer Matrix Composite Strength Related to Interface Condition," *Materials*, pp. 2216–2227, 2009.
[22] J. W. Bridge, A. E. Grabher, and D. W. Radford, "Preliminary Investigation of Geopolymer Matrix-Ceramic FIber Composites for High Temperature Structural Applications," presented at the The 22nd Asian-Pacific Technical Exchange and Advisory Meeting on Marine Structures, Istanbul, Turkey, 2008.
[23] P. T. Nivala and D. W. Radford, "The effectiveness of toughness modifications of inorganic polymer matrix composites as measured by static flexure testing," in *2010 SAMPE Fall Technical Conference and Exhibition, October 11, 2010 - October 14, 2010*, 2010, p. SAMPE's Utah Chapter.
[24] K. A. Keller, T.-I. Mah, T. A. Parthasarathy, and C. M. Cooke, "Fugitive Interfacial Carbon Coatings for Oxide/Oxide Composites," *J. Am. Ceram. Soc.*, vol. 83, no. 2, pp. 329–336, Feb. 2000.
[25] Y. Wang, H.-T. Liu, H.-F. Cheng, and J. Wang, "Effective fugitive carbon coatings for the strength improvement of 3D Nextel™ 440/aluminosilicate composites," *Mater. Lett.*, vol. 126, pp. 236–239, Jul. 2014.
[26] R. S. Hay, M. D. Petry, K. A. Keller, M. K. Cinibulk, and J. R. Welch, "Carbon and Oxide Coatings on Continuous Ceramic Fibers," in *Materials Research Society Symposium*, 1995, vol. 365, pp. 377–382.
[27] Y. Tang, L. Liu, W. Li, B. Shen, and W. Hu, "Interface characteristics and mechanical properties of short carbon fibers/Al composites with different coatings," *Appl. Surf. Sci.*, vol. 255, no. 8, pp. 4393–4400, 2009.
[28] A. S. Rahman and D. W. Radford, "Cure cycle optimization of an inorganic polymer matrix material for high temperature fiber reinforced composites," *Compos. Part Appl. Sci. Manuf.*
[29] P. R. Jackson and D. W. Radford, "Effect of initial cure time on toughness of geopolymer matrix composites," *Ceram. Int.*
[30] M. Welter, M. Schmucker, and K.J.D. MacKenzie, "Evolution of the Fibre-Matrix Interactions in Basalt-Fibre-Reinforced Geopolymer-Matrix Composites after Heating," *J. Ceram. Sci. Technol.*, vol. 6, no. 1, pp. 17–24, Oct. 2014.
[31] P. He and D. Jia, "Interface evolution of the Cf/leucite composites derived from Cf/geopolymer composites," *Ceram. Int.*, vol. 39, no. 2, pp. 1203–1208, Mar. 2013.
[32] D. W. Radford and P. T. Nivala, "Dynamic mechanical analysis assessment of the effectiveness of toughness modifications of inorganic polymer matrix composites," in *SAMPE 2010 Conference and Exhibition "New Materials and Processes for a New Economy", May 17, 2010 - May 20, 2010*, 2010, p. Seattle and Eastern Canada SAMPE Chapters.
[33] P. R. Jackson and D. W. Radford, "Monazite Fiber Coating for Strength and Toughness Improvement of Geopolymer Matrix Composites," in *2016 SAMPE Fall Technical*

Conference and Exhibition, May 23, 2016 - May 26, 2016, 2016, p. SAMPE's Utah Chapter.
[34] P. Duxson, G. C. Lukey, and J. S. J. van Deventer, "Thermal evolution of metakaolin geopolymers: Part 1 – Physical evolution," *J. Non-Cryst. Solids*, vol. 352, no. 52–54, pp. 5541–5555, Dec. 2006.
[35] P. Duxson, G. C. Lukey, and J. S. J. van Deventer, "The thermal evolution of metakaolin geopolymers: Part 2 – Phase stability and structural development," *J. Non-Cryst. Solids*, vol. 353, no. 22–23, pp. 2186–2200, Jul. 2007.
[36] V. F. F. Barbosa and K. J. D. MacKenzie, "Thermal behaviour of inorganic geopolymers and composites derived from sodium polysialate," *Mater. Res. Bull.*, vol. 38, no. 2, pp. 319–331, Jan. 2003.
[37] V. F. F. Barbosa and K. J. D. MacKenzie, "Synthesis and thermal behaviour of potassium sialate geopolymers," *Mater. Lett.*, vol. 57, no. 9–10, pp. 1477–1482, Feb. 2003.
[38] Samsur A. Rahman, "Nanofiber Reinforcement of a Geopolymer Matrix for Improved Composite Materials Mechanical Performance," PhD, Colorado State University, 2015.
[39] R. W. Hertzberg, *Deformation and fracture mechanics of engineering materials*. J. Wiley & Sons, 1996.
[40] M. E. Launey and R. O. Ritchie, "On the Fracture Toughness of Advanced Materials," *Adv. Mater.*, vol. 21, no. 20, pp. 2103–2110, May 2009.
[41] A. G. Evans and D. B. Marshall, "Overview no. 85 The mechanical behavior of ceramic matrix composites," *Acta Metall.*, vol. 37, no. 10, pp. 2567–2583, Oct. 1989.
[42] H. Ming-Yuan and J. W. Hutchinson, "Crack deflection at an interface between dissimilar elastic materials," *Int. J. Solids Struct.*, vol. 25, no. 9, pp. 1053–1067, 1989.
[43] V. Gupta, J. Yuan, and D. Martinez, "Calculation, Measurement, and Control of Interface Strength in Composites," *J. Am. Ceram. Soc.*, vol. 76, no. 2, pp. 305–315, Feb. 1993.
[44] R. J. Kerans, T. A. Parthasarathy, F. Rebillat, and J. Lamon, "Interface Properties in High-Strength Nicalon/C/SiC Composites, As Determined by Rough Surface Analysis of Fiber Push-Out Tests," *J. Am. Ceram. Soc.*, vol. 81, no. 7, pp. 1881–1887, Jul. 1998.
[45] W. Lee, S. J. Howard, and W. J. Clegg, "Growth of interface defects and its effect on crack deflection and toughening criteria," *Acta Mater.*, vol. 44, no. 10, pp. 3905–3922, Oct. 1996.
[46] P. D. Jero and R. J. Kerans, "The contribution of interfacial roughness to sliding friction of ceramic fibers in a glass matrix," *Scr. Metall. Mater.*, vol. 24, no. 12, pp. 2315–2318, Dec. 1990.
[47] R. J. Kerans, P. D. Jero, and T. A. Parthasarathy, "Issues in the control of fiber/matrix interfaces in ceramic composites," *Compos. Sci. Technol.*, vol. 51, no. 2, pp. 291–296, Jan. 1994.
[48] D.R. Mumm and K.T. Faber, "Interfacial Debonding and Sliding in Brittle-Matrix Composites, Measured Using an Improved Fiber Pullout Technique," *Acta Metall. Mater.*, vol. 43, no. 3, pp. 1259–1270, 1995.
[49] F. F. Lange, W. C. Tu, and A. G. Evans, "Processing of damage-tolerant, oxidation-resistant ceramic matrix composites by a precursor infiltration and pyrolysis method," *Mater. Sci. Eng. A*, vol. 195, pp. 145–150, Jun. 1995.
[50] F. W. Zok and C. G. Levi, "Mechanical properties of porous-matrix ceramic composites," *Adv. Eng. Mater.*, vol. 3, no. 1–2, pp. 15–23, 2001.

[51] K. K. Chawla and C. Coffin, “Interface engineering in oxide fibre/oxide matrix composites,” *Int. Mater. Rev.*, vol. 45, no. 5, pp. 165–189, 2000.
[52] D. B. Marshall, J. B. Davis, P. E. D. Morgan, and J. R. Porter, “Interface materials for damage-tolerant oxide composites,” *Proc. 1996 1st Int. Conf. Ceram. Met. Matrix Compos. CMMC 96 Part 2 2 Sept. 9 1996 - Sept. 12 1996*, vol. 127–131, no. Pt 1, pp. 27–36, 1997.
[53] J. P. Singh, D. Singh, and M. Sutaria, “Ceramic composites: roles of fiber and interface,” *Compos. Part Appl. Sci. Manuf.*, vol. 30, no. 4, pp. 445–450, Apr. 1999.
[54] T. A. Parthasarathy, R. J. Kerans, and N. J. Pagano, “Effective Fiber Properties to Incorporate Coating Thermoelastic Effects in Fiber/Matrix Composite Models,” *J. Am. Ceram. Soc.*, vol. 82, no. 3, pp. 579–584, Mar. 1999.
[55] K. M. Prewo and J. J. Brennan, “High-strength silicon carbide fibre-reinforced glass-matrix composites,” *J. Mater. Sci.*, vol. 15, no. 2, pp. 463–468, Feb. 1980.
[56] B. Bender, D. Shadwell, C. Bulik, L. Incorvati, and D. Lewis III, “EFFECT OF FIBER COATINGS AND COMPOSITE PROCESSING ON PROPERTIES OF ZIRCONIA-BASED MATRIX SiC FIBER COMPOSITES.,” *Am. Ceram. Soc. Bull.*, vol. 65, no. 2, pp. 363–369, 1986.
[57] J. J. Brennan, “Interfacial Chemistry and Bonding in Fiber Reinforced Glass and Glass-Ceramic Matrix Composites,” in *Ceramic Microstructures ’86*, J. A. Pask and A. G. Evans, Eds. Springer US, 1987, pp. 387–399.
[58] R. N. Singh and M. K. Brun, “Effect of Boron Nitride Coating on Fiber-Matrix Interactions,” in *11th Annual Conference on Composites and Advanced Ceramic Materials: Ceramic Engineering and Science Proceedings*, W. Smothers, Ed. John Wiley & Sons, Inc., 1987, pp. 636–643.
[59] E. Bischoff, M. Ruhle, O. Sbaizero, and A. G. Evans, “Microstructural studies of the interfacial zone of a SiC-fiber-reinforced lithium aluminum silicate glass-ceramic,” *J. Am. Ceram. Soc.*, vol. 72, no. 5, pp. 741–745, 1989.
[60] M. D. Thouless, O. Sbaizero, L. S. Sigl, and A. G. Evans, “Effect of interface mechanical properties on pullout in a SiC-fiber-reinforced lithium aluminum silicate glass-ceramic,” *J. Am. Ceram. Soc.*, vol. 72, no. 4, pp. 525–532, 1989.
[61] R. Naslain *et al.*, “Boron Nitride Interphase in Ceramic-Matrix Composites,” *J. Am. Ceram. Soc.*, vol. 74, no. 10, pp. 2482–2488, Oct. 1991.
[62] J. J. Brennan, “Interfaces in BN coated fiber reinforced glass-ceramic matrix composites,” *Scr. Metall. Mater.*, vol. 31, no. 8, pp. 959–964, Oct. 1994.
[63] J. B. Davis, J. P. A. Löfvander, A. G. Evans, E. Bischoff, and M. L. Emiliani, “Fiber Coating Concepts for Brittle-Matrix Composites,” *J. Am. Ceram. Soc.*, vol. 76, no. 5, pp. 1249–1257, May 1993.
[64] Y. Wang, H. Liu, H. Cheng, and J. Wang, “Interface engineering of fiber-reinforced all-oxide composites fabricated by the sol-gel method with fugitive pyrolytic carbon coatings,” *Compos. Part B Eng.*, vol. 75, pp. 86–94, 2015.
[65] J. H. Weaver, J. Yang, and F. W. Zok, “Control of Interface Properties in Oxide Composites Via Fugitive Coatings,” *J. Am. Ceram. Soc.*, vol. 91, no. 12, pp. 4003–4008, Dec. 2008.
[66] P. E. D. Morgan and D. B. Marshall, “Ceramic composites of monazite and alumina,” *J. Am. Ceram. Soc.*, vol. 78, no. 6, pp. 1553–1563, 1995.

[67] F. W. Zok, "Developments in Oxide Fiber Composites," *J. Am. Ceram. Soc.*, vol. 89, no. 11, pp. 3309–3324, Nov. 2006.
[68] J. B. Davis, D. B. Marshall, R. M. Housley, and P. E. D. Morgan, "Machinable Ceramics Containing Rare-Earth Phosphates," *J. Am. Ceram. Soc.*, vol. 81, no. 8, pp. 2169–2175, Aug. 1998.
[69] D. B. M. Peter E. D. Morgan, "Functional Interfaces in Oxide—Oxide Composites," *Mater. Sci. Eng. A*, vol. 162, no. 1, pp. 15–25, 1993.
[70] J. B. Davis, D. B. Marshall, and P. E. D. Morgan, "Oxide Composites of Al2O3 and LaPO4," *J. Eur. Ceram. Soc.*, vol. 19, no. 13–14, pp. 2421–2426, Oct. 1999.
[71] K. K. Chawla, H. Liu, J. Janczak-Rusch, and S. Sambasivan, "Microstructure and properties of monazite (LaPO4) coated saphikon fiber/alumina matrix composites," *J. Eur. Ceram. Soc.*, vol. 20, no. 5, pp. 551–559, May 2000.
[72] J. B. Davis, D. B. Marshall, and P. E. D. Morgan, "Monazite-containing oxide/oxide composites," *Int. Workshop OxideOxide Compos. June 22 1998 - June 24 1998*, vol. 20, no. 5, pp. 583–587, 2000.
[73] K. A. Keller, T.-I. Mah, T. A. Parthasarathy, E. E. Boakye, P. Mogilevsky, and M. K. Cinibulk, "Effectiveness of Monazite Coatings in Oxide/Oxide Composites after Long-Term Exposure at High Temperature," *J. Am. Ceram. Soc.*, vol. 86, no. 2, pp. 325–332, Feb. 2003.
[74] Anthony G. Evans, "Perspective on the Development of High-Toughness Ceramics," *J. Am. Ceram. Soc.*, vol. 73, no. 2, pp. 187–206, 1990.
[75] R. J. Kerans and T. A. Parthasarathy, "Theoretical Analysis of the Fiber Pullout and Pushout Tests," *J. Am. Ceram. Soc.*, vol. 74, no. 7, pp. 1585–1596, Jul. 1991.
[76] T. A. Parthasarathy, P. D. Jero, and R. J. Kerans, "Extraction of interface properties from a fiber push-out test," *Scr. Metall. Mater.*, vol. 25, no. 11, pp. 2457–2462, Nov. 1991.
[77] M. K. Ferber, E. Lara-Curzio, S. E. Russ, and K. K. Chawla, "Single-Fiber Push-In vs. Single-Fiber Push-Out: A Comparison Between Two Test Methods to Determine the Interfacial Properties of Brittle Matrix Composites," in *Symposium M – Ceramic Matrix Composites–Advanced High-*, 1994, vol. 365.
[78] P. D. Jero, T. A. Parthasarathy, and R. J. Kerans, "Measurement of Interface Propertes from Fiber Push-Out Tests," in *Proceedings of the 16th Annual Conference on Composites and Advanced Ceramic Materials: Ceramic Engineering and Science Proceedings*, J. B. W. Jr, Ed. John Wiley & Sons, Inc., 1994, pp. 54–63.
[79] W. M. Mueller, J. Moosburger-Will, M. G. R. Sause, and S. Horn, "Microscopic analysis of single-fiber push-out tests on ceramic matrix composites performed with Berkovich and flat-end indenter and evaluation of interfacial fracture toughness," *J. Eur. Ceram. Soc.*, vol. 33, no. 2, pp. 441–451, Feb. 2013.
[80] G. Rausch, B. Meier, and G. Grathwohl, "A push-out technique for the evaluation of interfacial properties of fiber-reinforced materials," *J. Eur. Ceram. Soc.*, vol. 10, no. 3, pp. 229–235, 1992.
[81] F. Rebillat, J. Lamon, R. Naslain, E. Lara-Curzio, M. K. Ferber, and T. M. Besmann, "Interfacial Bond Strength in SiC/C/SiC Composite Materials, As Studied by Single-Fiber Push-Out Tests," *J. Am. Ceram. Soc.*, vol. 81, no. 4, pp. 965–978, Apr. 1998.
[82] M. Rodríguez, J. M. Molina-Aldareguía, C. González, and J. LLorca, "A methodology to measure the interface shear strength by means of the fiber push-in test," *Compos. Sci. Technol.*, vol. 72, no. 15, pp. 1924–1932, Oct. 2012.

[83] J. Davidovits, “30 Years of Successes and Failures in Geopolymer Applications: Market Trends and Potential Breakthroughs,” presented at the Geopolymer 2002, Melbourne, Australia, 2002.
[84] Andrew Edwin Grabher, “Processing techniques and evaluation of geopolymer as a matrix material in fiber reinforced composite engine exhaust valves,” Colorado State University. Department of Mechanical Engineering., 2008.
[85] J. Davidovits, “Geopolymers: Inorganic Polymeric New Materials,” *Symp. Chem. Thermodyn. Calorim. Therm. Anal. 1989 Sept. 10 1989 - Sept. 14 1989*, vol. 37, no. 8, pp. 1633–1656, 1991.
[86] P. Duxson, A. Fernandez-Jimenez, J. L. Provis, G. C. Lukey, A. Palomo, and J. S. J. Van Deventer, “Geopolymer technology: The current state of the art,” *Spec. Sect. Adv. Geopolymer Sci. Technol. Guest Ed. Grant C Lukey Angel Palomo John Provis Jannie J Van Deventer*, vol. 42, no. 9, pp. 2917–2933, 2007.
[87] K. J. D. MacKenzie, “What are these things called geopolymers? A physico-chemical perspective,” in *Advances in Ceramic Matrix Composites IX, Proceedings, April 27, 2003 - April 30, 2003*, 2004, vol. 153, pp. 175–186.
[88] W. M. Kriven, J. L. Bell, and M. Gordon, “Microstructure and microchemistry of fully-reacted geopolymers and geopolymer matrix composites,” in *Advances in Ceramic Matrix Composites IX, Proceedings, April 27, 2003 - April 30, 2003*, 2004, vol. 153, pp. 227–250.
[89] C. Panagiotopoulou, E. Kontori, T. Perraki, and G. Kakali, “Dissolution of aluminosilicate minerals and by-products in alkaline media,” *J. Mater. Sci.*, vol. 42, no. 9, pp. 2967–2973, Dec. 2006.
[90] H. Xu and J. S. J. Van Deventer, “Geopolymerisation of alumino-silicate minerals,” *Int. J. Miner. Process.*, vol. 59, no. 3, pp. 247–266, 2000.
[91] L. Weng and K. Sagoe-Crentsil, “Dissolution processes, hydrolysis and condensation reactions during geopolymer synthesis: Part I—Low Si/Al ratio systems,” *J. Mater. Sci.*, vol. 42, no. 9, pp. 2997–3006, Jan. 2007.
[92] Joseph Davidovits, “GEOPOLYMERS II: Processing and Applications of Ultra-High Temperature, Inorganic Matrix Resin for Cast Composite Structures, Molds, Tools for RP/C and Metal Industries Stable to 2,100F (1,150C),” presented at the SPE PACTTEC ’83, Anaheim, California, 1983, pp. 222–230.
[93] J. G. S. Van Jaarsveld, J. S. J. Van Deventer, and L. Lorenzen, “The potential use of geopolymeric materials to immobilise toxic metals: Part I. Theory and applications,” *Miner. Eng.*, vol. 10, no. 7, pp. 659–669, Jul. 1997.
[94] P. Rovnaník, “Effect of curing temperature on the development of hard structure of metakaolin-based geopolymer,” *Constr. Build. Mater.*, vol. 24, no. 7, pp. 1176–1183, Jul. 2010.
[95] E. Rill, D. R. Lowry, and W. M. Kriven, “Properties of Basalt Fiber Reinforced Geopolymer Composites,” in *Strategic Materials and Computational Design*, W. M. Kriven, Y. Zhou, M. Radovic, Sanjaythur, and T. Ohji, Eds. John Wiley & Sons, Inc., 2010, pp. 57–67.
[96] S. S. Musil, G. Kutyla, and W. M. Kriven, “The Effect of Basalt Chopped Fiber Reinforcement on the Mechanical Properties of Potassium Based Geopolymer,” in *Developments in Strategic Materials and Computational Design III*, W. M. Kriven, A. L.

Gyekenyesi, G. Westin, J. Wang, M. Halbig, and Sanjaythur, Eds. John Wiley & Sons, Inc., 2012, pp. 31–42.
[97] "Online Materials Information Resource - MatWeb." [Online]. Available: http://www.matweb.com/index.aspx. [Accessed: 13-Nov-2015].
[98] A. J. Foden, P. Balaguru, and R. E. Lyon, "Mechanical properties and fire response of GEOPOLYMER structural composites," *Proc. 41st Int. SAMPE Symp. Exhib. Part 1 2 March 24 1996 - March 28 1996*, vol. 41, no. 1, pp. 748–758, 1996.
[99] B. Nair, Q. Zhao, T. Rahimian, R. F. Cooper, and P. N. Balaguru, "Matrix and interphase design of geopolymer composites," in *107th Annual Meeting of the American Ceramic Society, April 10, 2005 - April 13, 2005*, 2006, vol. 175, pp. 253–263.
[100] C. Defazio, M. D. Arafa, and P. N. Balaguru, "Functional Geopolymer Composites for Structural Ceramic Applications," Jun. 2006.
[101] T. Lin, D. Jia, P. He, and M. Wang, "Thermal-mechanical properties of short carbon fiber reinforced geopolymer matrix composites subjected to thermal load," *J. Cent. South Univ. Technol.*, vol. 16, no. 6, pp. 881–886, Dec. 2009.
[102] J. L. Bell, P. E. Driemeyer, and W. M. Kriven, "Formation of Ceramics from Metakaolin-Based Geopolymers. Part II: K-Based Geopolymer," *J. Am. Ceram. Soc.*, vol. 92, no. 3, pp. 607–615, Mar. 2009.
[103] T. S. Lin, D. C. Jia, P. G. He, and M. R. Wang, "Thermo-mechanical and Microstructural Characterization of Geopolymers with α-Al2O3 Particle Filler," *Int. J. Thermophys.*, vol. 30, no. 5, pp. 1568–1577, Aug. 2009.
[104] P. He, D. Jia, and S. Wang, "Microstructure and integrity of leucite ceramic derived from potassium-based geopolymer precursor," *J. Eur. Ceram. Soc.*, vol. 33, no. 4, pp. 689–698, Apr. 2013.
[105] D. Pernica, P. N. B. Reis, J. a. M. Ferreira, and P. Louda, "Effect of test conditions on the bending strength of a geopolymer-reinforced composite," *J. Mater. Sci.*, vol. 45, no. 3, pp. 744–749, Nov. 2009.
[106] P. Duxson, J. L. Provis, G. C. Lukey, S. W. Mallicoat, W. M. Kriven, and J. S. J. Van Deventer, "Understanding the relationship between geopolymer composition, microstructure and mechanical properties," *Colloids Surf. Physicochem. Eng. Asp.*, vol. 269, no. 1–3, pp. 47–58, 2005.
[107] "3M Nextel (TM) Ceramic Textiles Technical Notebook." 3M, Nov-2004.
[108] P. E. D. Morgan and D. B. Marshall, "Functional interfaces for oxide/oxide composites," *Mater. Sci. Eng. A*, vol. 162, no. 1, pp. 15–25, Apr. 1993.
[109] E. E. Boakye, R. S. Hay, P. Mogilevsky, and L. M. Douglas, "Monazite Coatings on Fibers: II, Coating without Strength Degradation," *J. Am. Ceram. Soc.*, vol. 84, no. 12, pp. 2793–2801, Dec. 2001.
[110] R. S. Hay, "United States Patent: 5164229 - Method for coating continuous tow," 5164229, 17-Nov-1992.
[111] R. S. Hay and D. Petry, "United States Patent: 5951764 - Coating apparatus for continuous tow," 5951764, 14-Sep-1999.
[112] R. S. Hay and E. E. Boakye, "Monazite Coatings on Fibers: I, Effect of Temperature and Alumina Doping on Coated-Fiber Tensile Strength," *J. Am. Ceram. Soc.*, vol. 84, no. 12, pp. 2783–2792, Dec. 2001.
[113] C28 Committee, "ASTM C1341-06. Test Method for Flexural Properties of Continuous Fiber-Reinforced Advanced Ceramic Composites," ASTM International, 2011.

[114] C28 Committee, "ASTM 1275-15. Test Method for Monotonic Tensile Behavior of Continuous Fiber-Reinforced Advanced Ceramics with Solid Rectangular Cross-Section Test Specimens at Ambient Temperature," ASTM International, 2011.
[115] L. T. Drzal, "The role of the fiber-matrix interphase on composite properties," *Vacuum*, vol. 41, no. 7–9, pp. 1615–1618, Jan. 1990.
[116] H. c. Cao *et al.*, "Effect of Interfaces on the Properties of Fiber-Reinforced Ceramics," *J. Am. Ceram. Soc.*, vol. 73, no. 6, pp. 1691–1699, Jun. 1990.
[117] R. S. Hay, "Monazite and Scheelite Deformation Mechanisms," in *24th Annual Conference on Composites, Advanced Ceramics, Materials, and Structures: B: Ceramic Engineering and Science Proceedings*, T. Jessen and E. Ustundag, Eds. John Wiley & Sons, Inc., 2000, pp. 203–217.
[118] *MIL-HDBK-727: Design Guidance For Producibility*, 1984th ed. Military Governmnet Specs & Standards (Naval Publications and Form Center) (NPFC), 1990.
[119] K. Okada, A. Ooyama, T. Isobe, Y. Kameshima, A. Nakajima, and K. J. D. MacKenzie, "Water retention properties of porous geopolymers for use in cooling applications," *J. Eur. Ceram. Soc.*, vol. 29, no. 10, pp. 1917–1923, Jul. 2009.
[120] C. G. Levi, J. Y. Yang, B. J. Dalgleish, F. W. Zok, and A. G. Evans, "Processing and Performance of an All-Oxide Ceramic Composite," *J. Am. Ceram. Soc.*, vol. 81, no. 8, pp. 2077–2086, Aug. 1998.
[121] J. J. Haslam, K. E. Berroth, and F. F. Lange, "Processing and properties of an all-oxide composite with a porous matrix," *J. Eur. Ceram. Soc.*, vol. 20, no. 5, pp. 607–618, May 2000.
[122] Committee B09, "ASTM B962-15. Standard Test Methods for Density of Compacted or Sintered Powder Metallurgy (PM) Products Using Archimedes' Principle," ASTM International, 100 Barr Harbor Drive, PO Box C700, West Conshohocken, PA 19428-2959, 2015.
[123] C. Kaya, F. Kaya, E. G. Butler, A. R. Boccaccini, and K. K. Chawla, "Development and characterisation of high-density oxide fibre-reinforced oxide ceramic matrix composites with improved mechanical properties," *J. Eur. Ceram. Soc.*, vol. 29, no. 9, pp. 1631–1639, Jun. 2009.
[124] G. H. Zhou, S. W. Wang, J. K. Guo, and Z. Zhang, "The preparation and mechanical properties of the unidirectional carbon fiber reinforced zirconia composite," *J. Eur. Ceram. Soc.*, vol. 28, no. 4, pp. 787–792, 2008.
[125] "Fig. 3. Bending test configurations and corresponding shear/moment...," *ResearchGate*. [Online]. Available: https://www.researchgate.net/figure/275329880_fig2_Fig-3-Bending-test-con-figurations-and-corresponding-shearmoment-diagrams-for-a. [Accessed: 25-Aug-2017].
[126] D. O. Adams and D. F. Adams, "Tabbing Guide for Composite Test Specimens," *DOTFAAAR-02106*, p. 74, Oct. 2002.
[127] D30 Committee, "ASTM D2344/D2344M-13. Test Method for Short-Beam Strength of Polymer Matrix Composite Materials and Their Laminates," ASTM International, 100 Barr Harbor Drive, PO Box C700, West Conshohocken, PA 19428-2959, 2013.
[128] C. Berg, J. Tirosh, and M. Israeli, "Analysis of Short Beam Bending of Fiber Reinforced Composites," in *Composite Materials: Testing and Design (Second Conference)*, H.

Corten, Ed. 100 Barr Harbor Drive, PO Box C700, West Conshohocken, PA 19428-2959: ASTM International, 1972, pp. 206-206–13.
[129] J. M. Whitney and C. E. Browning, "On short-beam shear tests for composite materials," *Exp. Mech.*, vol. 25, no. 3, pp. 294–300, Sep. 1985.
[130] J. L. Sullivan and H. Van Oene, "An elasticity analysis for the generally and specially orthotropic beams subjected to concentrated loads," *Compos. Sci. Technol.*, vol. 27, no. 2, pp. 133–155, Jan. 1986.
[131] D.F. Adams and J.M. Busse, "Suggested Modifications of the Short Beam Shear Test Method," presented at the Proceedings of teh 49th International SAMPE Symposium, Long Beach, CA, 2004.
[132] T. A. Parthasarathy, D. B. Marshall, and R. J. Kerans, "Analysis of the effect of interfacial roughness on fiber debonding and sliding in brittle matrix composites," *Acta Metall. Mater.*, vol. 42, no. 11, pp. 3773–3784, Nov. 1994.
[133] G. Tolf and P. Clarin, "Comparison between flexural and tensile modulus of fibre composites," *Fibre Sci. Technol.*, vol. 21, no. 4, pp. 319–326, Jan. 1984.
[134] F. Mujika, "On the difference between flexural moduli obtained by three-point and four-point bending tests," *Polym. Test.*, vol. 25, no. 2, pp. 214–220, Apr. 2006.
[135] L. Brancheriau, H. Bailleres, and D. Guitard, "Comparison between modulus of elasticity values calculated using 3 and 4 point bending tests on wooden samples," *Wood Sci. Technol.*, vol. 36, no. 5, pp. 367–383, Nov. 2002.
[136] J. A. DiCarlo, "Fibers for Structurally Reliable Metal and Ceramic Composites," *JOM*, vol. 37, no. 6, pp. 44–49, Jun. 1985.
[137] D. B. Marshall, P. E. D. Morgan, R. M. Housley, and J. T. Cheung, "High-Temperature Stability of the Al2O3-LaPO4 System," *J. Am. Ceram. Soc.*, vol. 81, no. 4, pp. 951–956, Apr. 1998.
[138] Y. Katoh, T. Nozawa, L. L. Snead, and T. Hinoki, "Effect of neutron irradiation on tensile properties of unidirectional silicon carbide composites," *J. Nucl. Mater.*, vol. 367–370, pp. 774–779, Aug. 2007.
[139] C. Sauder, A. Brusson, and J. Lamon, "Influence of Interface Characteristics on the Mechanical Properties of Hi-Nicalon type-S or Tyranno-SA3 Fiber-Reinforced SiC/SiC Minicomposites," *Int. J. Appl. Ceram. Technol.*, vol. 7, no. 3, pp. 291–303, May 2010.
[140] T. A. Parthasarathy, E. E. Boakye, K. A. Keller, and R. S. Hay, "Evaluation of Porous ZrO2-SiO2 and Monazite Coatings Using NextelTM 720-Fiber-Reinforced Blackglas™ Minicomposites," *J. Am. Ceram. Soc.*, vol. 84, no. 7, pp. 1526–1532, Jul. 2001.
[141] M. Takeda, A. Urano, J. Sakamoto, and Y. Imai, "Microstructure and oxidative degradation behavior of silicon carbide fiber Hi-Nicalon type S," *J. Nucl. Mater.*, vol. 258, pp. 1594–1599, Oct. 1998.
[142] S. S. Musil, P. F. Keane, and W. M. Kriven, "Green Composite: Sodium-Based Geopolymer Reinforced with Chemically Extracted Corn Husk Fibers," in *Developments in Strategic Materials and Computational Design IV*, W. M. Kriven, J. Wang, Y. Zhou, A. L. Gyekenyesi, S. Kirihara, and S. Widjaja, Eds. John Wiley & Sons, Inc., 2013, pp. 123–133.
[143] P. Duxson, G. C. Lukey, and J. S. J. van Deventer, "Physical evolution of Na-geopolymer derived from metakaolin up to 1000 °C," *J. Mater. Sci.*, vol. 42, no. 9, pp. 3044–3054, Feb. 2007.